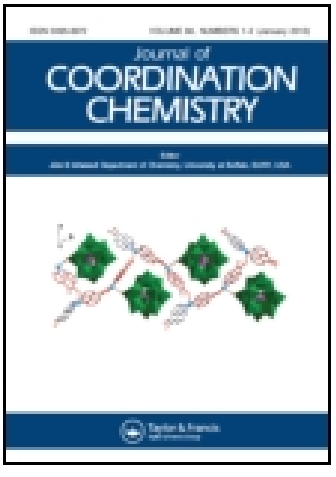

Journal of Coordination Chemistry
Publication details, including instructions for authors and subscription information:
http://www.tandfonline.com/loi/gcoo20

Review: A gentle introduction to magnetism: units, fields, theory, and experiment

Christopher P. Landee[a] & Mark M. Turnbull[a]

[a] Department of Physics and Carlson School of Chemistry and Biochemistry, Clark University, Worcester, MA, USA

Accepted author version posted online: 05 Feb 2014.Published online: 24 Mar 2014.

To cite this article: Christopher P. Landee & Mark M. Turnbull (2014) Review: A gentle introduction to magnetism: units, fields, theory, and experiment, Journal of Coordination Chemistry, 67:3, 375-439, DOI: 10.1080/00958972.2014.889294

To link to this article: http://dx.doi.org/10.1080/00958972.2014.889294

Journal of Coordination Chemistry, 2014
Vol. 67, No. 3, 375–439, http://dx.doi.org/10.1080/00958972.2014.889294

Review: A gentle introduction to magnetism: units, fields, theory, and experiment[†]

CHRISTOPHER P. LANDEE* and MARK M. TURNBULL

Department of Physics and Carlson School of Chemistry and Biochemistry, Clark University, Worcester, MA, USA

(*Received 13 December 2013; accepted 10 January 2014*)

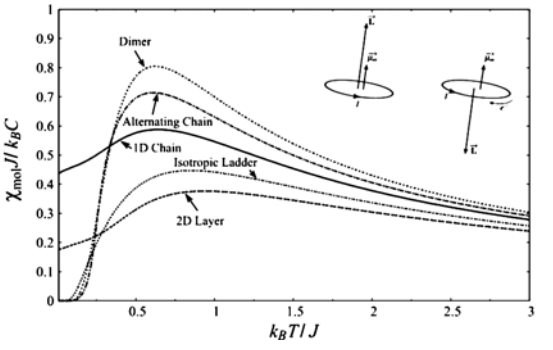

We present an introduction to the workings, units of measure, and general properties of magnetic materials. This is intended as a "primer to interpretation of magnetic data" for those who are entering the field, or those who are encountering magnetic measurements in the literature. We expect this work will serve as an initial guide to the reader to familiarize them with the basics in the hope that those working in the field of magnetochemistry will wish to explore additional, more detailed literature as their specific investigations demand. Topics covered include: magnetic fields and units (SI and cgs), paramagnetism (magnetization and magnetic susceptibility), Curie and Curie–Weiss behavior, magnetic exchange interactions, magnetic anisotropy, dimeric systems and exchange-coupled networks (including chains, ladders, and layers), and long-range order.

Keywords: Magnetochemistry; Magnetic exchange; Magnetic lattices; Exchange-coupled networks; Magnetic susceptibility; Magnetization; Magnetic units

1. Introduction

Over the past several decades, a significant number of chemical research groups have begun incorporating magnetic data into their work. There are a variety of reasons for this

*Corresponding author. Email: clandee@clarku.edu
[†]This manuscript is lovingly dedicated to Laura and Susan for near infinite patience.

development: the greater access to SQUID magnetometers with user-friendly software; increased collaborations between synthetic and physical chemistry groups; increased collaborations between chemists and physicists; and the greater ability to form international collaborations. However, as is frequently the case, many of these scientists are not simply new to collecting magnetic data; they are also new to the field of magnetism and especially to understanding the influence of magnetic interactions. Using a room temperature magnetic moment to determine whether an *isolated* ion is high spin or low spin can be a straightforward matter, but the presence of interactions frequently leads to complex temperature- and field-dependent data. The interpretation of such data is much more challenging to those without sufficient experience.

This increase in reported magnetic data and magnetic behavior in materials extends beyond the researchers themselves. As more chemists report magnetic data, it becomes incumbent upon referees and readers to also be more familiar with routine interpretation of temperature- and field-dependent magnetic data. This can be especially confusing to the novice when the literature is taken into account. Historically, different systems of units have been used for reporting magnetic data, and converting between them is not trivial. Even the question of the simplest form of the magnetic exchange Hamiltonian can be a daunting task given the variety of forms used. Is there a factor of two incorporated or not? What is the meaning of the sign of J?

We present here a "Primer to interpreting magnetic data" that is intended as an introduction for those new to the field, whether new students or senior scientists, and we hope it will serve as a stepping-stone to the more in-depth and specific reviews that are already available in the literature. Please note that there is nothing original in this document; everything presented here is standard magnetism as described in a long series of books, monographs, and review articles [1–12].

1.1. *Magnetic fields and units in the SI system*

The International System of Units [13] (SI for the French name "Système International d'unités") is the modern form of the metric system, founded upon seven base units. For magnetism, it is only necessary to use four of them: meters, kilograms, seconds, and amperes (MKSA). All other units can be derived from these units plus fundamental equations of science. For instance, the metric unit for electric charge, the Coulomb (C), is defined to be the charge transferred by a current of one ampere (A) in one second.

The SI system is universally used in education and employs the mechanical and electrical units with which we are all familiar: joules, watts, newtons, volts, ohms, farads, etc. The units of magnetism are less familiar but can all be readily derived, as we shall see in the following paragraphs. Unfortunately, much of the research in magnetism is still reported in the older cgs (centimeters, grams, seconds) system of units and converting from one system to the other is an endless source of confusion. Following this introduction to SI magnetism, cgs magnetism will be discussed, along with the appropriate conversion factors, in Section 1.2.

We begin with the most important field, B, which can be defined in terms of the force on a moving charge through the equation $\mathbf{F} = q\mathbf{v} \times B$, where the respective units are Newtons (N) for force, Coulombs (C) for charge, $\mathrm{m\,s^{-1}}$ for velocity, and Tesla (T) for B. One tesla is thus equivalent to one $\mathrm{N\,A^{-1}\,m^{-1}}$, where the current is expressed in amps. The name of the

B-field is the *magnetic flux density*[†], because it equals the number of magnetic flux lines (in units of Webers (Wb)) passing through an area of one square meter: $1\,\mathrm{T} = 1\,\mathrm{Wb\,m^{-2}}$.

The *B*-field is related to the two other magnetic fields, *H* and *M*, by equation (1), in which the proportionality constant μ_0 is named the permeability of free space and has a value of exactly $4\pi \times 10^{-7}\,\mathrm{T\,m\,A^{-1}}$.

$$B = \mu_0 (H + M) \tag{1}$$

The *H*-field, named *the magnetic field*, arises from electrical currents passing through wires. (The field created by current in a solenoid is the *H*-field.) The magnitude of the magnetic field at a distance *r* from a long straight wire carrying a current *I* is given by the equation

$$H = \frac{1}{2\pi}\frac{I}{r} \tag{2}$$

Consequently the units for the *H*-field are amperes per meter, $\mathrm{A\,m^{-1}}$. As shown later, one $\mathrm{A\,m^{-1}}$ is a very small field. It is also clear from equation (1) that *M* and *H* must have the same unit, $\mathrm{A\,m^{-1}}$. It is essential to realize that the magnetization appearing in equation (1) is the magnetization *per unit volume*, and not the more common magnetization per mole used in experimental work.

The volume magnetization *M* equals the vector sum of all the magnetic moments per cubic meter. Magnetic moments[‡] arise from circulating currents (whether quantum or free currents) and are equal to the product of the current in the loop times the area of the loop; moments have units of amp-meter^2 ($\mathrm{A\,m^2}$). The moment is normal to the plane of the loop and in the direction such that the *H*-field generated by the current passes through the loop according to the right-hand rule.

$$M = \left(\sum_i \mu_i\right) / \textit{unit volume} \tag{3}$$

The units of the volume magnetization are $\mathrm{A\,m^2}$ per cubic meter, or $\mathrm{A\,m^{-1}}$, the same as that of the magnetic field *H*.

Scientists rarely know the volumes of their samples, but they can measure the masses. For this reason, the magnetization per unit mass M_{kg} is more useful. It is obtained from the volume magnetization by dividing *M* by the sample's density expressed in the SI units of density, kilograms per cubic meter, equation (4).

$$M_{kg}(\mathrm{A\,m^2\,kg^{-1}}) = \frac{M(\mathrm{A\,m^{-1}})}{\rho(\mathrm{kg\,m^{-3}})} \tag{4}$$

One can then obtain the magnetization per mole M_{mol} by multiplying the mass magnetization by the formula weight (FW), equation (5).

$$M_{mol}(\mathrm{A\,m^2 mol^{-1}}) = M_{kg}(\mathrm{A\,m^2\,kg^{-1}}) \times \mathrm{FW(kg\,mol^{-1})} \tag{5}$$

[†]The *B*-field is also known as the *magnetic induction.*

[‡]This topic is addressed more completely in Section 2.

The magnetic susceptibility χ is usually the first quantity measured for a new compound. The *volume* susceptibility is defined as the ratio of the sample's *volume* magnetization to the applied *H*-field, in the limit of a vanishingly small field, equation (6):

$$\chi_{vol}(\text{dimensionless}) = \lim_{H\to 0} \frac{M}{H} \tag{6}$$

The *volume* susceptibility is dimensionless because the units of the volume magnetization and the magnetic field are the same, equation (1). Nevertheless, in the laboratory, we measure the magnetization per unit of mass, and calculate the magnetization per mole, so the corresponding mass and molar susceptibilities are defined as follows:

$$\chi_{kg}(\text{m}^3\,\text{kg}^{-1}) = \lim_{H\to 0} \frac{M_{kg}}{H} \tag{7a}$$

$$\chi_{mol}(\text{m}^3\,\text{mol}^{-1}) = \lim_{H\to 0} \frac{M_{mol}}{H} \tag{7b}$$

The units for the mass and molar susceptibilities are those of the inverse density and the molar volume, respectively.

This section concludes with the important connection between SI magnetic units and energy. In a *B*-field, a magnetic moment experiences a torque that tends to align the moment parallel to the field. The energy *U* required to rotate the moment away from the field direction is given as

$$U = -\mu \cdot B(\textit{the Zeeman equation}) \tag{8}$$

with the minimum energy configuration occurring when the moment and field are parallel. As seen from the units of this equation, the SI unit of moment μ (A m^2) is also equal to the ratio of energy to field, one joule per tesla: 1 A m^2 = 1 J T^{-1}.

1.2. *Magnetic fields and units in the CGS system*

> The SI is the legal system, but legality is not science. Indeed, this system is particularly inappropriate in molecular magnetism and, like most researchers involved in this field, we prefer to use the cgs-emu system. Olivier Kahn [1]

People studied magnetism long before the advent of the SI system and they created unit systems to suit their own purposes, usually to make a set of fundamental equations as simple as possible. Length, mass, and time were always in units of centimeters, grams, and seconds so these unit systems became known as cgs systems. However, *multiple* cgs systems were created, each one for the study of one particular branch of physics.

As an example, in the study of electrostatics, the fundamental unit of charge was defined such that two identical charges, separated by one centimeter, exerted mutual forces of one dyne (1 g cm s^{-2} = 10^{-5} N). In the cgs-*electrostatic* unit system (cgs-esu), Coulomb's Law has the simple form

$$\text{Coulomb's Law (cgs} - \text{esu)}: F = \frac{q_1 q_2}{r^2} \tag{9}$$

The charge thus defined is the *esu unit of charge,* the statcoulomb (1 sC = 3.33×10^{-10} C). One statampere is the flow of one statcoulomb per second and equals 3.33×10^{-10} A.

In contrast, for the study of magnetism, the cgs-*electromagnetic* system was created (cgs-emu) based on the definition of one unit of magnetic moment such that two equal moments separated by one centimeter repel each other with a force equal to one dyne. Given that the magnetic moment is equal to the product of a current times an area, this definition of moment defines the cgs-emu current, known as the absolute current or abamp (1 abA = 10 A) which is different from the stat-amp. Ultimately, the Gaussian system of cgs units evolved which uses esu units for charges and emu units for magnetic fields and moments. For the study of magnetism in this Tutorial, the Gaussian and cgs-emu units are identical. The relationships between the Gaussian and MKSA units are given in Appendix A. Additional sources for studying this confusing topic are available [14].

In the cgs-emu system, B, H, and M are related as shown in equation (10). The units of B and H are equivalent but are given different names to help identify the field under discussion. The unit of the B-field is the gauss (G, 1 G = 10^{-4} T) and those of the H-field are oersteds (Oe, 1 Oe = $10^3/4\pi$ A m^{-1} = 79.6 A m^{-1}). The volume magnetization consists of the vector sum of individual magnetic moments per unit volume, equation (3), and is often said to have units of emu/cm^3. This is unfortunate nomenclature for it leads people to believe that the emu is the cgs-emu unit of magnetic moment; it is *not*! This use of *emu* simply means that the magnetization is given in the emu system, with the cm^3 identifying the magnetization as the volume magnetization. Likewise, the mass and molar magnetizations in cgs units are commonly written as emu g^{-1} and emu mol^{-1}, respectively (see Appendix A).

$$B = H + 4\pi M \tag{10}$$

If not the emu, what is the cgs unit of magnetic moment? It is identified from equation (8), the Zeeman equation, for the energy (in ergs) of a moment in an applied field (in G). The cgs moment has units of ergs G^{-1} and is smaller than the SI unit of moment, the A m^2, by exactly 1000.

$$1\,\frac{\text{erg}}{\text{G}} = \frac{10^{-7}\text{J}}{10^{-4}\text{T}} = 10^{-3}\,\text{A m}^2 \tag{11}$$

Do we get the same numerical result when we compare definitions of moments (as a product of currents times area) from the cgs and SI systems? Does 1 A cm^2 = 10^{-3} A m^2? Clearly not, because 1 m^2 = 10^4 cm^2. The inequality arises because the cgs-emu unit of current is not the ampere, but the *abampere*, equal to 10 amperes. This example reveals a severe disadvantage of the Gaussian system; its units for electrical variables (charge, current, voltage, and resistance) are all different from the SI units in everyday use.

The cgs volume magnetization therefore has units of erg G^{-1} cm^{-3}, usually expressed as emu cm^{-3}. From equation (10), we see that volume magnetization also has the units of oersteds, so 1 Oe = 1 erg G^{-1} cm^{-3} = 1 emu cm^{-3}. However, it is also seen in equation (10) that $4\pi M$ has the unit of gauss! In the cgs system, both the free currents in wires and the bound currents in magnetized matter produce magnetic flux lines but the free currents are weighted more heavily. This difference does not occur in the SI system, equation (1).

For low fields, and in the absence of any permanent moments or hysteresis, the magnetization is proportional to the H-field, $M = \chi H$, equation (6), with the proportionality constant χ defined as the magnetic susceptibility. The ratio of M/H is dimensionless so 1 emu/cm^3 = 1 Oe = 1 G. Under these conditions, equation (10) can be written as

$$B = (1 + 4\pi\chi_{vol})H = \mu H \tag{12}$$

where the ratio of B/H is defined as the magnetic permeability μ. Since B and H have equal units, both the permeability and volume susceptibility are dimensionless.

As described in Section 1.1, for experimental work, it is convenient to work with the mass and molar magnetizations. These are calculated by the same procedure used previously, with the following results:

$$M_g(\text{emu g}^{-1}) = \text{M}(\text{emu cm}^{-3})/\rho(\text{g cm}^{-3}) \tag{13a}$$

$$M_g(\text{emu mol}^{-1}) = M_{mol}(\text{emu g}^{-1}) \times \text{FW}(\text{g mol}^{-1}) \tag{13b}$$

The mass and molar susceptibilities are defined in terms of the M_g and M_{mol} as before.

$$\chi_g(\text{cm}^3\ \text{g}^{-1}) = \lim_{H\to 0} \frac{M_g}{H} \tag{14a}$$

$$\chi_{mol}(\text{cm}^3\ \text{mol}^{-1}) = \lim_{H\to 0} \frac{M_{mol}}{H} \tag{14b}$$

The units for the mass and molar susceptibilities are once again those of inverse density and molar volume, respectively, just as found for the equivalent SI susceptibilities in equation (7).

We conclude this section by evaluating the conversion factors between the cgs and SI susceptibilities. In addition to powers of 10 that arise from converting base units ($1\ \text{cm}^3\ \text{mol}^{-1} = 10^{-6}\ \text{m}^3\ \text{mol}^{-1}$), a factor of 4π appears, due to the existence of 4π in equation (10) and its absence in equation (1). For this reason, a cgs molar susceptibility in units of $\text{cm}^3\ \text{mol}^{-1}$ equals $4\pi \times 10^{-6}$ times the SI molar susceptibility, equation (14). See Appendix A.

$$\chi_{mol}(\text{cm}^3\ \text{mol}^{-1}) = 4\pi \times 10^{-6}\chi_{mol}(\text{m}^3\ \text{mol}^{-1}) \tag{15}$$

We have just defined the susceptibilities in the two unit systems, and learned how to convert from one system to the other. *However, we are not done.* As shown in Section 2, application of a magnetic field to a magnetic material will induce a moment that is determined by the B-field, not the H-field. When calculating the susceptibility, the ratio B/H will appear. This ratio is dimensionless in cgs-emu system [equation (10)], but B/H has the units of (T m A^{-1}) in the SI system, equation (1), so the conversion of susceptibility units is more complex than shown in Appendix A.

2. Paramagnetism – magnetization and susceptibility of a mole of independent spins

In this section, we begin the study of magnetism itself. The connection between angular momentum and magnetic moments is reviewed in Section 2.1, both for classical currents and at the quantum level. Section 2.2 explores the effects of temperature and field upon a collection of non-interacting moments; the case of $S = 1/2$ is worked out in detail. It is seen that the net magnetization is due to a competition between the aligning effect of the B-field

and the randomizing influence of the thermal energy. In the limit of small B/T, the magnetization is linear with the field and the equation for the paramagnetic magnetic susceptibility is derived. Section 2.3 discusses Curie's Law for the paramagnetic susceptibility and the Curie constant is derived. Surprisingly, in SI units, the Curie constant needs to be multiplied by μ_0 to have the correct units for the susceptibility. Section 2.4 describes the need for demagnetization corrections that are necessary when working with large susceptibilities. A table of the fundamental physical constants in both SI and cgs units is available in Appendix B. A table of energy units used in magnetism, and their conversion factors, appears in Appendix C.

2.1. *Magnetic moments of quantum spins*

The origins of electricity and magnetism are fundamentally different. Electricity arises from two distinct electric charges, positive and negative, exemplified by the proton and electron. In an otherwise neutral molecule, such as H_2O, the centers of the positive and negative charge densities are displaced from each other, leading to an electric dipole moment. The same cannot be said for magnetism. No one has ever isolated an individual magnetic pole (magnetic monopole) even though there is no theoretical reason why monopoles cannot exist. Consequently, every magnet is a dipole. This distinction exists because, in contrast to electricity, all of magnetism arises from charges *in motion*.

The simplest possible illustration of this principle is a small circular loop of radius R, in which a charge q circulates at speed v. Experience shows that the magnetic behavior of any current loop can be described as arising from a magnetic moment μ that equals the product of the current and the area A of the loop, $\mu = IA$. Since current in SI units is given in amperes (A) and areas in square meters, the units of magnetic moments are A m^2. The direction of the moment is perpendicular to the plane of the loop, in accordance with the right-hand rule. The thumb of the right hand points in the direction of the positive current and the fingers of the right hand curl through the loop in the same sense as the magnetic moment.

We calculate the magnetic moment of the simplest possible system, the circular current loop. The period of the motion (T) is the ratio of the circumference, $2\pi R$, to the velocity, v: $T = 2\pi R/v$. The current (in Coulombs per sec) is given by the charge divided by the period, $I = q/(2\pi R/v) = qv/2\pi R$. As the magnetic moment equals the product of the current and the area A of the circular loop ($A = \pi R^2$),

$$\mu = \frac{qvR}{2} \text{ (circular loop)} \tag{16}$$

Two important points immediately follow. First is the recognition that the magnetic moment is proportional to the angular momentum L of the moving charge. Recall that the angular momentum of an object moving about a point is given as the vector product $L = R \times mv = mvR \sin(\theta)$, where mv is the momentum of the object, R is the vector from the point in question to the location of the object, and θ is the angle between v and R. For circular motion, R is simply the radius of the circle, $p = mv$, and the two vectors are orthogonal ($\theta = 90°$). Therefore $L = mvR$ and $vR = L/m$. The product vR also appears in equation (16) for the magnetic moment, so the equation can be rewritten

$$\mu = \frac{qL}{2m} \tag{17}$$

(Even though we have derived equation (17) only for the special case of a circular loop, it can be shown to be true for a current loop of any shape.)

For a current due to the rotation of positive charges, the magnetic moment vector is parallel to that of the angular momentum. However, and this is the second important point, we are usually interested in currents arising from negatively charged electrons. For electrons, μ and L point in opposite directions, figure 1. Equation (17) can be rewritten for the case of electrons using the electron mass m_e and the electron charge, $-e$ (the symbol e represents the absolute value of 1.602×10^{-19} C).

$$-\mu = \frac{eL}{2m_e} \tag{18}$$

Equation (18) can be used to calculate the magnetic moment of an atom that has one electron with orbital momentum L. The total magnetic moment resulting from the orbital motion of all the electrons in the atom is the vector sum L_{tot} where the sum is over all the electrons in unfilled shells,

$$L_{tot} = \sum_i L_i \tag{19}$$

Equation (18) brings us to one of the fundamental units of magnetism, the Bohr magneton. Orbital angular momentum at the atomic level is quantized and appears as an integer multiple of Planck's constant $\hbar$: $L = \sqrt{l(l+1)}\,\hbar$, $L_z = l\hbar$. Consequently, the magnetic moment arising from an electron in a quantized orbit, equation (18), will also be quantized.

$$\mu_l = -\frac{e\hbar}{2m_e}\sqrt{l(l+1)} = -\mu_B \frac{L}{\hbar} \text{ (orbital electron moment)} \tag{20}$$

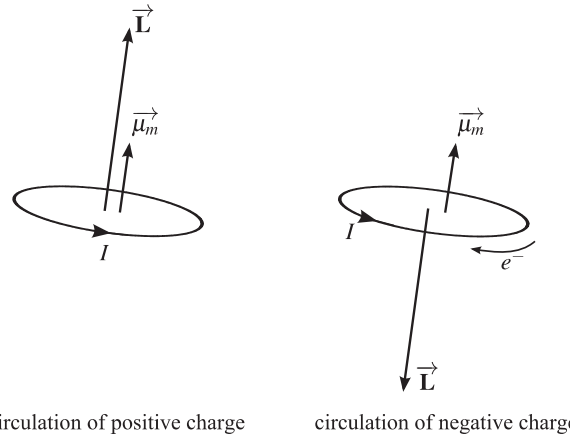

Figure 1. Relationship between angular momentum and magnetic moment for currents of positive and negative charges.

This ratio of basic units ($e\hbar/2m_e$) is one of the fundamental constants in science and is given the symbol μ_B and named the Bohr magneton. It has the very small value of 9.274×10^{-24} J T^{-1} in SI units, and 9.274×10^{-21} erg G^{-1} in cgs units. It is the conversion factor between quantum units of angular momentum and the resulting magnetic moment.[†]

The quantum mechanics of orbital angular momentum show that the magnitude of the angular momentum is related to the quantum number l in the following manner: $L = \sqrt{l(l+1)}\,\hbar$. The component of angular momentum along a particular axis z (L_z) is given as $L_z = m_l\,\hbar$, where m_l can assume values over the range $l, l-1, l-2, \ldots, -l+1, -l$.

Similar rules apply for the *intrinsic*, or *spin* angular momentum of the electron. Even an electron at rest has an angular momentum $S = \hbar/2$, with components $S_z = m_s\hbar$, $m_s = \pm 1/2$. Consequently, each electron also has an *intrinsic* magnetic moment $\mu_e = -g\mu_B S/\hbar$, where the negative sign arises from the electron's negative charge. The constant g (2.0023) is the electron g-factor and reflects the different proportionality between spin and orbital angular momentum in creating magnetic moments.

The important conclusion of this section is that the magnetic moments of atoms and ions can be evaluated by summing over the orbital and spin angular momenta and the result can be expressed as some number of Bohr magnetons. The average moment per atom can still be given in Bohr magnetons even in more complicated cases, such as magnetic metals, in which some of the electrons are no longer constrained to individual atoms. For example, at room temperature, iron has a moment of 2.14 μ_B per atom.

2.2. *Magnetization of a mole of independent spins*

2.2.1. The spin $S = 1/2$ case. We will first consider the magnetic properties of one mole of electron magnetic moments, with $m_s = \pm 1/2$ and $\mu_z = -g\mu_B m_s$. When a magnetic field B is applied in the z-direction, the energy U of each moment will vary according to the Zeeman equation, equation (8):

$$U = -\mu \cdot B = -\left(-\frac{g\mu_B}{\hbar} S \cdot B\right) = g\mu_B m_s B \tag{21}$$

The moments parallel to the field ($m_s = -1/2$) have their energies lowered as the field increases, while those antiparallel experience the opposite effect (figure 2). The energy splitting Δ between the two states is given as

$$\Delta = g\mu_B m_s B - (-g\mu_B m_s B) = 2g\mu_B m_s B = g\mu_B B \tag{22}$$

The molar magnetization M_{mol} equals the product of the *net* number of spins aligned with the field with the moment of each spin:

$$M_{mol} = \mu_e(N^+ - N_-), \tag{23}$$

where N_+ and N_- represent the number of moments respectively parallel and antiparallel to the field; the sum of N_+ and N_- equals Avogadro's number, N_A. The values of N_+ and N_- are related through the Boltzmann relation, $N_-/N_+ = e^{-\Delta/k_B T}$. Simple algebra then reveals that $N_+ = N_A/(1 + e^{-\Delta/k_B T})$ and $N_- = N_A e^{-\Delta/k_B T}/(1 + e^{-\Delta/k_B T})$. As the temperature decreases

[†]It is a good exercise in the use of SI units to prove that the Bohr magneton does have units of A m^2.

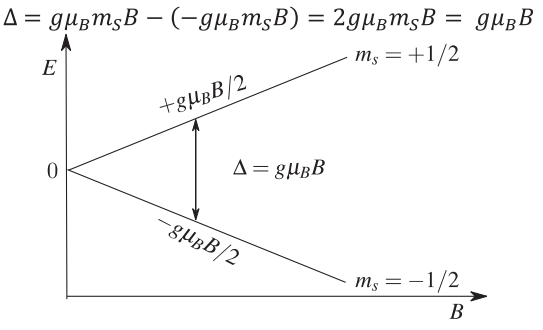

Figure 2. Energy level diagram of an $S = 1/2$ moment in a magnetic field B.

to zero, the exponential terms rapidly vanish, and N_+ and N_- reach their limiting values of N_A and zero, respectively, and the molar magnetization reaches its saturation value, M_{sat}.

$$M_{sat} = N_A g \mu_B S \tag{24}$$

Using the values for the fundamental constants (Appendix A), the saturation moment per mole for $S = 1/2$ in both unit systems can be calculated as follows:

$$M_{sat}(cgs) = 5.585 \left(\frac{g}{2}\right) \times 10^3 \,\text{emu mol}^{-1}$$

$$M_{sat}(SI) = 5.585 \left(\frac{g}{2}\right) \text{A m}^2 \,\text{mol}^{-1} \tag{25}$$

The full equation for the field and temperature dependence of the molar magnetization is quickly obtained using the formulae for N_+ and N_- in equation (23), resulting in equation (26).

$$\begin{aligned} M_{mol} &= \mu_e \left(N_A \frac{1 - e^{-\frac{\Delta}{k_B T}}}{1 + e^{-\frac{\Delta}{k_B T}}} \right) \times \left(\frac{e^{\frac{\Delta}{2k_B T}}}{e^{\frac{\Delta}{2k_B T}}} \right) = N_A \mu_e \left(\frac{e^{\frac{\Delta}{2k_B T}} - e^{-\frac{\Delta}{2k_B T}}}{e^{\frac{\Delta}{2k_B T}} + e^{-\frac{\Delta}{2k_B T}}} \right) \\ &= N_A g \mu_B m_s \tanh\left(\frac{\Delta}{2k_B T}\right) = M_{sat} \tanh\left(\frac{g\mu_B B}{2k_B T}\right) \end{aligned} \tag{26}$$

where tanh represents the hyperbolic tangent.

Notice that the argument of the hyperbolic tangent in equation (26) is simply the ratio of the Zeeman energy of an $S = 1/2$ moment in field B to the thermal energy at temperature T. The magnetization is determined by the energetic competition between the aligning nature of the magnetic field and the randomness of thermal energy. When the ratio B/T is sufficiently large, the magnetization approaches saturation at its upper limit M_{sat}. As B/T ratio decreases, so does the magnetization, ultimately going to zero in the limit of zero field or extreme temperature. The full dependence of the hyperbolic tangent upon its argument is shown in figure 3. It is seen that tanh(x) is zero at the origin, equals its argument within one percent up to $x = 0.15$, and rapidly reaches its saturation value of one: tanh(1) = 0.761, tanh(2) = 0.964, and tanh(3) = 0.995.

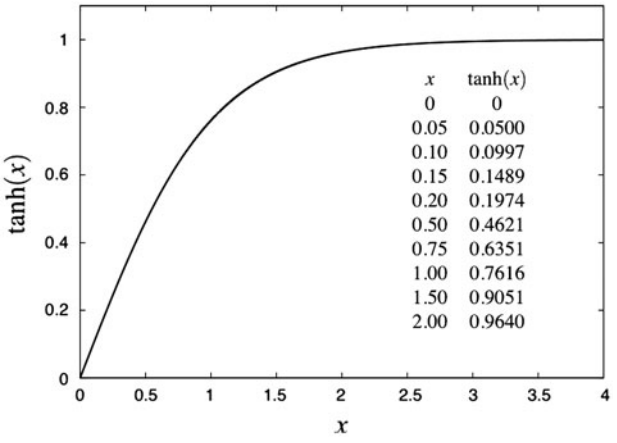

Figure 3. Dependence of the hyperbolic tangent function, tanh(x), upon its argument x.

The magnetic susceptibility is defined as the *limiting* low-field value of the ratio of magnetization to the applied field [equation (6)]. Measurements of the susceptibility must be done in fields for which the M/H ratio is linear. For a mole of non-interacting $S = 1/2$ moments, the argument of the tanh(x) function ($g\mu_B B/2k_B T$) must be less than 0.15. The ratio μ_B/k_B equals 0.6717 TK^{-1} so the linear range is obtained so long as the B-field is less than 0.22 T (2.2 kG) for every degree of temperature (assuming $g = 2.00$). For example, if the lowest temperature is 4.2 K, fields up to 9 kG (0.9 T) can be used to determine the susceptibility of paramagnetic samples. This fact is useful when deciding on an experimental field for a study of the temperature dependence of susceptibility, provided interactions are negligible.

The final expression for the magnetization (in cgs units) for a mole of $S = 1/2$ moments is

$$M(B,T) = M_{sat} \tanh\left(6.717 \times 10^{-5} \left(\frac{g}{2}\right)\frac{B(G)}{T(K)}\right) \tag{27}$$

where the magnetic field is expressed in units of Gauss. For example, in a 5 T (50,000 Oe) field at 1.8 K, the argument in equation (26) equals 1.87(g/2). For a copper(II) sample with $\langle g \rangle = 2.10$, the argument equals 1.96, enough to reach 95% of the saturation field. This is a useful expression for comparing experimental molar magnetization data collected as a function of field at constant temperature. M, B, and T are all measured variables and g is the only free parameter. If the experimental data can fit to this expression with a reasonable value for g (2.10 ± 0.05), that means that no significant exchange interactions are present. The existence of ferromagnetic interactions would cause the magnetization to increase faster with applied field than the hyperbolic tangent function, while antiferromagnetic interactions would cause the magnetization to increase at a slower rate.

2.2.2. The case when $S > 1/2$. The calculation above for the magnetization of independent moments was carried out for the limiting case of $S = 1/2$ with only two discrete energy levels in an applied field. For larger values of the spin, $2S + 1$ levels arise from Zeeman splitting and the calculation of the magnetization becomes more complex. As demonstrated in the standard reference books [1, 4], the molar magnetization of a collection of non-interacting spins can be written in the form

$$M_{mol}(B,T) = M_{sat}B_s\left(\frac{g\mu_B SB}{k_B T}\right), \text{ where} \tag{28}$$

$$B_s\left(\frac{g\mu_B SB}{k_B T}\right) \equiv \left(\frac{2S+1}{2S}\right)\coth\left(\frac{(2S+1)}{2S}\frac{g\mu_B SB}{k_B T}\right) - \frac{1}{2S}\coth\left(\frac{1}{2S}\frac{g\mu_B SB}{k_B T}\right) \tag{29}$$

$B_S(x)$ is known as the Brillouin function and coth stands for the hyperbolic cotangent. In the limit of $S = 1/2$, the Brillouin function reduces to the hyperbolic tangent. In figure 4, the relative magnetization curves (M_{mol}/M_{sat} *versus* B/T) for $S = 1/2$, 1, 3/2, 2, and 5/2, are shown on the same plot for B/T values from zero up to 40 kG/Kelvin. Notice that the smaller the spin value, the easier the system is to magnetize.

In the classical limit ($S \to \infty$), the projection of the moment along the field can vary continuously so the Zeeman energy varies continuously. The summation over all possible levels then becomes an integral rather than a discrete sum. In this limit, the magnetization is given by the expression

$$M_{mol}(B,T) = M_{sat}L(\frac{g\mu_B B}{k_B T}), \tag{30}$$

where $L(x)$ is the Langevin function: $L(x) \equiv \coth(x) - x^{-1}$.

2.3. *Magnetic susceptibility of a mole of independent spins: Curie's law*

The magnetic susceptibility for a mole of paramagnetic $S = 1/2$ moments can be immediately calculated from the definition of the molar susceptibility, equation (7b), and the low-field limit of the molar magnetization, equation (26), recalling that the saturation magnetization $M_{sat} = N_A g\mu_B S$. For small arguments, the hyperbolic tangent equals its argument and the susceptibility has the following form:

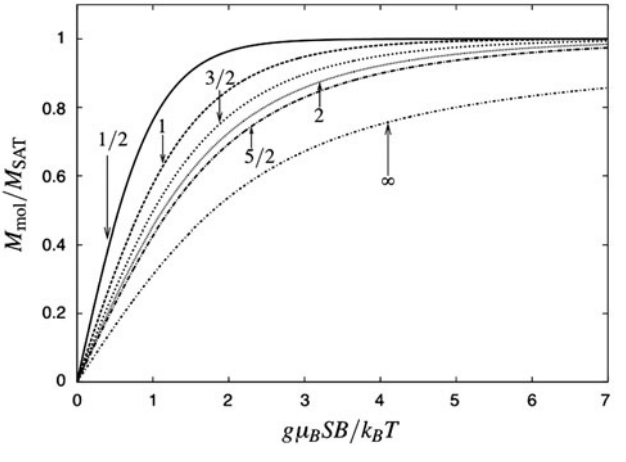

Figure 4. The B/T dependence of the Brillouin function for spin values 1/2, 1, 3/2, 2, and 5/2. The lowest curve shows the dependence of the Langevin function, appropriate for classical spin ($S = \infty$).

$$\chi_{mol}\left(S=\frac{1}{2}\right)=\lim_{H\to 0}\frac{M_{mol}}{H}=M_{sat}\left(\frac{g\mu_B SB}{k_BT}\frac{1}{H}\right)=\frac{N_A(g\mu_B)^2S^2}{k_BT}\frac{B}{H}=\frac{N_A(g\mu_B)^2}{4k_BT}\frac{B}{H} \tag{31}$$

For other values of the spin, the Brillouin function must be used and the S^2 appearing in equation (31) is replaced by $S(S+1)$.

$$\chi_{mol}(S)=\lim_{H\to 0}\frac{M_{mol}}{H}=M_{sat}\left(\frac{g\mu_B SB}{k_BT}\frac{1}{H}\right)=\frac{N_A(g\mu_B)^2S(S+1)}{3k_BT}\frac{B}{H} \tag{32}$$

This equation contains three experimental parameters (B, H, and T) and a series of constants. The ratio of constants is known as the Curie constant C and the resulting expression for the susceptibility of a mole of spin S moments follows:

$$\chi_{mol}(S)=\lim_{H\to 0}\frac{M_{mol}}{H}=\frac{C}{T}\frac{B}{H},\ \text{where}\quad C=\frac{N_A(g\mu_B)^2S(S+1)}{3k_B} \tag{33}$$

Equation (33) is known as Curie's Law, but it is not yet in final form. It surprisingly contains the B/H ratio that is defined as the magnetic permeability[†], equation (12). The final forms of Curie's Law in the two unit systems depend on the two different expressions for the permeability.

For the cgs-emu system, the permeability is dimensionless (strictly speaking, G Oe^{-1}) and has the form $\mu(cgs)=1+4\pi\chi_{vol}$. If $4\pi\chi_{vol}\ll 1$, the permeability can be replaced by unity and the familiar textbook form of Curie's Law is recovered. (This approximation is frequently the case for antiferromagnetic systems. Discussion of the correct form of the susceptibility when the approximation is *not* valid appears in the following section.)

$$\text{Curies's law}\,(cgs-emu):\ \chi_{mol}=\frac{C}{T}(1+4\pi\chi_{vol})\approx\frac{C}{T} \tag{34}$$

In the SI system, the permeability is found from equation (1): $B/H=\mu_0(1+M/H)=\mu_0(1+\chi_{vol})$. This ratio is *not* dimensionless but has the dimensions of μ_0 (T m A^{-1}). In the limit of $\chi_{vol}\ll 1$, the SI permeability reduces to μ_0 and the SI version of Curie's Law is found.

$$\text{Curies's law}\,(SI):\ \chi_{mol}=\mu_0(1+\chi_{vol})\frac{C}{T}\approx\mu_0\frac{C}{T} \tag{35}$$

2.3.1. Curie constants. The units of molar susceptibility in the two unit systems were derived in Section 1 and found to be $cm^3\,mol^{-1}$ and $m^3\,mol^{-1}$ for the cgs and SI systems, respectively. The expression for the Curie constant of spin S is given as equation (33). The units of C arise from those of Avogadro's number (mol^{-1}), the Bohr magneton (erg G^{-1} or J T^{-1}), and Boltzmann's constant (erg K^{-1}, or J K^{-1}). Using the values of these fundamental constants listed in Appendix A leads to the following expressions for the respective Curie Constants.

[†]The symbol for the permeability is unfortunately the same as that of magnetic moment. To avoid confusion, the B/H ratio will be used in this section.

$$C(cgs) = 0.12505\, g^2 S(S+1)\frac{erg \cdot K}{G^2 \cdot mol} = 0.500\left(\frac{g}{2}\right)^2 S(S+1)\frac{emu \cdot K}{G \cdot mol}. \tag{36}$$

In determining the final set of units above, the equality $1\,\text{erg}\,\text{G}^{-1} = 1\,\text{emu}$ was used. Curie's Law requires that the units of M_{mol}/H (emu $\text{G}^{-1}\,\text{mol}^{-1}$) must equal those of the molar susceptibility, $\text{cm}^3\,\text{mol}^{-1}$ [equation (14a)] so an additional step is required.

$$\chi_{mol}\left(\frac{cm^3}{mol}\right) = \frac{C}{T}\left(\frac{emu}{G\,mol}\right)\cdot\frac{B}{H}\left(\frac{G}{Oe}\right) = \frac{C}{T}\frac{B}{H}\left(\frac{emu}{\left(\frac{emu}{cm^3}\right)mol} = \frac{cm^3}{mol}\right), \tag{37}$$

where the equality from Section 1.2 (one Oe = one emu cm^{-3}) was used. Notice that the units of the B/H ratio were required to recover the correct susceptibility units.

Repeating the calculation for the Curie constant in SI units leads to the following expression:

$$C(SI) = 1.2505\, g^2\, S(S+1)\left(\frac{J^2K}{T^2 mol}\right) = 5.002\left(\frac{g}{2}\right)^2 S(S+1)\frac{A\,m^2K}{T\,mol} \tag{38}$$

The numerical factor is 10 times that of $C_S(cgs)$ but the units of $C_S(SI)$ divided by temperature are not equal to those of the SI susceptibility, $\text{m}^3\,\text{mol}^{-1}$. This discrepancy occurs because $C_S(SI)$ must be multiplied by μ_0 (T m A^{-1}) to equal $\chi_{mol}(SI)$. The product $\mu_0 C_S(SI)$ does have the units of the SI molar susceptibility.

$$\mu_0 C(SI) = 5.002\,\mu_0\left(\frac{g}{2}\right)^2 S(S+1)\frac{m^3K}{mol} \tag{39}$$

Permeabilities vary with the size of the applied field and need to be determined experimentally. For this reason, many scientists new to magnetism in SI units are surprised to find an *experimental* ratio (B/H) in the *theoretical* expression for the Curie constant. However, the definition of the magnetic susceptibility assumes the *limiting* case of a vanishing H-field so it is always possible to use the limiting value of μ_0 for the permeability. This justification is explained at greater length in the following section.

2.4. *Demagnetization corrections to experimental susceptibilities*

The fundamental definition of the susceptibility, equation (6), depends on the value of the H-field applied to each individual moment; in this section, this value is designated as the *internal* field, H_{int}. For an unmagnetized sample, the external field H_{ext} (created by a solenoid or electromagnet) equals the internal field. However, once the sample becomes magnetized, H_{int} is reduced by an amount which depends both on the shape of the sample and its magnetization,

$$H_{\text{int}} = H_{\text{ext}} - NM_{\text{vol}}, \tag{40}$$

where N is known as the *demagnetizing factor*. (In SI units N varies between 0 and 1, while the range is between 0 and 4π for cgs units.) The *true* susceptibility depends on the value of H_{int} but the *measured* susceptibility is based on the value of the external H-field, H_{ext}.

$$\chi_{vol}(true) = \lim_{H\to 0}\left[\frac{M_{vol}}{H_{int}} = \frac{M_{vol}}{H_{ext} - NM_{vol}} = \frac{M_{vol}/H_{ext}}{1 - NM_{mol}/H_{ext}}\right] = \frac{\chi_{vol}(meas)}{1 - N\chi_{vol}(meas)}, \quad (41)$$

where $\chi_{vol}(meas) = M_{vol}/H_{ext}$. As the product $N\chi_{vol}(meas)$ becomes insignificant compared to one, the measured susceptibility approaches the true susceptibility.

The corresponding equation for the molar susceptibility follows from the equality $\chi_{vol} = \chi_{mol}\rho/FW$:

$$\chi_{mol}(true) = \frac{\chi_{mol}(meas)}{1 - \frac{N\rho}{FW}\chi_{mol}(meas)} \quad (42)$$

When studying antiferromagnets, it is rarely necessary to use equation (42) instead of the fundamental definition of M_{mol}/H. As an illustration of this point, consider the magnetic susceptibility of copper pyrazine *bis*nitrite, figure 5. This monoclinic compound [15] (C2/m) consists of chains of pyrazine-bridge copper(II) ions along the *b*-axis, with oxygen atoms from the nitrite ions completing the square planar coordination. Adjacent chains are well separated, creating a *magnetically* 1-D compound. The density of $CuPz(NO_2)_2$ is 2.13 g cm^{-3} with the formula weight of 235.7 g mol^{-1}. As seen in figure 5, the maximum susceptibility [16] of 0.032 cm^3 mol^{-1} occurs near 4.6 K. The sample was polycrystalline and enclosed in a gelatin capsule, so we use the demagnetizing factor of a sphere in cgs units, $4\pi/3$. Using these values, the maximum value of $\frac{N\rho}{FW}\chi_{mol} = 0.0013$, which is insignificant compared to 1 in the denominator of equation (41) so the demagnetization effects can be ignored.

There are certain conditions that require demagnetization corrections. Materials that order with spontaneous moments (ferromagnets, ferrimagnets) have extremely large susceptibilities near their critical temperatures and demagnetization corrections are essential. In addition, paramagnetic high-spin molecules have been found with spin values as large as 83/2 [17]. Since the Curie constant is proportional to $S(S+1)$, the measured susceptibility

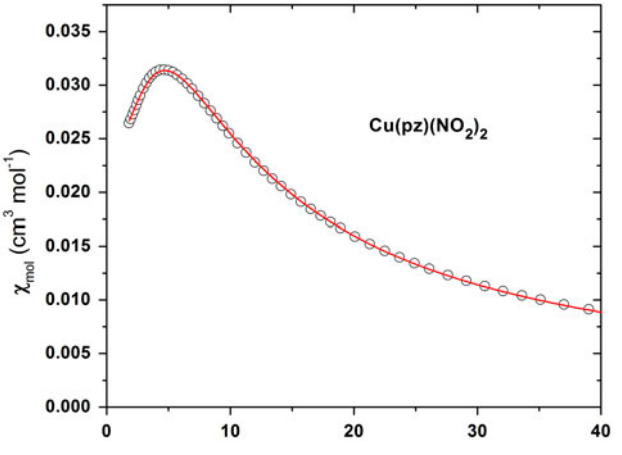

Figure 5. The temperature dependence of the magnetic susceptibility of copper pyrazine *bis*nitrite in cgs-emu units. The solid line corresponds to the prediction for the magnetic susceptibility of a 1-D Heisenberg $S = 1/2$ antiferromagnet with an exchange strength of 7.3 K, a Curie constant (CC) of 0.408 cm^3 K mol^{-1}, with zero correction due to paramagnetic impurities. Unpublished results.

becomes very large for these compounds, also requiring corrections. A third case involves measurements of paramagnets at *very* low temperatures. Thirty years ago, a temperature of 5 K was considered low by magnetochemists but now measurements down to 50 mK (0.05 K) are increasingly common. A paramagnetic compound with no need for a demagnetizing correction at 5 K will most likely need one at such low temperatures.

This section concludes with an interesting effect that occurs when studying compounds with spontaneous moments. Inverting equation (41) to solve for $\chi_{vol}(meas)$ in terms of the true susceptibility leads to equation (43):

$$\chi_{vol}(meas) = \frac{\chi_{vol}(true)}{1 - N\chi_{vol}(true)} \approx -\frac{1}{N}, \quad \text{for large } \chi_{vol}(true) \tag{43}$$

As the sample approaches the critical temperature, the true susceptibility $\chi_{vol}(true)$ increases without limit and the *measured* susceptibility approaches a limiting value of $-\mathrm{N}^{-1}$ as $T \rightarrow T_C$. For $T \leq T_C$, the measured response is a constant, with a value depending only on the shape of the crystal.

3. Interactions and anisotropies

Section 2 explored the effects of temperature and a magnetic field on a collection of non-interacting moments that had no preference for their orientation in space. The field-induced magnetization was the same for all orientations of the external field.

Magnetism becomes rich in possible behaviors when the moments interact with each other as well as with the field. When the interactions are 3-D in nature, spontaneous ordered states appear at temperatures proportional to the exchange strength. The nature of the resulting ordered state depends strongly on single-ion and exchange anisotropies present in the compound. These topics are explored in the present section.

3.1. *The molecular field and the Curie–Weiss law*

In the previous section, the magnetization of a collection of independent magnetic moments in an applied field was calculated as a function of temperature, leading to Curie's Law. The magnetic behavior resulted from competition between the Zeeman energy, minimized as the moments align with the field, and the thermal energy that induces fluctuations away from the energy minimum. (Mathematically, this competition appears as the argument of the Brillouin function.) Lowering the temperature reduces the size of the thermal fluctuations, resulting in an increased magnetization.

What if the spins are not independent but interacting? The ability of an external field to orient a specific moment against thermal fluctuations now also depends on the orientations of the moment's neighbors. However, their orientations depend on the value of the field, the temperature, and the orientations of *their* neighbors! This is a classic *many-body* problem in which we cannot derive an expression for the magnetization until we already know the orientation of all the moments. Many-body problems frequently display interesting complex behavior but are difficult to analyze.

The first successful solution of a magnetic many-body problem was obtained by Pierre Weiss in 1907 [18]. He considered a collection of N interacting moments and made the

simplest possible approximation[†] to describe the interaction. He assumed the field acting on a moment equaled the sum of two terms; the external field B itself, plus a "field" proportional to the magnetization of the sample. He called this new field the "molecular field" because it arose from the other molecules in the sample. The total field B_{tot} was then given as

$$B_{tot} = B + \lambda M, \tag{44}$$

where λ is the proportionality constant between the magnetization and the molecular field. The B_{tot} field was then used in the derivation of Curie's Law [equation (19)] and once again results in the hyperbolic tangent (for $S = 1/2$) but with the external field B replaced by B_{tot} in the argument:

$$M_{mol} = \frac{Ng\mu_B}{2}\tanh\left(\frac{g\mu_B B_{tot}}{2k_B T}\right) = M_{sat}\tanh\left(\frac{g\mu_B(B+\lambda M)}{2k_B T}\right) \tag{45}$$

There is no analytical solution for equation (45) for any temperature or field; we are seeking M_{mol} but its value depends on the hyperbolic tangent of itself. Solutions for the general case can be found graphically and numerically. However, in the high-temperature/low-field limit, this equation can be easily solved. This limit corresponds to the situation when the argument of the hyperbolic tangent is small compared to one. In this case, the value of the hyperbolic tangent is closely approximated by its argument: $\tanh(x) \approx x$, for $x \ll 1$.

$$M_{mol} = M_{sat}\tanh\left(\frac{g\mu_B(B+\lambda M_{mol})}{2k_B T}\right) = \frac{N(g\mu_B)^2}{4k_B T}(B+\lambda M_{mol}) = \frac{C}{T}(B+\lambda M_{mol}) \tag{46}$$

Collecting terms in M_{mol} leads to the following equation:

$$M_{mol}\left(1-\frac{\lambda C}{T}\right) = \frac{C}{T}B \Rightarrow M_{mol}\left(\frac{T-\lambda C}{T}\right) = \frac{C}{T}B \Rightarrow M_{mol} = \frac{C}{T-\lambda C}B \tag{47}$$

The final form of equation 47 shows that, in the limit of small B/T, M remains proportional to the field so the susceptibility can once again be defined. In the following equations, we replace the product λC by θ which we define as the Curie–Weiss temperature: $\theta \equiv \lambda C$.

$$\chi \equiv \lim_{H\to 0}\frac{M_{mol}}{H} = \lim_{H\to 0}\frac{C}{T-\theta}\frac{B}{H} \tag{48}$$

The ratio B/H appears in equation (48) just as it did for the derivation of Curie's Law in the previous section. Depending on the system of magnetic units being employed, the final forms appear as:

$$\text{Curie}-\text{Weiss law (cgs-emu)}: \ \chi_{mol} = \frac{C}{T-\theta}(1+4\pi\chi_{vol}) \cong \frac{C}{T-\theta} \tag{49a}$$

[†]Weiss's success proves that there is nothing wrong with making an assumption, even if it is clearly unreasonable. Having a solution to the problem can provide important insights even if the solution is quantitatively invalid.

$$\text{Curie}-\text{Weiss law (SI)}: \chi_{mol} = \mu_0(1+\chi_{vol})\frac{C}{T-\theta} \cong \mu_0 \frac{C}{T-\theta} \tag{49b}$$

The form of the susceptibility in equation (49) is known as the Curie–Weiss Law. It shows that an interaction between moments modifies Curie's Law by subtracting the Weiss temperature θ from the sample temperature T. If the interaction is positive (meaning the moments prefer to align parallel), λ is positive and the Weiss temperature is positive. As a result, at any temperature, the susceptibility in the presence of the interaction is greater than it would be in the absence of an interaction. A positive interaction is called a ferromagnetic one, as found in ferromagnets such as the elements iron, cobalt, nickel, and gadolinium.

It may seem curious that a stronger field, the *molecular field*, shows up as a reduced temperature in the susceptibility equation, but it is a natural consequence of Boltzmann's relationship. The magnetization is related to the argument of the hyperbolic tangent in equation (45) where the argument is $g\mu_B(B+\lambda M_{tot})/(2k_BT)$. Increasing the numerator has the same effect as decreasing the denominator; either action increases the argument. It follows that a negative interaction (an antiferromagnetic one), in which the moments tend to lie in opposite directions, has the effect of reducing the effective field; that in turn is equivalent to raising the temperature of the sample.

$$\chi_{mol} = \frac{C}{T-\theta} = \frac{C}{T-10K}, \text{ ferromagnetic interactions}, \theta = +10\text{K}$$

$$\chi_{mol} = \frac{C}{T-\theta} = \frac{C}{T+10K}, \text{ antiferromagnetic interactions}, \theta = -10\text{K} \tag{50}$$

In practice, the Curie–Weiss formula is able to reveal the existence of interactions, even when they are weak compared to the lowest measured temperature. Consider the behavior of the *inverse susceptibility,* $1/\chi$ [equation (51)]. It is proportional to $(T-\theta)$, with a slope equal to the reciprocal of the Curie constant and a temperature intercept equal to the Curie–Weiss constant. At temperatures high compared to $|\theta|$, χ^{-1} will increase linearly with temperature but with a non-zero intercept. (The plot of χ^{-1} *versus* temperature is known as a Curie–Weiss plot.) The intercept with the temperature axis provides information about both the sign and the magnitude of the dominant interaction.

$$\frac{1}{\chi_{mol}} = \frac{T-\theta}{C} = \frac{1}{C}(T-\theta) \tag{51}$$

The inverse susceptibilities for several low-dimensional magnetic models are plotted in figure 6, along with straight lines representing the high-temperature limiting behavior for the models. It is clear that at low temperatures, there are significant differences between the high-temperature limits and the low-temperature behavior. As will be shown in the following section, the inverse susceptibility for the $S = 1/2$ Heisenberg dimer agrees within 1% of its high-temperature limit only for temperatures exceeding 50 J/k_B. As observed in figure 6, the temperature intercept for the dimer is $\theta_{\text{dimer}} = -|J|/4k_B$, so the high-temperature limit is only found for $T > 200\ \theta_{\text{dimer}}$! For this reason, most experimental reports of Curie–Weiss parameters for dimers in the literature are inaccurate because the data have not been collected to high-enough temperatures.

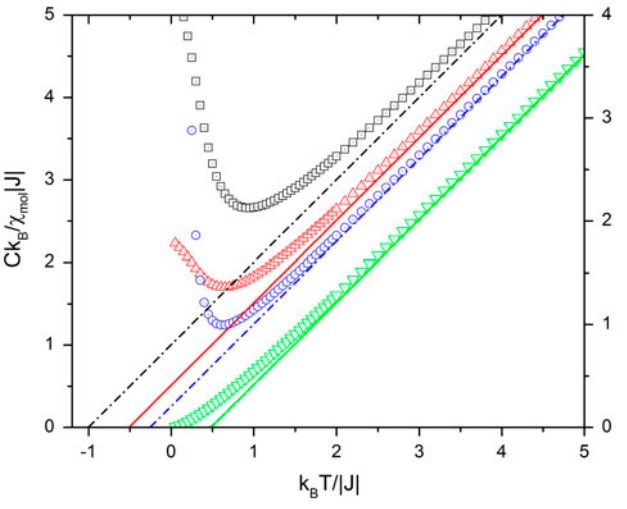

Figure 6. The inverse susceptibilities (in dimensionless units) are plotted as a function of relative temperature $k_BT/|J|$, where $|J|$ is magnetic interaction strength. The open symbols correspond to the calculated values for the 2-D $S = 1/2$ antiferromagnetic layer (□), the 1-D antiferromagnetic chain (Δ), the antiferromagnetic dimer (o), and the ferromagnetic chain (∇). The solid lines are the corresponding Curie–Weiss lines that represent the high-temperature behavior of these susceptibilities.

Molecular field theory [19] provides a formula for the Curie–Weiss constant in terms of the number of nearest neighbors z, the spin value S and the nearest-neighbor exchange strength J (single J format).

$$\theta(S) = \frac{zS(S+1)J}{3k_B}; \quad \theta\left(\frac{1}{2}\right) = \frac{zJ}{4k_B} \tag{52}$$

with J positive/negative for ferro/antiferromagnetic interactions. The Curie–Weiss intercepts in figure 6 are in agreement with this formula for the square lattice and chains have four and two nearest neighbors, respectively, yielding θ-values of $-J/k_B$ and $-J/2k_B$ and $+J/2k_B$ for the antiferromagnetic layer and the antiferromagnetic and ferromagnetic chains, respectively.

In our own research, we plot data in three standard formats: χ_{mol} *versus* T; χ_{mol}^{-1} *versus* T; and $\chi_{mol}T$ *versus* T. We find the third option (the "χT" plot) to be the most versatile in that it is the most sensitive to the presence of interactions. It also has the advantage that at high temperatures the $\chi_{mol}T$ product will numerically approach the value of the Curie constant. It is the only format in which the value of C is obvious. To illustrate these points, the susceptibility of the linear chain antiferromagnetic compound $Cu(pzdo)Cl_2(H_2O)_2$ (pzdo = pyrazine dioxide) is plotted in both the Curie–Weiss and χT formats [20] in figure 7. This compound has weak antiferromagnetic interactions, corresponding to $\theta = -6.3$ K and leading to a maximum in susceptibility at 7 K. However, although the Curie–Weiss parameter is small, the χT product very clearly shows a significant decrease from the room-temperature value by 150 K.

It is necessary to warn about *inappropriate* applications of the Curie–Weiss plot. There have been so many of these that Van Vleck, a pioneer in magnetism who shared the 1974

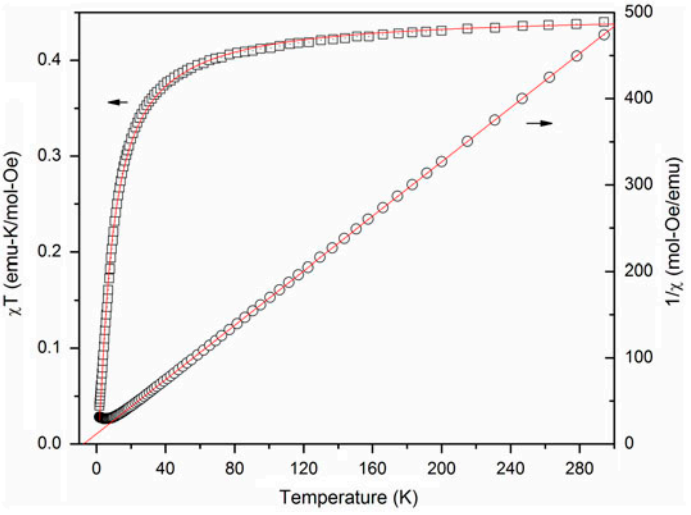

Figure 7. Magnetic susceptibility of $Cu(pzdo)Cl_2(H_2O)_2$ plotted both as $\chi_{mol}T$ *vs.* T and $1/\chi_{mol}$ *vs.* T.

Nobel prize in Physics, once wrote an article [21] entitled "The Curie–Weiss Law; the most overused equation in magnetism".

- Curie's law and the Curie–Weiss law are derived by assuming that the arguments of the hyperbolic tangent (and more generally, the Brillouin function) were very small, i.e. at the limit of *low fields/high temperatures*. These laws are *not* valid when the argument is greater than 0.15.

  In practice, it is not easy to say at what temperature the equation becomes valid but a good guide is that the temperature should be *many multiples* of the magnitude of the Curie–Weiss temperature; how many multiples depends on the dimensionality of the magnetic lattice, the number of nearest neighbors (NN), and the spin value. The Heisenberg dimer is an extreme case for each $S = 1/2$ moment has only one NN, but comparison of the susceptibilities of 1-D and 2-D $S = 1/2$ models to the Curie-Weiss expression shows that multiples of 80 θ and 40 θ are required to assess the θ-value to within 1%. In contrast, 3-D models are much better approximated by equation (51), with multiples of 3 θ being sufficient.
- The Curie Law and Curie–Weiss law are only valid for *temperature-independent* moments, such as Mn(II) and Cu(II). Ions with unquenched orbital angular momentum have internal energy levels corresponding to different m_l values and the populations of these levels change with temperature. Consequently, the size of the ion's moment changes with temperature and the Curie–Weiss law does *not* apply.
- The Curie–Weiss temperature θ (also known as the Weiss constant or Curie–Weiss constant) is sometimes, incorrectly, referred to as a *magnetic ordering temperature* at which the paramagnetic moments mutually align into a state of long-range order. The origin of this concept appears in figure 6. The Curie–Weiss constant for the ferromagnetic chain has a positive value of $0.5\,k_BT/|J|$, implying the formation of a spontaneous moment at finite temperature even in zero field. 3-D magnetic lattices do

order at temperatures comparable to θ, but as will be discussed in Section 4, 1-D lattices *never* do. The existence of a finite θ does *not* imply the existence of ordering.

3.2. *Exchange interactions: the S* = 1/2 Heisenberg Dimer

Magnetism exists because the orientation of a moment affects the orientations of other moments. Fundamentally, this interaction is an electrostatic one at the atomic level, where the rules of quantum mechanics apply. The electrostatic energy of two overlapping electronic wave functions is reduced if they have opposing moments, thus favoring antiferromagnetic alignments. If the two wave functions are orthogonal to each other, their moments align in a parallel fashion. Evaluating the electrostatic energy involves the exchange terms in the symmetric or antisymmetric wave functions, so this interaction energy is often called the *exchange* energy. The literature on exchange interactions is broad and deep and will not be summarized in this tutorial. References to many of the standard sources are provided in the first seven references.

The most common interaction is the Heisenberg interaction, for which the energy depends only on the *mutual orientation* between interacting spins, with the energy of interaction equal to the prefactor J times the spin's dot product. There is no contribution to the energy that would favor a preferential orientation along a specific axis. For this reason, the Heisenberg interaction is isotropic.

$$H = -JS_i \cdot S_j = -J \sum [S_i^x S_j^x + S_i^y S_j^y + S_i^z S_j^z] \tag{52a}$$

$$H = -2JS_i \,.\, S_j \tag{52b}$$

Equation (52a) has been written in the single-J format with a negative sign. The dot product is maximized by parallel spins; for a positive J, parallel spins have the lowest energy so a positive-J corresponds to a ferromagnetic interaction, with negative-J corresponding to the antiferromagnetic case.

For such a simple equation, a great deal of confusion appears in the literature because equation (52a) is not universally used. Until 30 years ago, the two-J format [equation (52b)] was the most common form in both the physics and chemistry literature. Physicists then began to employ the single-J form, which eliminated the need to carry around the factor of two.

It gets worse, for another variation of the Hamiltonian is common. When studying an explicitly *antiferromagnetic* system, via either theory or experiment, the need to use negative values for the exchange strength can be eliminated using the positive form of the Hamiltonian, equation (53). Using that format, a positive interaction corresponds to a ground state with antiparallel moments. As you would expect, both the single J and $2J$ forms are found. Currently, four common forms of the Heisenberg interaction are in use, those appearing in equations (52) and (53). If the authors of an article did not explicitly state the form they used, readers will be unsure of the magnitude of the exchange strength of the material,[†] to within a factor of two, as well as uncertain of the sign. To avoid confusion, it is necessary for every scientific article to display the Hamiltonian employed to facilitate comparison of results.

[†]Use of both thermal units (K) and spectroscopic units (cm^{-1}) also confuses the literature.

$$H = JS_i \cdot S_j \tag{53a}$$

$$H = 2JS_i \cdot S_j \tag{53b}$$

In the following discussion, we will use the positive, single-J form of the Hamiltonian [equation (53a)] because most of the examples to be presented will be antiferromagnetic.

We illustrate the use of the Heisenberg interaction by analyzing the simplest interacting system, the $S = 1/2$ Heisenberg dimer.[†] Two spins, S_1 and S_2, interact according to the Hamiltonian 53a. The spins can couple to form an $S_{tot} = 0$ singlet state and an $S_{tot} = 1$ triplet state, where S_{tot} is the total spin for the system. The energies of the states depend on their mutual orientation.

$$S_1 \cdot S_2 = \frac{1}{2}\left[S_{tot} \cdot S_{tot} - S_1 \cdot S_1 - S_2 \cdot S_2\right] = \frac{1}{2}\left[S_{tot}(S_{tot}+1) - \frac{3}{4} - \frac{3}{4}\right] \tag{54}$$

The respective energies for the singlet and triplet states are $-3J/4$ and $J/4$, respectively. The energy of the singlet state can be defined to be zero, placing the triplet state an energy J higher (figure 8).

It is a simple calculation to show that the susceptibility for a mole of dimers is given as

$$\chi_{mol\ dimers} = \frac{2N_A(g\mu_B)^2}{3k_BT}\frac{3exp(-J/k_BT)}{3+exp(-J/k_BT)} = \frac{C(S=1)}{T}\frac{3exp(-J/k_BT)}{3+exp(-J/k_BT)} \tag{55a}$$

The susceptibility of a mole of moments immediately follows by dividing that of the mole of dimers by two and using the relationship: $C(S=1) = 8C(S=1/2)/3$.

$$\chi_{mol\ moments} = \frac{4C(S=1/2)}{3T}\frac{3exp(-J/k_BT)}{3+exp(-J/k_BT)} \tag{55b}$$

The antiferromagnetic dimer has a rounded susceptibility (χ_{max} occurs at $T_{max} = 0.624\,J/k_B$) that descends to zero exponentially at low temperatures [figure (9a)]. In contrast, the susceptibility of the ferromagnetic dimer increases without limit at low temperatures.

More insight into the ferromagnetic behavior is provided by the $\chi_{mol}T$ product [figure (9b)]. As the temperature approaches zero, $\chi_{mol}T$ for the ferromagnetic dimer increases by one-third over its high-temperature value, approaching the $S = 1$ Curie constant, as all the dimers drop into the triplet ground state at low temperatures. For higher temperatures ($T > 4J/k_B$), the product drops to 0.75 $C(S=1)$, as all four energy levels are occupied equally. A rise in $\chi_{mol}T$ upon cooling is a signature of ferromagnetic interactions.

While the susceptibility (magnetic response as function of temperature at constant field) is calculated from the occupation fraction of the energy levels in the limit of zero field, the magnetization (induced moment as a function of field at constant temperature) is calculated from changing the occupation fractions of the energy levels as the field is varied. As seen above, the susceptibility is a function of the zero-field energy gap Δ between the singlet ground state and the triplet excited state; for the dimer, $\Delta = J$. For the magnetization, the

[†]It is important to recognize the distinction between a mole of *moments* and a mole of *dimers*. This leads to an additional factor-of-two confusion.

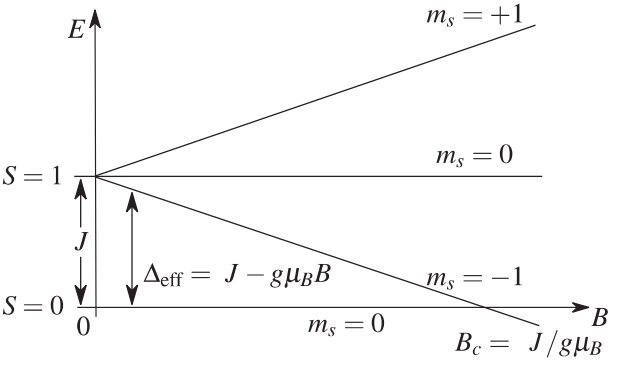

Figure 8. Energy level diagram for an antiferromagnetic Heisenberg $S = 1/2$ dimer in an applied field. Note that it is possible even in zero-field for the $S = 1$ state to be split into doublet ($m_s = \pm 1$) and singlet ($m_s = 0$) states. See Section 3.5.

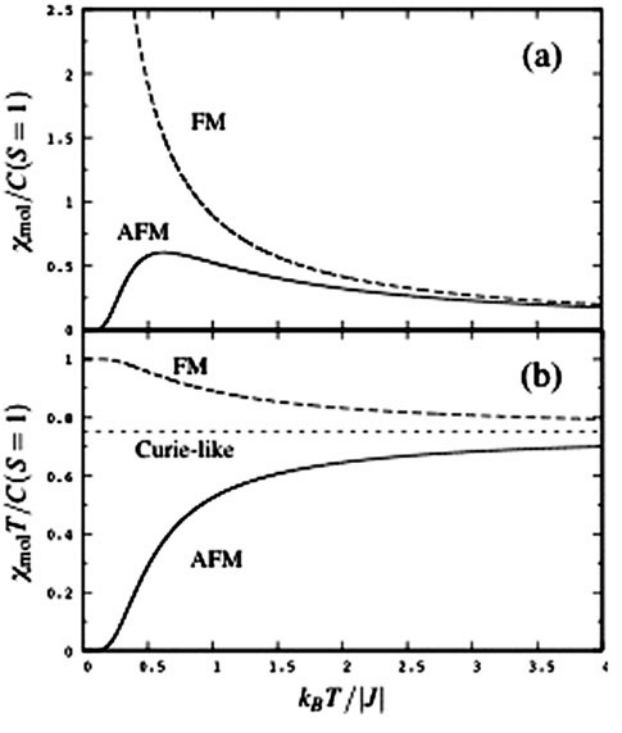

Figure 9. (a) The normalized molar susceptibilities (χ_{mol}/C(S = 1)) of the ferro-and antiferro-magnetic Heisenberg $S = 1/2$ dimer are plotted as a function of relative temperature $k_BT/|J|$. (b) The normalized $\chi_{mol}T$ products are plotted against the same temperature scale.

$m_S = \pm 1$ energy levels vary as a field is applied (figure 8); so, the occupation fractions of the levels vary with both temperature and field, leading to the following expression [equation (56)] for the magnetization of the $S = 1/2$ Heisenberg antiferromagnetic dimer.

$$M(B,T) = \frac{Ng\mu_B \sinh(g\mu_B B/k_B T)}{exp(-g\mu_B B/k_B T) + 2\cosh(g\mu_B B/k_B T) + 1} \tag{56}$$

The magnetization in figure 10 represents the balance of three different energies: the exchange energy J, the field energy $g\mu_B B$, and the thermal energy $k_B T$. The exchange strength determines the size of the zero-field energy gap, the field energy controls the size of the effective gap $\Delta_{\text{eff}} = J - g\mu_B B$, and the thermal energy controls the relative occupation of the energy levels.

In the antiferromagnetic dimer, when B and T are relatively small, only the singlet state is occupied and molar magnetization remains very small. With small T and increasing field, the effective gap is reduced by the Zeeman energy, and vanishes at the critical field $B_c = J/g\mu_B$. At B_c, the ground state changes from the singlet to the $m_s = -1$ sublevel, at which point the magnetization rapidly rises to its saturation value. As the temperature is raised, the magnetization process spreads over an increasingly broad range of field. At $T \approx 0.5\, J/k_B$, almost all of the upward curvature in the magnetization has disappeared; all trace of the existence of the critical field has vanished by $T \approx J/k_B$. Figure 10 provides a clear example of why magnetization experiments yield the most information when carried out at the lowest possible temperatures.

3.3. *Paramagnetic susceptibilities of exchange coupled spin networks*

The fundamental experiment for exploring a new magnetic material is a study of the temperature-dependent susceptibility. This data can be compared to the predicted susceptibility of an appropriate model by which one can learn the value of the Curie constant of the compound, the existence or absence of interactions, as well as the sign, magnitude, and nature (Ising, Heisenberg) of the interaction. Given the importance of the susceptibility, we discuss it in detail.

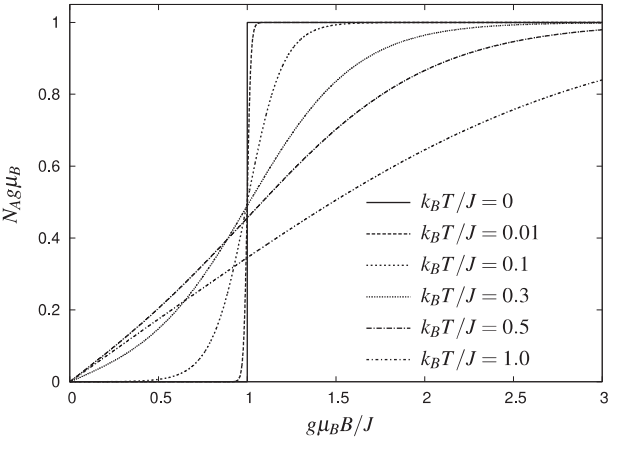

Figure 10. Magnetization of the $S = 1/2$ Heisenberg antiferromagnetic dimer as a function of temperature and field. At $T = 0$, the magnetization jumps discontinuously at the critical field $B_C = J/(g\mu_B)$. The dependence of the magnetization upon field and temperature [equation (56)] is characteristic of many systems with spin-singlet ground states.

Our examples will be taken from extended networks of spins, rather than from finite clusters. The primary reason for this choice is *simplicity*; even though there may be millions of spins in a linear chain compound, all the spins will be the same and there will be only one exchange interaction. The behavior of the susceptibility can be understood simply in terms of the competition between the exchange and Zeeman energies.

Contrast that simplicity with the complex nature of the fundamental molecular magnet [22] known as Mn_{12}. This compound contains two different ions (eight Mn(III) and four Mn(IV)) which have different moments and different single-ion anisotropies which are not co-axial (see the following section). There are at least four different exchange interactions present in this spin cluster and more than 10 million possible eigenstates [23]. Computation of the susceptibility of this compound, possible in principle, is beyond the power of current computers while an intuitive understanding of the role of the various parameters is likewise out-of-reach.

A secondary reason for the emphasis on extended magnetic lattices is the scarcity of good reviews of the advances in this field. In contrast, the high degree of research activity in high-spin molecules[†] for the past two decades has already created a growing number of review articles [24], books [25], and book chapters [26] in this field.

There are additional reasons for choosing examples of extended spin networks. Theoretical modeling of spin systems has advanced rapidly over the past dozen years due to improvements in simulation techniques such as Quantum Monte Carlo, the availability of user-friendly software [27], and the ever-increasing speed and memory of inexpensive computers. As a result, there are now numerical expressions for the susceptibility of a wide variety of low-dimensional (1-D or 2-D) magnetic models with one or more exchange parameters that can be used to characterize ever-more complex compounds. Use of these same techniques has also led to quantitative insight into the influence of an interaction in the third direction upon the transition to long-range order of the low-dimensional magnets [28] (see Section 4).

3.3.1. Paramagnetic susceptibilities of uniform exchange-coupled spin networks.

3.3.1.1. *One-Dimensional* $S = 1/2$ Heisenberg Antiferromagnet (1-D QHAF). The most common source of spin-1/2 ions with isotropic exchange is Cu(II) ions with one unpaired electron. The orbital angular momentum of this electron is mostly quenched by the ligand field so the average g-factor $\langle g \rangle \approx 2.12$–$2.15$ and the moment of the ion has nearly no preference for alignment along a particular crystalline axis.[‡] For this reason, the exchange interaction is essentially isotropic and is defined by the single J Heisenberg Hamiltonian $H = J\Sigma S_i \cdot S_{i+1}$, equation (53a), in which antiferromagnetic interactions have a positive sign.

One-dimensional lattices occur when the Cu(II) ions are joined by bridging ligands along an axis and when the coordination sites not involved in bridging are capped by terminal ligands. Two famous examples of such lattices are μ-pyrazine dinitrocopper(II) [29] and *bis*pyridine dichlorocuprate [30], as shown in figure 11. In the first compound, the copper atoms in $Cu(pz)(NO_3)_2$ are bridged into chains by the neutral 1,4-diazines while the nitrate anions serve as capping ligands about the metal, providing excellent 1-D isolation of the chains. In contrast, the anions in $Cu(py)_2Cl_2$ bridge the metal cation to form the chain. The copper ions have short bonds to two chloride ions (Cu–Cl = 2.298 Å) and the two pyridine

[†]Also known as single-molecule magnets (SMM) and nanomagnets.

[‡]Further details are included in Section 3.5.

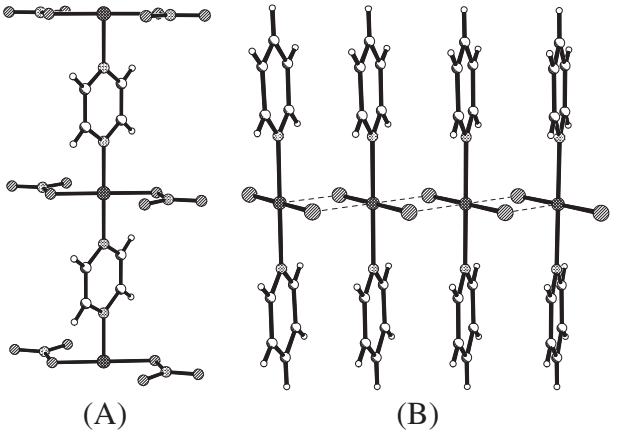

Figure 11. Uniform Cu(II) chains: (A) Cu(pyrazine)$(NO_3)_2$ (pyrazine-bridged Cu(II) ions). (B) Cu(pyridine)$_2Cl_2$ (bihalide-bridged Cu(II) ions).

molecules are coordinated to the coppers by the nitrogen atoms (Cu–N = 2.004 Å). The axial sites of the metal ions involve semi-coordinate bonds (Cu–Cl = 3.026 Å) to the chlorides bonded to the adjacent copper neighbors, forming a structural chain. The steric bulk of the pyridine molecules prevents adjacent chains interacting magnetically with each other, resulting in a 1-D magnetic lattice in a 3-D crystal.

The magnetic susceptibilities of Cu(pz)$(NO_3)_2$ (squares) and Cu(py)$_2Cl_2$ (circles) are presented in figure 12. Both data sets display rounded maxima at low temperatures but remain *finite* at the lowest temperatures. This is in contrast with the susceptibility of the previously discussed dimer (figure 9). Notice that the Cu(pz)$(NO_3)_2$ data set has a larger maximum

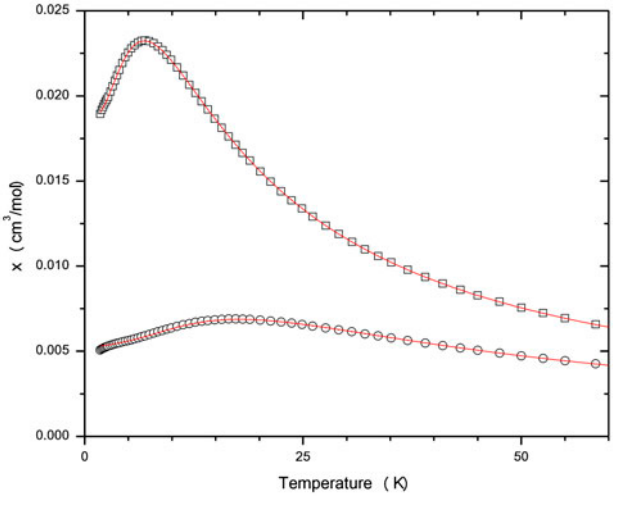

Figure 12. Magnetic susceptibilities of Cu(pz)$(NO_3)_2$ (□) and Cu(py)$_2Cl_2$ (o). The solid lines are the best-fit representations of the 1-D QHAF susceptibility with exchange constants of 10.6 K, and 27.3 K, respectively (single-J format).

susceptibility (χ^{max}) at a lower temperature (T^{max}) than the corresponding χ^{max}, T^{max} of the $Cu(py)_2Cl_2$ data set. Numerical studies [31] of the susceptibility of the 1-D QHAF have shown that this behavior is universal: T^{max} and χ^{max} are respectively, proportional to, and inversely proportional to, the strength of the exchange constant. Consequently, their product is independent of temperature.

$$T^{max} = 0.640851\,\frac{J}{k_B} \tag{57}$$

$$\chi^{max} = 0.146926\,\frac{Ng^2\mu_B^2}{J} \tag{58}$$

For molar susceptibilities with $N = N_A$, the product of $\chi^{max}T^{max}$ in cgs units is given below.

$$\chi^{max}T^{max} = 0.035323\,g^2\,\frac{cm^3K}{mol} \tag{59}$$

Based on analytical and numerical studies of the 1-D QHAF susceptibility [31 and references therein], a useful expression for the temperature dependence of the susceptibility has been obtained [equation (60)] where the coefficients N_i, D_i are given in table 1. Note that this expression is also based on the positive, single J form of the Hamiltonian [equation (53a)] for which a positive number corresponds to antiferromagnetic interactions.

$$\chi_{mol}\,(1D\,QHAF) = \frac{C_{mol}}{T}\left[\frac{1+\sum_{i=1}^{5} N_i\left(\frac{J}{k_BT}\right)^i}{1+\sum_{i=1}^{6} D_i\left(\frac{J}{k_BT}\right)^i}\right] \tag{60}$$

By comparing the experimental data in figure 12 to equation (60) and allowing the values of both J and C to vary, the solid lines in the figure were obtained, corresponding to exchange strengths of 10.6 K and 27.3 K for $Cu(pz)(NO_3)_2$ and $Cu(py)_2Cl_2$, respectively.

Table 1. Coefficients of the susceptibility formula for the 1-D QHAF and the 1-D QH FM [both equation (60)], and the 2-D QHAF [equation (61)].

Parameter	1-D QHAF	1-D QH FM	2-D QHAF
N_1	−0.053837836	1.736278	−0.998586
N_2	0.097401365	1.07588	−1.28534
N_3	0.014467437	0.12081	−0.656313
N_4	0.0013925193		0.235862
N_5	0.00011393434		−0.277527
D_1	0.44616216	1.24008	1.84279
D_2	0.32048245	0.42784	1.14141
D_3	0.13304199	0.00272	0.704192
D_4	0.037184126	−0.00002	−0.189044
D_5	0.00026467628		0.277545

It may seem curious that the susceptibility of the 1-D QHAF remains finite at zero temperature while that of the $S = 1/2$ Heisenberg antiferromagnetic dimer decreases exponentially to zero at low temperatures (figure 9) since each system contains $S = 1/2$ moments and antiferromagnetic interactions. This question was first answered in 1964 in a profoundly influential article by Bonner and Fisher [32]. In both systems, the ground state is a non-magnetic singlet with a triplet as the first excited state, and the singlet–triplet energy gap Δ is *proportional* to J. In this numerical study of finite chains with N-spins, it was found that the singlet–triplet gap Δ approaches a value $\Delta = J/N$ as N becomes large. In the limit $N \rightarrow \infty$, the gap vanishes and the energy spectrum becomes a continuum. At any finite temperature, moment-bearing states are thermally occupied and the material has a field-induced moment.

Surprisingly, the 1-D QHAF has a finite susceptibility even at absolute zero. Although the chain is in the singlet state *in zero-field,* any applied magnetic field is a perturbation to the Hamiltonian which mixes moment-bearing states into the ground state, resulting in a finite susceptibility.

1-D $S = 1/2$ Heisenberg ferromagnets (1-D QHFM) also exist [33] although they are less common than 1-D QHAF. The susceptibility of the 1-D QHFM has been obtained [34] and can be expressed in a similar form as equation (60). The corresponding coefficients for the ferromagnetic chain are also given in table 1. The susceptibilities of ferromagnets diverge at low temperature; for this reason, plots of these susceptibilities are often presented in the χT *versus* T format in which the paramagnetic T^{-1} dependence has been removed. The χT products of the 1-D and 2-D QHFMs are presented as a function of $k_B T/J$ in figure 13; a log–log scale has been used to accommodate the divergence at low temperatures.

3.3.1.2. *Two-Dimensional* $S = 1/2$ Heisenberg Antiferromagnets (2-D QHAF): isotropic and rectangular. Common 2-D lattices can be said to consist of a series of 1-D chains, exchange strength J, that are cross-linked into a 2-D net by a second interaction αJ, $0 \leq \alpha \leq 1$, scheme 1. In the limiting case $\alpha = 0$, the chains are isolated; when $\alpha = 1$, a square (or isotropic) lattice is formed. The intermediate cases of $0 < \alpha < 1$ correspond to rectangular lattices.

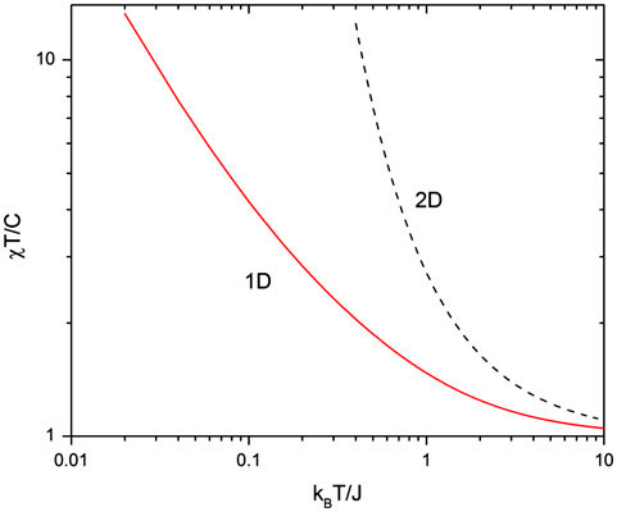

Figure 13. Theoretical predictions for the $\chi T/C$ products of the 1-D and 2-D QH ferromagnets. Notice the log–log scale.

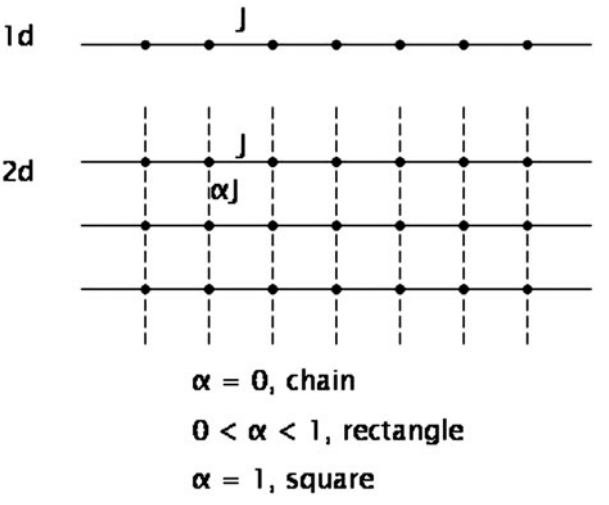

Scheme 1.

Note: in this section, we only discuss 2-D lattices that have an even number of nearest neighbors such as square or rectangular lattices. These are the so-called *bipartite* lattices in which there are no competing interactions and the Néel state of alternating up and down spins is applicable. Triangular, hexagonal, and kagomé lattices have an odd number of nearest neighbors and do not have unique antiferromagnetic ground states. For this reason, they are said to be *frustrated*. Their behavior is quite complex [35] and will be discussed further in Section 4.

Isotropic 2-D QHAF: Interest in the uniform 2-D QHAF model surged after the discovery of the copper-oxide-based high-temperature superconductors [36], such as $La_{2-x}Sr_xCuO_{4+y}$. These compounds contain layers of copper ions joined into a square lattice by bridging O^{2-} ions with an antiferromagnetic interaction estimated to be close to 2000 K. The high superconducting temperatures (in excess of 100 K, depending on the Sr-doping level) have been thought to arise from the antiferromagnetic interaction. To date, however, the explanation for these record superconducting temperatures remains unknown.

Based on many analytical and numerical studies [37] of the 2-D QHAF model, a useful expression [38] for the temperature dependence of the susceptibility has been obtained [equation (61)] which can be used to determine exchange strengths from experimental data. It has a similar, *but not identical*, form to equation (60). The appropriate coefficients for the 2-D case are contained in table 1. This expression is also based on the single-J form of the Hamiltonian, equation (53a).

$$\chi_{mol}\,(2D\,QHAF) = \frac{C_{mol}}{T}\left[1+\frac{\sum_{i=1}^{5} N_i\left(\frac{J}{k_BT}\right)^i}{1+\sum_{i=1}^{5} D_i\left(\frac{J}{k_BT}\right)^i}\right] \tag{61}$$

The dimensionless (reduced) susceptibility $\chi_{mol}J/(k_BC)$ of the 2-D QHAF is plotted as a function of the dimensionless (relative) temperature k_BT/J in figure 14. For comparison purposes, the figure also contains the reduced susceptibilities of other Heisenberg antiferromagnets: the $S = 1/2$ dimer, an alternating chain with $\alpha = 0.50$, the 1-D QHAF, and an isotropic spin ladder for which $J_{rung} = J_{rail}$.

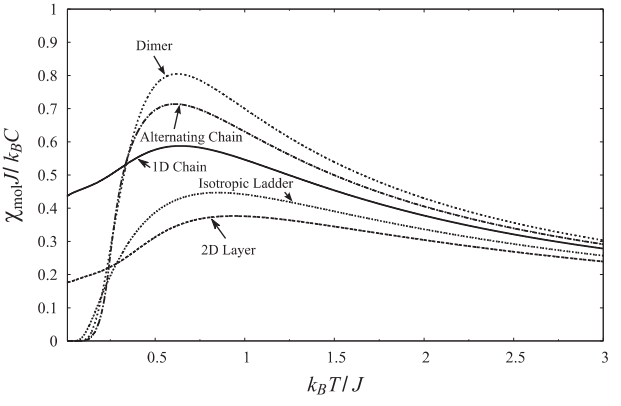

Figure 14. The dimensionless susceptibilities of two uniform lattices (1-D chain and 2-D square) and three dimerized lattices (dimer, alternating chain with $\alpha = 0.5$, and the isotropic spin ladder) are plotted *vs.* the relative temperature.

The 2-D QHAF is similar to the 1-D QHAF in that their energy spectra are continuous, leading to finite values of the susceptibilities at all temperatures. The 1-D and 2-D QHAF have two and four nearest neighbors (NN), respectively, resulting in the 2-D susceptibility having a smaller maximum value that occurs at a higher relative temperature; in addition, it has a smaller value at $T = 0$.

The 2-D QHAF model is based on a square lattice in which each moment has equivalent exchange interactions J to its four nearest neighbors. A good approximation to this 2-D model may be found in a 3-D crystal with a fourfold axis provided the interlayer interactions J' are much smaller than J. However, a true fourfold axis is not required; C-centered lattices also satisfy the requirement that all four NN-intralayer interactions are equivalent.[†] We have used this principle to synthesize a number of quasi-2-D QHAF.

Copper pyrazine perchlorate [39] [$Cu(pz)_2(ClO_4)_2$, figure (15A)] consists of layers of Cu (II) ions coordinated to four bridging pyrazine molecules within the layers while the perchlorate groups are located in the axial sites of the copper ions coordinate sphere in the common 4 + 2 configuration. At room temperature, the space group is *C2/m,* but it converts to *C2/c* below 180 K [40]. Due to the bulk of the perchlorate groups, adjacent layers are shifted by *a*/2, *b*/2, with the perchlorate ions packing into the volume surrounded by the pyrazine molecules. This arrangement leads to a large distance (8.54 Å) between nearest copper sites in adjacent layers and accounts for the small exchange ratio ($J'/J \approx 10^{-3}$) found for this compound [41]. The intralayer exchange through the pyrazine molecules is 17.5 K (single J format) which is the largest found for the family of copper/pyrazine molecules.

Analogous *C*-centered structures can be found in the family of compounds $(AH)_2CuX_4$ in which AH is a substituted pyridinium ion and X = Cl, Br. The steric bulk and hydrogen-bonding capabilities of the organic molecules determine the ultimate structure. Figure 15B illustrates the structure with A = 5-bromo-2-aminopyridine (aka 5BAP) and X = Br [42]. Similar structures [43] are found with 5-chloro-2-aminopyridine and 5-methyl-2-aminopyridine (5CAP and 5MAP, respectively) and with quinoline [44]. The magnetic interactions arise from halide–halide contacts [45]. With the exception of the quinolinium complex, the layers of CuX_4 dianions stack directly on top of one another so the interactions between the layers are considerably larger ($J'/J \approx 0.2$).

[†]We thank Roger D. Willett for this insight.

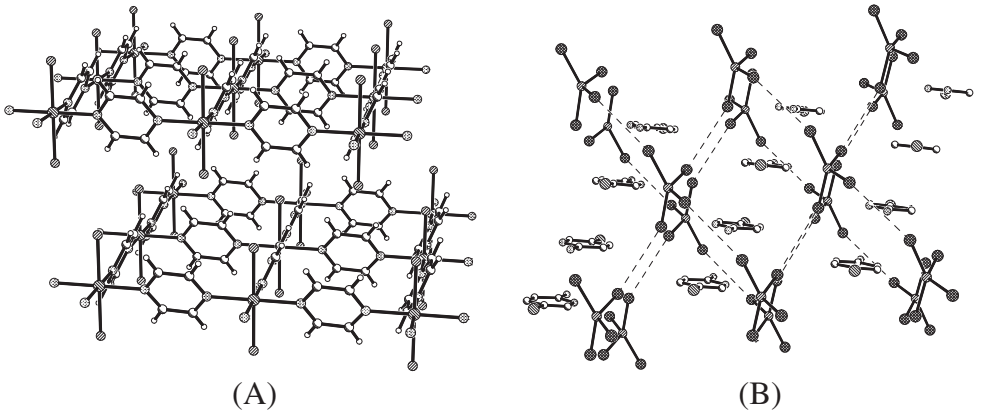

Figure 15. 2-D Cu(II) layers: (A) $Cu(pyrazine)_2(ClO_4)_2$ – The layers lie parallel to the *ab*-plane (two layers shown). Only the semi-coordinate O-atoms from the perchlorate ions, which separate the layers, are shown for clarity. (B) $(2\text{-amino-5-bromopyridinium})_2\ CuBr_4$ –The $CuBr_4^{2-}$ ions form a 2-D square magnetic lattice parallel to the *ab*-plane (two layers shown). The organic cations (H-atoms removed for clarity) lie between the layers and provide some isolation.

The magnetic susceptibilities of $(5BAPH)_2CuBr_4$ and $Cu(pyrazine)_2(ClO_4)_2$ are presented in figure 16 where it is seen that each susceptibility shows a rounded maximum characteristic of a low-dimensional Heisenberg antiferromagnet [figure (14)]. The solid curves represent the best-fit curves to the data using the function of equation (61). The 5BAP compound has the higher maximum at the lower temperature, consistent with weaker interaction ($J/k_B = 6.9$ K); the pyrazine compound has $J/k_B = 17.5$ K. The two compounds have 3-D ordering temperatures $T_N = 5.09$ K and 4.18 K, respectively. In spite of the poor isolation between the layers for the $CuBr_4$ compound, the 2-D susceptibility model describes the data very well, even in the ordered state.

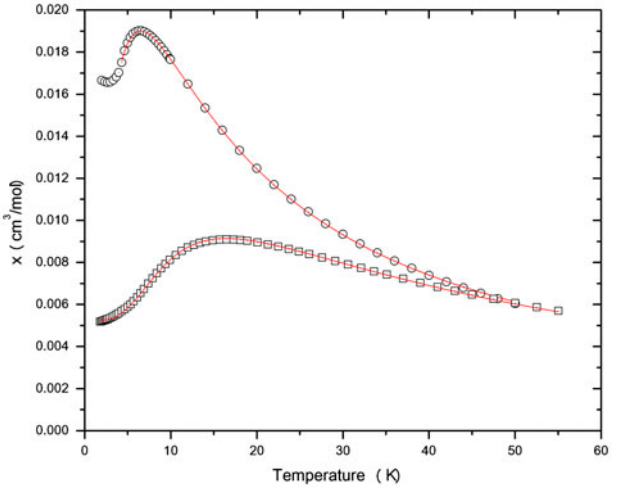

Figure 16. The magnetic susceptibilities of $Cu(pyrazine)_2(ClO_4)_2$ (□) and $(5BAPH)_2CuBr_4$ (O) are shown as well as the curves representing their susceptibilities with exchange constants $J/k_B = 17.5$ and 6.9 K, respectively.

2-D $S = 1/2$ Heisenberg ferromagnets (2-D QHFM) also exist [10], although they are less common and less studied than the 2-D QHAF. The susceptibility of the 2-D QHFM has been obtained [46] and is expressed as a power series of the ratio of the exchange strength to temperature, equation (62). The χT product of the 2-D QHFM is compared to that of the 1-D QHFM in figure 13. There it can be seen that the divergence of the 2-D system is much more rapid than that of the chain system. While the ferromagnetic chain susceptibility diverges as T^{-2}, that of the ferromagnetic layer diverges [47] as $\exp(4\pi JS^2/T)$. The explicit formula for the susceptibility of the 2-D QHFM is presented in Appendix D.

$$\frac{\chi T}{C} = 1 + \sum_{n=1}^{14} \frac{\alpha_n}{2^2 n!} K^n, \quad \text{where } K \equiv \frac{J}{2kT} \ (single - J\ format) \tag{62}$$

Rectangular 2-D QHAF: Rectangular lattices can be formed in a number of ways. A simple example begins with the linear chain compound $Cu(py)_2Cl_2$ [figure (11B)]. When the two capping pyridine molecules are replaced by one bridging pyrazine molecule, a rectangular lattice appears [48] [figure (17)] with magnetic interactions occurring through both the chloride ions and the pyrazine molecules.

Until recently, there was no magnetic model available to model the susceptibility of rectangular magnets with two exchange interactions, J and αJ, where J is the stronger interaction and $0 < \alpha < 1$. If one interaction was considerably stronger than the other, the susceptibility could be approximated as that of a linear chain with a Curie–Weiss parameter that would be proportional to the weaker interaction, equation (63). The approximation becomes valid only in the limit of a weak secondary interaction ($\alpha \rightarrow 0$) and is a poor representation of the susceptibility for $\alpha > 0.1$.

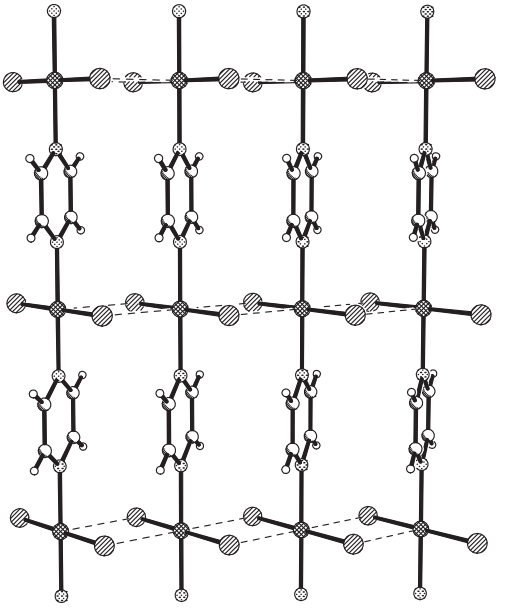

Figure 17. A rectangular magnetic lattice, $Cu(pyrazine)Cl_2$. The Cu(II) ions are bridged by the pyrazine molecules parallel to the *b*-axis and the chloride ions parallel to the *c*-axis.

$$\chi_{rectangle} \approx \chi_{1D}\left(\frac{T}{T-\theta}\right) \tag{63}$$

We have used Quantum Monte Carlo techniques to simulate the magnetic susceptibility of $S = 1/2$ magnetic rectangles [49]. For the most common case of antiferromagnetic interactions along both axes, the simulation results are presented in figure 18. Each set of data points corresponds to the temperature dependence of the rectangular susceptibility of a given value of the parameter α, ranging from $\alpha = 0$ (1-D QHAF) for the highest set of points to $\alpha = 1$ (2-D QHAF) for the lowest set. Each curve contains a rounded maximum $\chi^{max}(\alpha)$ at a temperature $T^{max}(\alpha)$, with χ^{max} decreasing and T^{max} increasing with α.

For the case of two antiferromagnetic interactions, it has been possible to generate a function that can be used to model experimental data. This function has three adjustable parameters: the $S = 1/2$ Curie constant C, the stronger interaction strength J/k_B, and the anisotropy parameter α. Due to the existence of the third parameter, the form of the function is more complex than that presented above for the 1-D QHAF or the isotropic 2-D QHAF [equations (60) or (61)]. The susceptibility is once again expressed as a ratio of polynomials in powers of J/k_BT [equation (64)], but the numerical coefficients N_i and D_i themselves are polynomials as well. For the convenience of the reader, equation (64) has been written out explicitly in Appendix D.

$$\chi_{mol}(\alpha, J) = \frac{C_{mol}}{T}\left[\frac{1 + \sum_{i=1}^{6} N_i\left(\frac{J}{k_BT}\right)^i}{1 + \sum_{i=1}^{6} D_i\left(\frac{J}{k_BT}\right)^i}\right] \tag{64}$$

where $N_i(\alpha) = \sum_{m=1}^{4} N_{i,m}\alpha^m$, and $D_i(\alpha) = \sum_{m=1}^{4} D_{i,m}\alpha^m$.

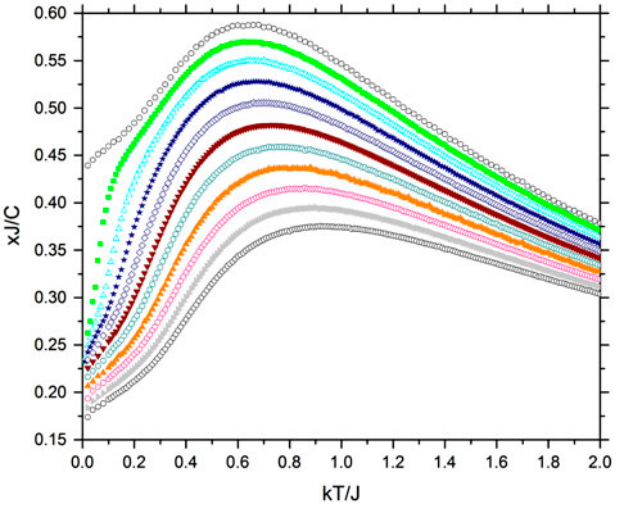

Figure 18. Dimensionless susceptibilities ($\chi J/k_BC$) of antiferromagnetic magnetic rectangles as a function of reduced temperature k_BT/J for different values of α. The top data set corresponds to the 1-D chain ($\alpha = 0$). The lower sets represent rectangular lattices in values α increasing by 0.1 down to the square lattice ($\alpha = 1$). [48]

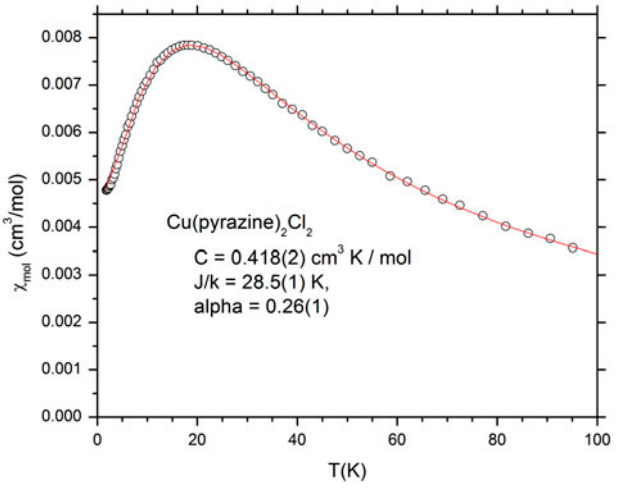

Figure 19. The susceptibility of $Cu(pz)Cl_2$ is presented along with the best fit to the antiferromagnet rectangular susceptibility function, equation (64).

The susceptibility function of equation (64) has been used to model the susceptibility of copper pyrazine dichloride, figure 19. Excellent agreement is found with the data between 2 and 300 K with a larger exchange strength $J/k_B = 28.5(1)$ K and $\alpha J/k_B = 7.6(1)$ K. At this point, it becomes the chemist's job to identify which exchange path within the compound corresponds to which exchange strength. This is a simple task for the case of $Cu(pz)Cl_2$; many bi-chlorobridged copper chains have been previously studied and the antiferromagnetic interaction through the chloride ions is typically in the range 25–28 K, as seen above for $Cu(py)_2Cl_2$, [$J/k_B = 27.3$ K, figure (12)]. In addition, pyrazine-bridged copper(II) compounds typically have exchange strengths between 5 and 12 K; the value of 17.5 K found in $Cu(pz)_2(ClO_4)_2$ is the largest yet discovered. Consequently, for $Cu(pz)Cl_2$, the dominant exchange is through the chloride bridges with the weaker interaction through the pyrazine molecules.

3.3.2. Paramagnetic susceptibilities of dimerized exchange-coupled spin networks. The previous section revealed that antiferromagnets in uniform 1-D or 2-D lattices have smoothly varying susceptibilities that remain finite at zero temperature. Very different behavior is found when antiferromagnetic dimers (exchange J) are present; as seen in Section 3.2, the energy gap above the singlet ground state leads to an exponentially changing susceptibility at low temperatures. Even when dimers are coupled together into an extended lattice by a second interaction αJ, they continue to possess a gapped, singlet ground state and a vanishing susceptibility at low-temperature.

Only 1-D lattices of dimers will be considered in this work. There are many crystalline materials that are good examples of the 1-D models to be described. In addition, sufficient analytical/simulation work has been done to provide expressions for the susceptibilities so exchange strengths can be derived from experimental data. The study of the magnetic behavior of 2-D lattices of dimers has not yet been sufficiently developed.

There are two ways of forming a bipartite lattice of dimers as seen in scheme 2. The first, known as an *alternating chain*, has alternating interactions $\cdots J, \alpha J, J, \alpha J \cdots$, ($\alpha < 1$) with each moment having two nearest neighbors. In the second form, known as a *spin ladder*, each moment has three nearest neighbors, its dimeric partner (interaction J_{rung}) and the two moments on neighboring dimers (interactions J_{rail}). The spin ladder may equivalently be thought of as two identical chains (J_{rail}) coupled together through J_{rung} to form a ladder.

3.3.2.1. *The $S = 1/2$ Heisenberg antiferromagnetic alternating chain*. In the alternating chain, the stronger interaction is defined to be J, so the weaker interaction (αJ) corresponds to a range of the alternation parameter $0 < \alpha < 1$, with the limiting values for α corresponding to the isolated dimer and the uniform chain, respectively. We recall [Section (3.2)] that the isolated dimer has a singlet ground state separated from its triplet state by a zero-field energy gap $\Delta_0 = J$. The ground state of the alternating chain is likewise a singlet but with a gap that also varies with the alternation parameter, $\Delta(\alpha,J)$. The gap decreases as α increases, and becomes zero as α approaches unity. For this reason, the low-temperature susceptibility of the alternating chain also decreases exponentially to zero at low temperatures ($T < \Delta_0(\alpha,J)/k_B$), figure 14.

At higher temperatures, the susceptibility of the alternating chain is less than that of the dimer but greater than that of the uniform chain; for $k_BT/J > 0.5$, the largest susceptibility is that of the dimer (only 1 NN), the second largest is the alternating chain (1.α NN), and the third largest is that of the uniform chain (2 full NN).

A full discussion of the alternating chain susceptibility [30] includes an analytic expression for the susceptibility. The temperature dependence is too complex to express as a simple ratio of polynomials, as is the case for uniform and rectangular 2-D magnetic systems and the uniform 1-D. This complexity is due to a two-parameter energy gap $\Delta(\alpha,J)$. For this reason, the full equation for the susceptibility of a $S = 1/2$ Heisenberg alternating antiferromagnetic chain is presented in Appendix D. (A similar expression for the $S = 1$ Heisenberg Antiferromagnetic chain is also available [50].)

A special case of an alternating chain is known as a Spin-Peierls (SP) chain in which a structural phase transition converts a high-temperature uniform (gapless) antiferromagnetic chain into an alternating (gapped) chain at a critical temperature T_{SP}. These chains are rare because the decrease in magnetic energy by the formation of the gap must outweigh the energy required to distort the lattice. Because the effective gap ($\Delta_{eff}(B) = \Delta_0 - g\mu_B B$) is field dependent, the critical temperature is also a function of the applied field. Detailed analysis of SP chains is challenging, due to the interaction between the magnetic and phonon sys-

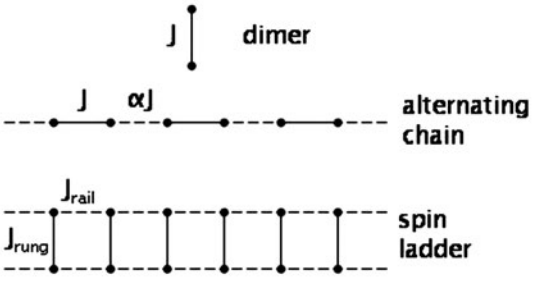

Scheme 2. One-dimensional arrays of dimers.

tems. The best-known Spin-Peierls chain is $CuGeO_3$, first reported [51] in 1993. A recent thorough review is available [52].

An interesting variation of the alternating chain is one in which both the magnitude and the sign of the interactions alternate, • • J_{af} • J_{fm} • J_{af} • J_{fm} • J_{af} • J_{fm} • •. Physical examples of such systems are found in antiferromagnetically coupled chains of ferromagnetic dimers, such as isopropylammonium copper trichloride [53]. A useful expression for the susceptibility [54] of such a chain has been obtained from calculations based on the negative single-J Hamiltonian with a positive J_{fm} and an anisotropy parameter $\alpha \equiv J_{fm}/|J_{af}|$. Expressions for the reduced susceptibility $\chi_r = \chi_{mol}|J_{af}|/C$ are given as ratios of polynomials of powers of $k_BT/|J_{af}|$ in which the coefficients are themselves third-order polynomials of the anisotropy parameter. Different sets of coefficients are used for $0 \le \alpha \le 1$ and $1 \le \alpha \le 8$. For the convenience of the reader, these functions are written out explicitly in Appendix D. In addition, information regarding the design of alternating ferromagnetic and antiferromagnetic exchange Cu(II) chains has been discussed in detail [55].

As seen in figure 20, the susceptibility curves are all dimer-like in that they decrease exponentially at low temperatures. The influence of the ferromagnetic interaction is to raise the value of the susceptibility at all temperatures, with the larger the anisotropy, the larger the susceptibility. The curves in this figure, starting at the smallest, correspond to values of α of 0.1, 0.5, 1.0, 1.5, and 2.0, respectively. If $J_{fm} > |J_{af}|$, the χT product will rise above the Curie constant upon warming, before ultimately decreasing to equal it at still higher temperatures.

3.3.2.2. *The $S = 1/2$ Heisenberg antiferromagnetic spin ladder.* The spin ladder shares many features with the alternating chain. Because they are both constructed from dimers, their magnetic behavior strongly resembles that of the dimer [Section (3.2)]. Each system has a gapped, singlet ground state, a susceptibility that decreases exponentially to zero at low temperatures [figure (14)], and a zero-temperature magnetization that remains zero until the

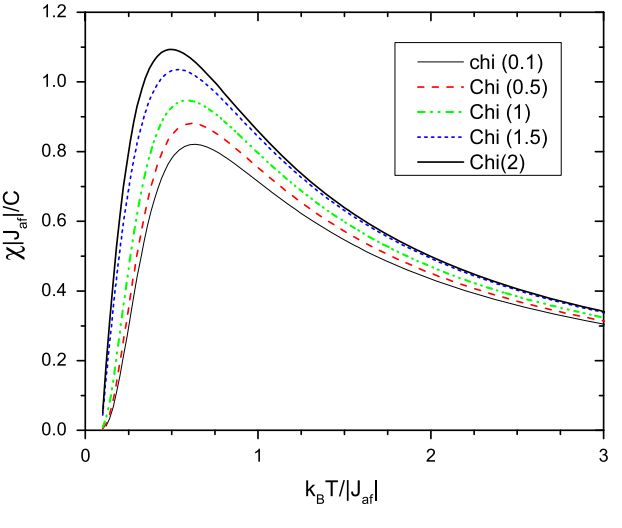

Figure 20. The reduced susceptibility for the ferromagnetic/antiferromagnetic alternating chain is plotted as a function of $k_BT/|J_{af}|$ for different values of the anisotropy factor $\alpha = J_{fm}/|J_{af}|$.

external field closes the gap at a critical field H_C [figure (10)]. In addition, as will be seen in the following section on field-dependent properties, for fields greater than H_C, the magnetization of spin ladders increases from zero until saturation is reached at a second critical field, H_{C2}.

The spin ladder [56] is considerably more complex and interesting than the alternating chain. The reason is that alternating chain only has one independent energy, J, with the second interaction constrained to be αJ, with $0 \le \alpha \le 1$. As α is varied, the chain transforms smoothly from isolated dimers to a uniform chain. In contrast, there are two *independent* energies for the spin ladder, J_{rung} and J_{rail}. Their ratio J_{rung}/J_{rail} can be much greater than one (*strong rung* limit), equal (*isotropic* case), or much less than one (*strong rail* limit). It was anticipated that the gap would vanish as the ratio went to zero (perfectly isolated chains), but surprisingly there always remains [57] an energy gap Δ proportional to J_{rung} no matter how small the J_{rung}/J_{rail} ratio. The characteristics of the excited states are very different in the three cases.

Numerical expressions for the susceptibility of a $S = 1/2$ Heisenberg antiferromagnetic spin ladder are available [58]. As is the case for the alternating chain, the temperature dependence is too complex to express as a simple ratio of polynomials. The full equations (one for strong rung, one for strong rail) for the susceptibility of a $S = 1/2$ Heisenberg alternating antiferromagnetic chain are presented in Appendix D.

Scheme 2 illustrates the two-leg ladder (2LL), but it is possible for additional legs to be added in parallel, while maintaining the same rung and rail interactions. It was originally thought that the 1-D QHAF could be smoothly converted into the 2-D QHAF by considering an N-leg ladder and letting $N \rightarrow \infty$. The discovery of a gap in the 2LL forced a reconsideration, particularly after it was realized that the 3LL does not have a gap in the energy spectrum. The ground state for the three moments on a rung has $S_{tot} = 1/2$, so the ground state of the 3LL is a doublet while that of the 2LL is a singlet ground state. In the general case, $N =$ odd leg ladders have doublet ground states while $N =$ even ladders have singlets.

Among the first known spin ladders [59, 60] were copper oxides with large exchange constants, $SrCu_2O_3$ and $Sr_{14}Cu_{24}O_{41}$. The two copper oxides share a common ladder structure in which copper ions are linked by 180° oxygen bridges along the rungs and rails. $Sr_{14}Cu_{24}O_{41}$ is a more complex structure in which CuO_2 linear chains coexist with the ladders. The magnitude of the energy gaps can be determined experimentally but without knowledge of the J_{rung}/J_{rail} ratio, it was not initially possible to determine an exchange strength from the energy gap. Later experiments [61] showed the J_{rung}/J_{rail} ratio for $Sr_{14}Cu_{24}O_{41}$ to be 0.5, with $J_{rung} \approx 950$ K.

Replacing some of the Sr ions by Ca in $Sr_{14}Cu_{24}O_{41}$ produces mobile holes on the ladders, with about 10% hole concentration appearing in the ladders for the compound $Sr_3Ca_{11}Cu_{24}O_{41}$. Although none of the Sr/Ca compounds become superconducting under ambient pressure, three compounds with different Sr/Ca ratios undergo insulator–superconductor transitions at low temperatures under pressures of several gigapascals [62]. This existence of superconductivity created great interest in spin ladders.

A molecular magnetism approach has created a second generation of spin ladders (table 2) with a wide variety of J_{rung}/J_{rail} ratios, excellent isolation between the ladders, and much smaller exchange strengths. This last feature has permitted investigations of these compounds in magnetic fields up to their saturation fields.

Figure 21 displays the ladder-like skeletons for two molecular-based spin ladders, *bis*-(2,3-dimethylpyridinium) tetrabromocuprate [67] (aka DIMPY) and copper quinoxaline

Table 2. Molecular-based spin ladders with accessible critical fields.

	J_{rung} (K)	J_{rail} (K)	J_{rung}/J_{rail}	Δ (K)	H_{c1} (tesla)	H_{c2} (tesla)	Ref.
Strong rung							
$(5iapH)_2CuBr_4 \cdot 2H_2O$	13	1	13	12	8.3	10.4	[63]
$(pipH)_2CuBr_4$	13.3	3.8	3.5	9.5	7.0	14.4	[64]
$Cu(quinox)Cl_2$	33.2	21.1	1.57	20	14	54	[65]
$Cu(2,3\text{-}dmpz)Cl_2$	29.0	16.0	1.8	22	15	>30	[65]
Isotropic							
$(5napH)_2CuBr_4 \cdot H_2O$	20.4	19.6	1.04	11.3	7.8	47	[66]
$Cu(quinox)Br_2$	35	30.3	1.16	20	14	60	[67]
Strong rail							
$(cpaH)_2CuBr_4$	5.5	11.6	0.45	2.3	1.6	20	[68]
$Cu(2,3\text{-}dmpyH)_2Br_4$	9.0	17.0	0.53	3.6, 4.5	2.5	~35	[69]
$(dmaH)(3,5dmpH)\ CuBr_4$	4.1	7.9	0.52	1.8*	1.2*	13.5*	[70]

*Values are estimated but have not yet been experimentally verified. 5iapH = 5-iodo-2-aminopyridinium; pipH = piperidinium; quinox = quinoxaline; 2,3-dmpz = 2,3-dimethylpyrazine; 5napH = 5-nitro-2-aminopyridinium; cpaH = cyclopentylammonium; 2,3-dmpyH = 2,3-dimethylpyridinium.

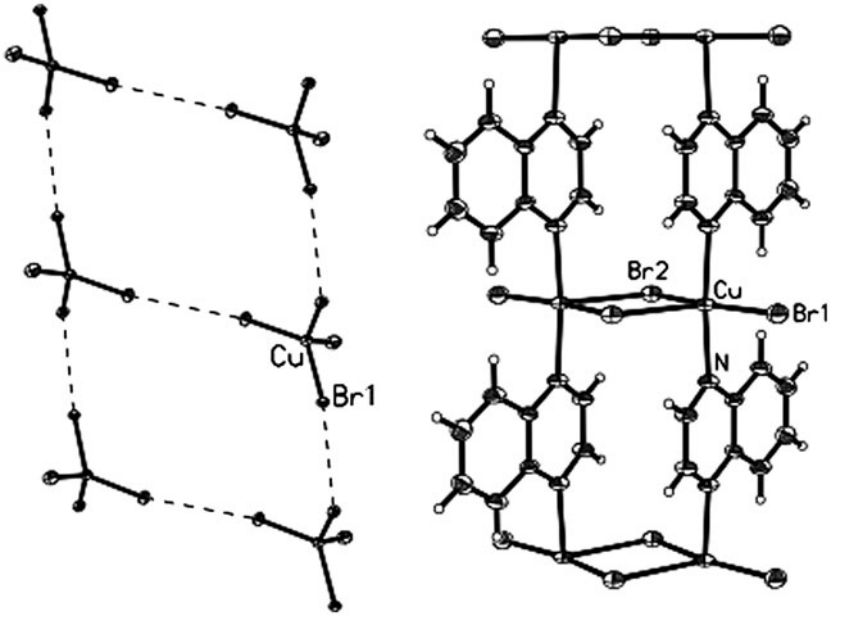

Figure 21. Examples of molecular-based spin ladders. Left: *bis*-(2,3-dimethylpyridinium) tetrabromocuprate (DIMPY). Only the $CuBr_4$ dianions are shown, along with the bromide–bromide close contacts (dashed lines). Right: Copper quinoxaline dibromide, $Cu(quinox)Br_2$.

dibromide [65]. The structure of DIMPY consists of a two-leg ladder of $CuBr_4^{2-}$ radicals with the ladders separated by the organic cations (not shown). The rails of the ladder are formed via unit cell translations of the $CuBr_4$ dianions with a Br···Br separation of 3.905 Å. The rungs are formed by short contacts between inversion-related $CuBr_4^{2-}$ ions with a Br···Br distance of 4.328 Å. Susceptibility studies reveal the characteristic temperature dependence of a singlet-ground state antiferromagnet (figure 14) with a rounded maximum

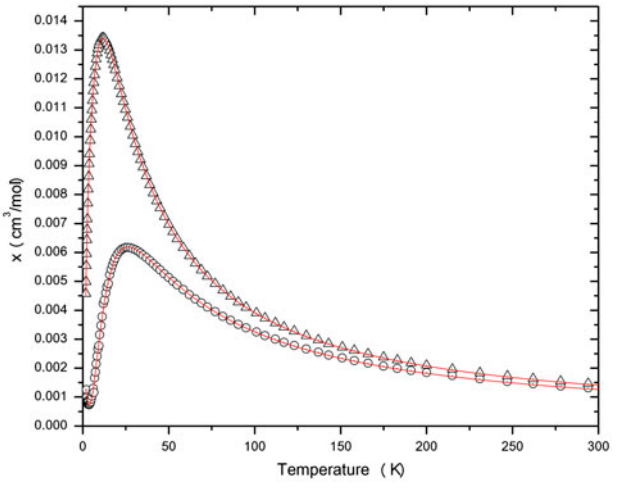

Figure 22. The magnetic susceptibilities of the spin ladders *bis*-(2,3-dimethylpyridinium) tetrabromocuprate (Δ) and copper quinoxaline dibromide (O) are shown as a function of temperature. The solid lines correspond to the fits to the data with the exchange parameters ($J_{rung}/k_B = 8.7$ K, $J_{rail}/k_B = 16.9$ K) and ($J_{rung}/k_B = 35.0$ K, $J_{rail}/k_B = 30.3$ K), respectively.

at 11 K and a rapid decrease towards zero at lower temperature (figure 22). The data were fit to the models of isolated dimers, alternating chains, as well as strong-rail and strong-rung ladders. Equivalently excellent fits were obtained to the model of a strong-rail ladder ($J_{rung}/k_B = 8.7$ K, $J_{rail}/k_B = 16.9$ K, $J_{rung}/J_{rail} = 0.51$) and an alternating chain with different parameters. Given the structure, the data were interpreted in terms of the spin ladder model, an interpretation later confirmed by neutron scattering experiments [71]. DIMPY and $(cpaH)_2CuBr_4$ [66] were the first *strong-rail* spin ladders to be discovered. The best-studied spin ladder is *bis*piperidinium copper tetrabromide [62] (BPCB); it is the first compound to display [72] a form of 1-D behavior (Luttinger liquid) that had been predicted 50 years ago; DIMPY has recently [73] been shown to be the second. Because one of these compounds is *strong rung* while the other is *strong rail*, the natures of their excited states are markedly different.

Copper quinoxaline dibromide is an example of a covalently bonded spin ladder. It consists of neutral Cu_2Br_4 dibromo-bridged dimers (rungs) that are linked to adjacent dimers by bridging quinoxaline molecules (rails). Susceptibility studies showed a rounded maximum near 22 K and a rapid decrease upon further cooling (figure 22). Fitting to the model of a spin ladder yielded parameters for a reasonably isotropic spin ladder: $J_{rung}/k_B = 35.0$ K, $J_{rail}/k_B = 30.3$ K, $J_{rung}/J_{rail} = 1.16$. These values were confirmed by subsequent neutron scattering experiments [67b].

3.4. *Magnetization of exchange coupled spin networks*

Magnetization experiments (isothermal measurement of the moment as a function of applied field) are useful complements to basic susceptibility studies. Through magnetization, information is obtained that can reveal the magnitude and nature of the exchange interactions, the dimensionality of the magnetic lattice, the existence (or absence) of an energy gap, and the presence (or absence) of field-induced phase transitions. Magnetization studies of

single-crystals reveal even more information but examination of polycrystalline materials is still important. Figure 23 displays the low temperature ($k_BT/J = 0.02$) magnetization curves for four Heisenberg $S = 1/2$ antiferromagnets.

The magnetization curves in uniform lattices are straightforward. The 1-D QHAF and 2-D QHAF have a continuous distribution of energy levels so the susceptibilities remain finite at zero temperature. The initial slope of the magnetization curve equals the susceptibility at that temperature but increased fields change the slope until full saturation is achieved. For these lattices, there is only one critical field, the saturation field itself.

Dimerized magnetic systems, such as spin ladders and alternating chains, resemble the dimer; they too have spin-singlet ground states and critical fields H_{C1} at which the magnetization first appears at $T = 0$. However, they contain two exchange strengths (J and αJ for the alternating chain, J_{rung} and J_{rail} for the spin ladder) that lead to the existence of two critical fields, H_{C1}, the gap-closing field, and H_{C2}, the saturation field. The lower critical field marks the closing of the energy gap, at which one of the antiferromagnetic bonds is broken, while the saturation field occurs when the second interaction also is overcome.

It is easy to calculate the relationship between the saturation fields and the exchange strengths in a system. In a mean-field approximation, the Zeeman energy of a moment in the saturation field ($g\mu_B SH_{sat}$) equals the exchange energy of a spin with its neighboring spins (equation (53)), where z represents the number of neighbors. Canceling out a common factor of S, we obtain the following,

$$g\mu_B SH_{sat} = zJ/2 \tag{65}$$

where J has units of Joules (in SI) or ergs (cgs). In practical cases, when the exchange strength is reported in Kevin, the product J/k_B (K) appears in equation (65). A useful expression for the saturation field (in kiloOersteds) follows:

$$H_{sat}(kOe) = \left(\frac{k_B}{\mu_B}\right)\frac{zJ(K)}{2gS} = \frac{14.89}{2gS}\,zJ(K) \tag{66}$$

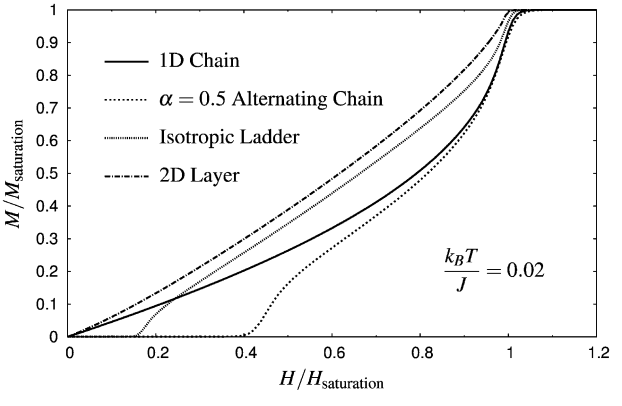

Figure 23. The relative magnetizations (M/M_{sat}) as a function of relative field (H/H_{sat}) for the four low-dimensional, Heisenberg antiferromagnetic $S = 1/2$ lattices. The magnetizations for the uniform 1-D chain and 2-D square lattices are gapless; those for the gapped alternating chain ($\alpha = 0.5$) and isotropic spin ladder have lower critical fields as well as saturation fields.

Table 3. Nearest neighbors and zJ equivalents for several lattices.

Lattice	# nearest neighbors	zJ equivalent
Uniform chain	2	$2J$
Alternating chain	1 + 1	$(1+\alpha)J$
Spin ladder	1 + 2	$J_{rung} + 2J_{rail}$
Uniform layer	4	$4J$
Rectangular layer	2 + 2	$2(1+\alpha)J$

As an example, copper pyrazine dinitrate (figure 11) is a uniform $S = 1/2$ chain with $z = 2$, $g_{ave} \approx 2.14$, and $J = 10.6$ K. Using equation (66), H_{sat} is calculated to be 146 kOe, equivalent to 14.6 T, in excellent agreement with experiment [74]. A uniform 2-D lattice has four nearest neighbors so for a given exchange strength, twice as much field is required to saturate a square lattice as a uniform chain. Copper pyrazine perchlorate [figure (15a)] is a square lattice with $J/k_B = 17.6$ K. The calculated saturation field is 490 kOe, also consistent with the observed value [41].

When lattices contain more than one exchange strength, the equation for the saturation field must be modified (table 3). An alternating chain has two neighbors, one with an exchange strength J and the other with exchange αJ. For this case, the product zJ is replaced by $(1+\alpha)J$. The rectangular lattice has four interactions, two with J and two others with αJ so the product $zJ = 2(1+\alpha)J$. Each moment in a spin ladder has one neighbor in the rung (J_{rung}) and two neighbors in the chain (J_{rail}); consequently the zJ product for the spin ladder is $J_{rung} + 2J_{rail}$.

3.5. *Anisotropies: exchange and single-ion*

Geographers say that every map is a *lie*. In this way, they remind themselves that every map is an *approximation* that excludes information; the map may nevertheless be useful provided the missing information is not relevant to the task at hand. In the same spirit, it is time to acknowledge that the Heisenberg Hamiltonian [equation (53)] is also a lie. It assumes that the moments are free to orient in any direction in space, with the only constraint being that they will be parallel, or antiparallel to, the moments with which they interact. It ignores all other factors that may give a preference for a specific direction in space.

There are two immediate objections to the assumption inherent in the Heisenberg Hamiltonian: dipolar interactions and crystal fields. The inevitable existence of long-range dipolar interactions $(\propto r^{-3})$ necessitates an additional term to the overall Hamiltonian, a term that can lead to a preferred direction as a consequence of minimizing the dipolar energy. A much stronger influence is due to the presence of crystal fields that lead to a set of orbital levels for each magnetic ion; lower symmetry creates fewer degeneracies and a greater number of levels [4, 9, 75]. The presence of unquenched angular momentum in the thermally occupied levels will sometimes lead to the moment preferentially orienting along an axis or within a plane. In these conditions, the Heisenberg Hamiltonian is inappropriate for modeling magnetic behavior.

In spite of these entirely valid objections, the Heisenberg Hamiltonian can be successfully applied to a wide variety of magnetic materials, as seen by all of the compounds discussed previously in this section. Dipolar interactions and crystal field splittings are always present but often only provide weak perturbations.

Ions with half-filled shells (Mn(II) d^5; Gd(III) f^7) and organic radicals make excellent Heisenberg compounds. The absence of any orbital angular momentum ($g = 2.00$) creates

ideal spin-only moments so crystal-field effects are negligible. However, the large moments of these metal ions create relatively large dipolar fields, whose strength is proportional to the square of the moment. If the exchange interactions are small, the influence of dipolar fields may be found at low temperatures.

Cu(II) is very well described as a Heisenberg ion due to the quenching of the orbital angular momentum by the crystal field. In sufficiently high symmetry, $\langle L \rangle = 0$ for this ion but Cu(II) is a Jahn–Teller ion *extrordinaire* and will distort its coordination sphere to minimize its electronic energy. In the presence of an axially distorted coordination sphere, the existence of unquenched angular momentum typically leads to an axial $g_z \approx 2.25$, and transverse $g_x = g_y \approx 2.06$. For this reason, the moment of Cu(II) has different values along different axes. This is a minor perturbation to the Hamiltonian, however. In the paramagnetic state, the normalized susceptibilities (χ_i/g_i^2) have the same temperature dependence. Until reaching the ordered state, Cu(II) is an isotropic ion. In contrast, the normalized susceptibilities depend on temperature differently for non-Heisenberg ions.

Transition metal ions with unquenched angular momentum are anisotropic ions. Such ions include Fe(II), d^6 and Co(II), d^7. The Co(II) ion in a slightly anisotropic tetrahedral symmetry is discussed in [10]. The ground state of the cubic field is an orbital singlet with $S = 3/2$. The axial field splits the $S = 3/2$ and $S = 1/2$ doublet by 10 K of energy, with the $\pm 3/2$ state lower, figure (24a). For low temperatures, compared to 10 K, small fields will not induce any moment transverse to the axis, but will induce large moments parallel to it. At these temperatures, the isotropic Heisenberg Hamiltonian fails completely. For more detailed information regarding magnetic properties related to unquenched angular momentum in high-spin six-coordinate Co(II) complexes, see [76].

$$H = J \sum_{nn} [a(S_i^x S_{i+1}^x + S_i^y S_{i+1}^y) + bS_i^z S_{i+1}^z] \tag{66}$$

Equation (66) displays a more versatile Hamiltonian that can model anisotropic interactions. For the case with the parameters $a = b = 1$, the Heisenberg form is recovered. For the extreme case of purely axial moments, the parameters are $a = 0$, $b = 1$; this form is known as the Ising Hamiltonian.

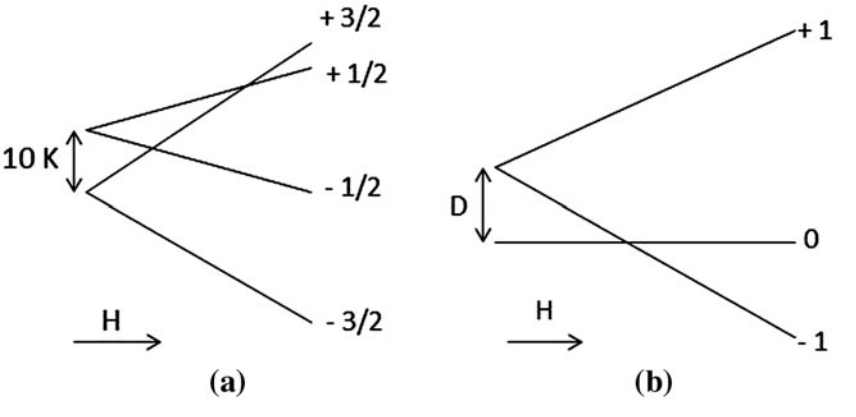

Figure 24. Effects of anisotropy on ground states of transition metal ions. (a) Splitting of the $S = 3/2$ ground state for Co(II) in an axially distorted tetrahedral field. Adapted from Ref. [10]. (b) Splitting of the $S = 1$ ground state of high-spin Ni(II) by single ion anisotropy.

$$H_{Ising} = J \sum_{nn} S_i^z S_{i+1}^z \tag{67}$$

For the remaining extreme case, in which the moments may only lie perpendicular to an axis, the parameters are $a = 1$, $b = 0$, and the model is the XY Hamiltonian, equation (68).

$$H_{XY} = J \sum_{nn} (S_i^x S_{i+1}^x + S_i^y S_{i+1}^y) \tag{68}$$

It is important to note that the appropriate Hamiltonian for a particular ion may change as a function of temperature. Consider the Co(II) ion energy levels in figure (24a). For temperatures well below the 10 K gap between the $S = 3/2$ and $S = 1/2$ doublets, the behavior of the ion is distinctly Ising-like. However, for temperatures high compared to the 10 K gap, both doublets are thermally occupied and the ion behaves as a $S = 3/2$ Heisenberg ion!

Another form of the exchange Hamiltonian is sometimes used, particularly with Ni(II) compounds. Ni(II) has a d^8 configuration and in octahedral crystal fields the t_{2g} sub-orbitals are filled while one electron occupies each of the e_g states, $S = 1$; at high temperatures, it behaves as a $S = 1$ Heisenberg ion. Unquenched orbital angular momentum leads to a small splitting of the $S = 1$ triplet state, with a gap D between the $m_s = \pm 1$ doublet, and the $m_s = 0$ singlet state, figure (24b). This splitting is said to arise from *Single Ion Anisotropy* (SIA) and can be described by a contribution to the Hamiltonian $H_{SIA} = D(S_z)^2$. If $D < 0$, the doublet state is low and Ising-like behavior is found; for $D > 0$, there is preference for the moments to align within an easy plane, but at low temperatures, the moment disappears as the singlet ground state is increasingly occupied. If the Ni(II) ions are exchange coupled, the gap may remain. One such compound is $NiCl_2 \cdot 4SC(NH_2)_2$, to be discussed further in Section 4.

4. Long-range order

As described earlier, magnetism results from the competing tendencies of interactions and anisotropies to align moments, and the randomizing effects of thermal energy. At high-enough temperatures, thermal energy dominates and paramagnetism results. The effect of interactions on the susceptibility is to induce a finite Curie–Weiss parameter, but in the absence of a field, there is no spontaneous moment. However, upon cooling the sample to a sufficiently low temperature, the interactions are able to stabilize a lattice of aligned moments and magnetic long-range order (LRO) occurs. This order need not lead to a spontaneous moment; if the interactions are antiferromagnetic, half of the moments orient in one direction and the other half in the opposite direction so complete cancelation is found in zero field.

Magnetic order is formally defined in terms of the correlation length, ξ. Two spins located n lattice sites apart are correlated if the normalized[†] expectation value of their dot product, $\langle S_i \cdot S_{i+n} \rangle / \langle S_i \cdot S_i \rangle$ is finite. Two moments that share parallel components have a positive expectation value while antiferromagnetically correlated spins have negative values.

[†]By dividing the expectation value for two different spins by the value for any spin with itself, the normalized expectation value ranges between zero and one.

Interacting nearest neighbors ($n = 1$) will have finite expectation values that decrease as the temperature is raised. As the two spins are further separated ($n = 2, 3, \ldots$), the magnitude steadily grows smaller, either as a power law or exponentially. The long-range correlation length ξ is defined as the number of lattice spacings n required to reduce the expectation value to a value of $e^{-1} = 0.37$. In an interacting paramagnetic material, the correlation length is finite and increases upon cooling. Short-range order is found within a correlated cluster but the clusters are not correlated with others far away. *Long-range* magnetic order occurs at the temperature at which the correlation length diverges to include all the moments in the same material.

4.1. *Long-range order in 3-D lattices*

The molecular-field model (Section 3.1) provides a simple illustration of the process by which LRO is achieved. The model assumes that each moment experiences a total field equal to the external field plus a contribution proportional to the magnetization of the sample: $B_{tot} = B + \lambda M$ [equation (44)]. The total field was placed into the expression for the molar magnetization of a paramagnetic assembly of $S = 1/2$ moments [equation (16)] to yield equation (45), repeated below.

$$M_{mol} = \frac{Ng\mu_B}{2} \tanh\left(\frac{g\mu_B(B + \lambda M)}{2k_BT}\right) \tag{45}$$

In Section 3.1, this equation was solved in the limiting case of small field and high temperature, so the hyperbolic tangent is easily approximated as $\tanh(x) \approx x$ the Curie–Weiss approximation for the susceptibility in the presence of interactions was then derived.

We now examine how equation (45) can lead to spontaneous order, even in the absence of an external field. First the field B is set to zero, yielding

$$M_{mol} = \frac{Ng\mu_B}{2} \tanh\left(\frac{g\mu_B\lambda M_{mol}}{2k_BT}\right) = M_{sat} \tanh(x), \tag{69}$$

$$\text{where} \qquad x = \frac{g\mu_B\lambda M_{mol}}{2k_BT} \tag{70}$$

and $M_{sat} = N_A g\mu_B/2$. Equation (70) can be inverted to show the linear dependence of M_{mol} upon the parameter x, equation (71a).

$$M_{mol} = \frac{2k_BT}{\lambda g\mu_B} x, \tag{71a}$$

$$\frac{M_{mol}}{M_{sat}} = \frac{4k_BT}{\lambda N_A (g\mu_B)^2} x = \frac{T}{\lambda C} x \tag{71b}$$

(In equation (71b), the $S = 1/2$ Curie constant has been substituted.) Equations (69) and (71b) are two valid equations relating the dependence of the relative magnetization M_{mol}/M_{sat} as a function of the parameter x [figure (25)]. Their joint solutions are found where the linear term and hyperbolic tangent curves intersect (values indicated by arrows). At low

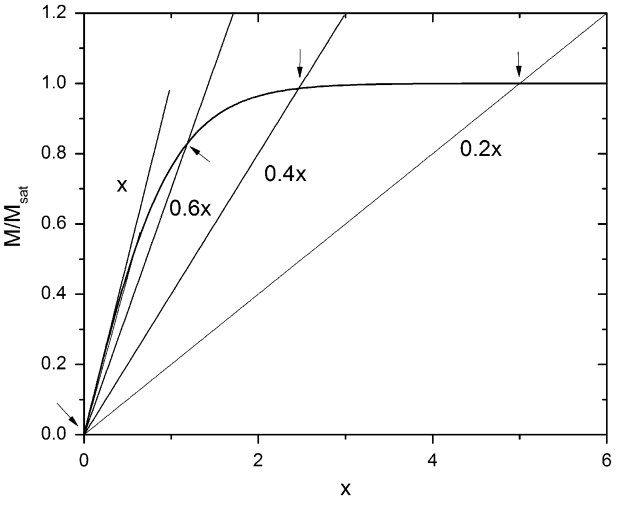

Figure 25. The ratio of $M_{mol}(T)/M_{sat} = \tanh(x)$ is plotted against the parameter x as the curved line, where x is defined in equation (70). In addition, straight lines $y = (T/T_C)x$ are plotted for T/T_C ratios of 1, 0.6, 0.4, and 0.2. The intersections of the straight lines with the $\tanh(x)$ (marked by arrows) mark the ratios $M_{mol}(T)/M_{sat}$ for the corresponding T/T_C ratios.

temperatures, the linear term has a small slope so the intersection occurs at larger values of relative magnetization. As the temperature gets larger, the intersection moves to lower values of x, indicating a lower relative magnetization. The spontaneous magnetization vanishes at the critical temperature T_C at which initial slope of $\tanh(x)$ equals that of equation (71b).

$$\frac{T_C}{\lambda C}x = x \tag{72a}$$

$$T_C = \lambda C \tag{72b}$$

As expected, the critical temperature is proportional to the molecular field parameter λ [equation (72b)]; the stronger the coupling between the moments, the greater the ability of the moments to remain correlated against thermal fluctuations. The resulting curve of the relative magnetization as a function of relative temperature (T/T_C) appears as figure (26), and is qualitatively similar to plots of experimental magnetization *versus* temperature. There are distinct quantitative differences with experimental data, particularly for the rate at which the magnetization vanishes as the temperature approaches the critical point, but the molecular field approximation does offer qualitative insight into magnetic behavior.

An alternate molecular-field model [77] offers further insight into the formation of LRO. In this model, the critical temperature is said to occur at the temperature at which the available thermal energy is comparable to the interaction energy within the 3-D cluster of correlated spins with z nearest neighbors (a is the separation between adjacent moments):

$$k_B T_C/|J| \approx zS(S+1)\left(\frac{\xi(T_C)}{a}\right)^3 \tag{73}$$

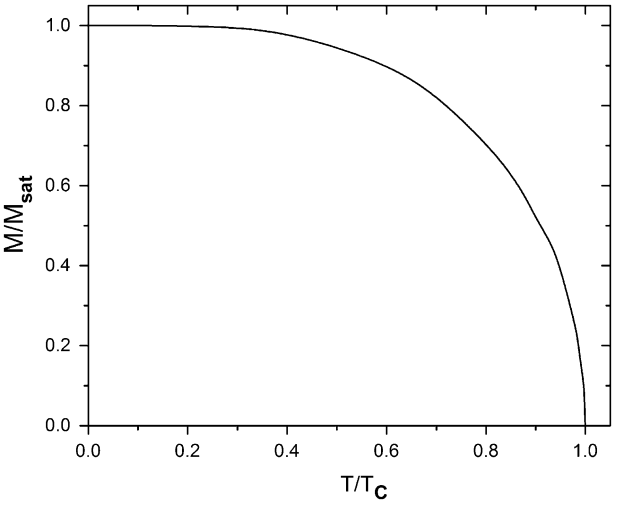

Figure 26. The relative magnetization $M_{mol}(T)/M_{sat}$ is plotted as a function of the relative temperature T/T_C. These values are obtained from the molecular-field approximation for the development of long-range order in a $S = 1/2$ Heisenberg ferromagnet.

The importance of exchange anisotropy in the ordering process is revealed in equation (73). The correlation length for Ising-like systems grows exponentially with temperature ($\xi_I/a \propto \exp(|J|/k_BT)$) in lattices of every dimension due to the confinement of the moment along the preferred axis, while the correlation lengths for XY and Heisenberg systems grow more slowly. In 1-D, the Heisenberg correlation length ξ_H varies inversely with temperature; ξ_{XY} grows more rapidly than ξ_H and less rapidly than ξ_I. Due to the rapid growth of the Ising correlation length upon cooling, the condition for ordering is achieved at relatively high temperatures. Ising systems are the most stable against thermal fluctuations.

4.2. *Long range order in low-dimensional lattices*

Magnetic ordering in *ideal* low-dimensional magnets (1-D and 2-D) cannot be described by equation (73) without modification. As mentioned above, the correlation length of a 1-D $S = 1/2$ Heisenberg magnet diverges as T^{-1}, that of the equivalent *XY* magnet diverges twice as rapidly, and that of an Ising magnet diverges as $\exp(J/k_BT)$. In every case, these correlation lengths diverge as T approaches zero so LRO would seem inevitable. However, the ground state is not determined by a minimum in the energy U but by a minimum in the free energy F:

$$dF = U - TdS$$

At any finite temperature, the free energy can be reduced by increasing the entropy. This increase can be accomplished with the smallest increase of energy by simply reversing the orientations of all spins to the right of the nth spin. There are N possible locations for the break in an N-spin chain so the entropy gain is significant, the broken chain is favored, and the correlation length is rendered finite. At any finite temperature, an ideal 1-D magnet does

not order. (This argument does not apply for higher dimensional lattices. A single reversed spin in a 2-D lattice does not reduce the size of a correlated area because all the spins around the reversed spin retain their original alignment.)

Many *quasi*-1-D magnets have been studied during the past 50 years, as described in Section 3. These are physical realizations of 3-D crystals that contain predominately 1-D-correlations. Inevitably[†], there are interactions J' between magnetic chains that lead to correlations between the chains and induce LRO at some temperature. The molecular field relationship of equation (73) can be modified to reflect the presence of both the intrachain and interchain interactions [78, 79]. The 1-D correlations grow at a rate determined by the dominant exchange strength, J, and the nature of the interactions (H, XY, I). The weaker interaction, J', couples the correlated blocks of moments together until the interaction energy is larger than the available thermal energy. At this temperature, LRO is achieved. The number of spins in a block is proportional to the correlation length for a 1-D system and the square of the correlation length for 2-D materials. This approximation leads to the following result for the dependence of the ordering temperature upon the parameters J and J':

$$k_B T_C/|J| \approx z'|J'|S(S+1)\left(\frac{\xi(T_C)}{a}\right)^n,\ n = 1\ \text{(1-D) or 2 (2-D)} \tag{74}$$

The importance of the exchange anisotropy is illustrated in figure (27), in which the relative correlation lengths of Heisenberg, *XY*, and Ising $S = 1/2$ chains are plotted as a function of the relative temperature k_BT/J. Also plotted is a line proportional to the thermal energy k_BT with a slope equal to $1/\{z'|J'|S(S+1)\}$; the intersection of this line with the respective correlation curves determines the critical temperature for that model system. It is clear that the exponential growth of correlations in the Ising chain leads to LRO at significantly higher temperatures than those with *XY* or Heisenberg interactions.

This molecular-field approximation leads to the following results for the dependence of the ordering temperature of 1-D and 2-D magnets upon the parameters J and J':

$$\begin{aligned} &\textit{Quasi-1D}: k_B T_C/|J| \approx z'S(S+1)\sqrt{J'/J}; \\ &\textit{Quasi-2D}: k_B T_C/|J| \approx z'S(S+1)\ln(J'/J) \end{aligned} \tag{75}$$

This relation for the 1-D magnet is plotted as the dot–dash line in figure 28, a plot of k_BT_C *versus* $|J'/J|$ for 1-D and 2-D Heisenberg antiferromagnets.

More accurate numerical methods are now available for studying the relationship between T_C and $|J'/J|$. A significant advance [28] was made in 2005 using quantum Monte Carlo (QMC) simulations and fast processors. The Néel temperatures of quasi-1-D and -2-D Heisenberg antiferromagnetic lattices were determined as a function of the J'/J ratio and empirical formulas proposed to determine the value of J' from knowledge of J and T_N [80]. The results for the 1-D and 2-D models are also plotted in figure 28. Note that the temperature scale for the quasi-1-D magnets (left axis) covers five orders of magnitude while the analogous scale for the 2-D magnets (right axis) spans less than one decade.

[†]Dipolar interactions are always present, even in the absence of superexchange pathways.

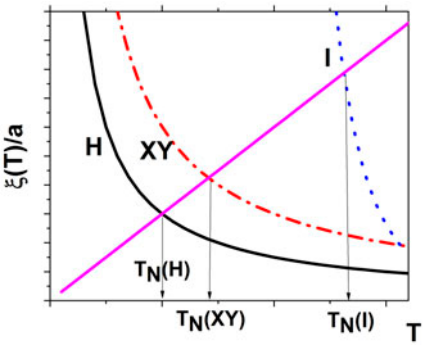

Figure 27. The relative correlation lengths for $S = 1/2$ Heisenberg, *XY*, and Ising antiferromagnetic chains are plotted as a function of temperature. The intercepts with the straight line correspond to the MF values for the respective critical temperatures.

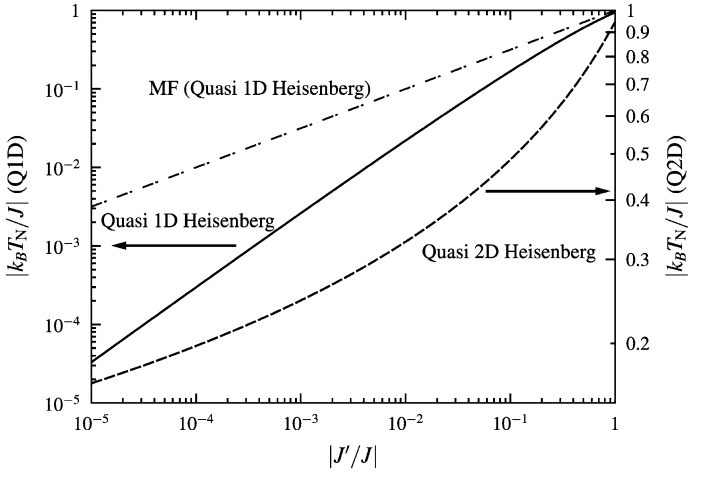

Figure 28. The critical ratios, k_BT_N/J, of the quasi-1-D (solid line) and -2-D (dashed line) $S = 1/2$ Heisenberg antiferromagnets are plotted as a function of the exchange ratios J'/J, where J' is the interchain or interlayer interaction, respectively. The critical temperatures are normalized to the ordering temperature of the 3-D $S = 1/2$ Heisenberg antiferromagnet for which $J' = J$. The dot–dash line corresponds to the mean-field (MF) prediction for the quasi-1-D antiferromagnet according to the formula in equation (76).

These numerical studies have confirmed the qualitative predictions for the molecular field model stated in equation (75). The k_BT_N/J ratio for quasi-1-D and 2-D Heisenberg antiferromagnets do scale with $(J'/J)^{0.5}$ and $\ln(J'/J)$, respectively, although the molecular field models always predict higher critical temperatures than are observed. This is understood in terms of the basic MF approach of assuming an infinite range interaction, as well as ignoring the effect of thermal and quantum fluctuations which inhibit ordering. More recent [81] MF models based on equation (75) that include the effects of interchain interactions are significantly improved and agree qualitatively with the results in figure 28.

$$Quasi\text{-}1D: \frac{k_B T_N}{J} = \left(\frac{J'}{J}\right) \times \left[0.932\sqrt{\ln\left(\frac{2.6J}{k_B T_N}\right) + \frac{1}{2}\ln\ln\left(\frac{2.6J}{k_B T_N}\right)}\right] \tag{76}$$

$$Quasi\text{-}2D: \frac{k_B T_N}{J} = \frac{2.30}{\left[2.43 - \ln\left(\frac{J'}{J}\right)\right]} \tag{77}$$

The numerical results of reference [28] can be expressed as the empirical equations (76) and (77). Note that these are only valid for $S = 1/2$ Heisenberg antiferromagnets but similar results are also found for classical spin systems ($S = \infty$). These equations can readily be inverted to solve for the J'/J ratio in terms of the measured value of $k_B T_N/J$. Direct knowledge of the interchain or interlayer J' is of great interest for testing models of low-dimensional magnetism but is rarely available experimentally. Two cases in which J' can be measured are mentioned. Spin wave dispersion curves of low-dimensional magnets can be determined by inelastic neutron scattering [82]. Analysis of the dispersion for scattering *normal* to the magnetic chain or layer directly reveals the value of J'. The second case involves metamagnets (easy-axis ferromagnetic layers coupled antiferromagnetically by J'); application of a field parallel to the easy axis will align all the moments at a critical field proportional to J'.

A striking feature of figure 28 is the much greater stability of the 2-D antiferromagnets relative to the 1-D. While a J'/J ratio of 10^{-5} reduces the $k_B T_N/J$ ratio of the 1-D magnet by nearly five orders of magnitude, the same exchange ratio only reduces the critical ratio of the 2-D system by a factor of six. This difference is due to the much more rapid growth of the correlations in 2-D. Even for the isotropic Heisenberg interactions, most subject to thermal and quantum fluctuations, the correlation length grows exponentially [47, 83] with decreasing temperature $\xi_H \propto \exp\left(\frac{J}{k_B T}\right)$. Inserting this rapidly diverging correlation length into equation (74), it is seen that the right-hand side of the equation grows so rapidly upon cooling than even a J'/J ratio of 10^{-5} does lead to LRO.

The ideal ($J' = 0$) 2-D QHAF only has LRO at $T = 0$; any thermal fluctuations are sufficient to render it paramagnetic [85a]. In contrast, the XY- and Ising $S = 1/2$ systems order at finite temperatures. The 2-D Ising system was shown to spontaneously order [84] at $k_B T_N = 1.134\,J$ (single-J format). The 2-D XY antiferromagnet forms vortices and antivortices of moments within the XY plane, the diameters of which grow upon cooling. The vortices come into contact at the critical temperature $k_B T_{BKT} = 0.342\,J$ [85] and a unique form of LRO is predicted to appear with a divergent susceptibility but no spontaneous magnetization. This transition is known as the Berezinskii–Kosterlitz–Thouless (BKT) transition after the theorists [86] who first predicted its existence. While multiple quasi-2-D Heisenberg [40] and Ising magnets are known [11], no crystalline compounds have been found in which a BKT transition is definitive [87].

The results of figure 28 were obtained for purely Heisenberg antiferromagnetic 1-D and 2-D lattices (J) in the presence of inter-lattice exchange (J'). In crystalline systems, purely isotropic exchange is rare. Even for transition metal $S = 1/2$ moments, there remains some unquenched orbital angular momentum that induces a preferential orientation in the crystal and leads to anisotropy in the g-factor[†]. It is common to find values of $g_x = g_y = 2.06$ while $g_z = 2.20$. Spin-orbital coupling yields a preference to the moment to orient along the z-axis

[†]In contrast, organic magnetic radicals are pure Heisenberg materials.

Table 4. Dimensionality of spin anisotropy compared with lattice dimensionality.

Spin → ↓ Lattice	3 (Heisenberg)	2 (XY)	1 (Ising)
3-D	Yes	Yes	Yes
2-D	No	BKT	Yes
1-D	No	No	No

and the ion is no longer isotropic. The exchange Hamiltonian is more correctly described by the anisotropic form of equation (78) rather than equation (53a).

$$H = J \sum_{nn} [S_i^x S_j^x + S_i^y S_j^y + (1 - \Delta) S_i^z S_j^z] \tag{78}$$

The anisotropy parameter Δ corresponds to *XY* or Ising anisotropy when Δ is negative or positive, respectively. The anisotropy values determined for Cu^{2+} ions have been found [41] to be small, $|\Delta| \leq 0.01$ Numerical studies [88, 89] show that even such small anisotropies significantly affect the ordering process of purely 2-D, quasi-Heisenberg antiferromagnets. In the absence of any interlayer interactions ($J' = 0$), an Ising-like anisotropy $\Delta = 0.01$ creates an ordering ratio $T_N/J = 0.28$; an equivalent *XY*-anisotropy $\Delta(XY) = -0.01$ leads to a considerably smaller value $T_N/J = 0.22$. Evidently, the Ising anisotropy has an influence 20-fold that of the *XY* type. Referring to the isotropic exchange results in figure 28, these same ordering ratios would be induced by J'/J ratios of 5×10^{-3} and 2×10^{-4}, respectively. Well-isolated magnetic layers are found to have ordering temperatures in the region $0.2 < T_N/J < 0.35$, where both interlayer exchange and exchange anisotropy are relevant. For this reason, detailed understanding of the origin of the LRO in these compounds remains elusive.

A graphical summary of the influence of lattice and exchange anisotropy upon long-range order is presented in table 4. The horizontal axis represents the number of spin degrees of freedom, three for the isotropic Heisenberg model, two for *XY* anisotropy, and one for the Ising case. The vertical axis represents the dimensionality of the magnetic lattice in which correlations can form. The contents of the cells (Yes, No, BKT) refer to the presence (Yes), absence (No), or special case (BKT) of long-range order at $T = 0$. The stability of the ordered state is increased by *increasing* the number of lattice dimensions and *decreasing* the number of spin degrees of freedom.

4.3. *Absence of long-range order*

This review has concentrated on magnetically ordered materials but many magnetic systems never undergo finite temperature transitions to LRO. The explanation in all cases is found in the definition of LRO in terms of the diverging correlation length. Examples include the following:

- finite magnets;
- magnets with singlet-ground states; and
- highly frustrated magnets.

4.4. *Finite magnets*

Magnetic order is lost at a temperature when the available thermal energy becomes comparable to the energies holding the moments into alignment. These energies include both exchange and anisotropy contributions. For traditional ferro- and ferri-magnets (metals and oxides), both types of energy are present and ordering temperatures are high. However, the ordered state does not possess the saturation magnetization; the dipolar fields of one section of the magnet are oriented antiparallel to moments in neighboring sections. The overall energy is minimized by subdividing the sample into domains. If the dominant anisotropy is axial, adjacent domains have moments oriented antiferromagnetically. For some cubic crystals, such as metallic nickel, the easy axes are along the cube diagonals so additional domain orientations are possible.

In zero field and at temperatures well below T_C, the net magnetization of a sample may be zero. Application of an external field along a symmetry axis can saturate the sample once the anisotropy energy is overcome. When reducing the field back to zero, *hard* magnets retain most of their magnetization while *soft* magnets readily break into domains, leaving little, if any bulk magnetization.

The volume of a magnet can be reduced to the size of a domain (typically a micron in dimension) without significantly affecting the critical temperature or the volume magnetization.[†] Further reduction in volume changes the balance of anisotropy energy to thermal energy. Once the sample is below a certain size (≈50 nm), the anisotropy energy (proportional to the volume of the sample) becomes too low to prevent the orientation of sample moment from thermally fluctuating. The magnetization of a collection of randomly oriented particles becomes equivalent to the paramagnetism of a collection of randomly fluctuating atomic moments. The primary difference between the two situations is the size of the moments involved; the atomic moments are on the order of Bohr magnetons while the moment of the particle is $\mu = MV$, where the volume incorporates thousands of individual atomic moments. This condition is known as *superparamagnetism*, first predicted by Néel [90].

Typically, superparamagnets have an axial anisotropy of the type $U = (CV/2)\sin^2\varphi$, where C depends on the magnitude of the anisotropy, V is the volume of the domain, and φ is the angle between the moment and the axis. The energy barrier has a height of $\frac{1}{2}CV$; the moment is stable for $\varphi = 0$ or π unless an external source of energy induces a transition. The energy could be thermal or from an external field. The flipping process occurs more rapidly if the volume is low or if the temperature is high. In the presence of a small external field, one alignment is favored with the fraction of domains in the two energy states determined by the Boltzmann factor.[‡] For this reason, the rate of flipping Γ is proportional to the Boltzmann factor [equation (79)], where the relaxation time τ is the reciprocal of the flipping rate Γ.

$$\Gamma \equiv \frac{1}{\tau} \propto e^{-CV/2k_BT}, \tag{79}$$

The exponential dependence of the flipping rate upon domain volume leads to an extreme variation in relaxation times. As pointed out in [3], under identical conditions the relaxation time for a spherical domain with radius 17 Å is 10^{-1} s while it is 10^8 s for a radius of 22 Å! The ability to understand the relaxation processes in single domain particles was greatly

[†]See sections 7 and 8 in Refs. [3] and [6], respectively.
[‡]This is analogous to the problem of a $S = 1/2$ moment in an external field described in section 2.

limited by the inevitable distribution of domain sizes of metallic or metal oxide samples, or the clusters of iron atoms found in the protein ferritin [91].

The relaxation process of identical domains can be readily studied with ac-susceptibility.[†] An oscillating field of angular frequency ω is applied to the sample. If this frequency is low compared to the relaxation rate ($\omega \ll \Gamma$), the sample has time to equilibrate with the field and a normal paramagnetic susceptibility is measured; the out-of-phase component of the susceptibility χ'' (which measures the rate of energy absorbed by the sample) is zero. For $\omega \approx \Gamma$, the sample does not have sufficient time to equilibrate and the measured susceptibility falls below the equilibrium value. In addition, χ'' becomes a maximum. In the condition $\omega >> \Gamma$, the external field is changing much more quickly than the sample can relax so both the in-phase χ and out-of-phase χ'' responses go to zero.

Identical domains are found in crystals of high-spin molecules, also known as nanomagnets. The contents of each unit cell are identical and the alignments of the easy axes are parallel (in the absence of canting). In practice, these compounds are studied as a function of temperature at a fixed frequency, with the temperature dependence remeasured at other frequencies. It is found that the maximum in χ decreases in magnitude and moves to higher temperatures with increasing frequency. The behavior of χ'' is similar. The ability to study nanomagnets, such as Mn_{12}, using relaxation methods has provided great insight into the dynamics and the Hamiltonians of these compounds.

The relatively small moments of nanomagnets, compared to those of superparamagnetism, led to one of the most important developments in molecular magnetism, the discovery of macroscopic quantum tunneling [92]. A nanomagnet is selected with uniaxial anisotropy and a high-spin (S) ground state. A single crystal is cooled to low temperatures in a field; each moment is then in one of the lowest energy states, with the distribution determined by the Boltzman factor, equation (79). At $T = 0$, only the $m_S = S$ state is occupied. The field is then brought to zero, at which point the energies of the m_S and $-m_S$ states are equal. This is not an equilibrium situation because the occupied states are prevented from relaxing by the energy barrier. As the field reverses direction, the occupied states are increasingly unstable. If the temperature is raised, they may relax via the ordinary thermal process.

There is an alternative process, quantum tunneling. As the field slowly reverses, the $m_S = S$ state rises in energy and becomes degenerate with the $-m_{S-1}$ state which decreases in energy. The two states are mixed by a small transverse field and relaxation occurs. If the field continues to grow in the reverse direction, additional degeneracies occur at higher discrete values of field and the magnetization increases in steps. Quantum tunneling had been proposed long before the existence of Mn_{12} [93] but the unavailability of monodisperse superparamamagnets with relatively small ground state spin values left the concept purely theoretical. The ability to study nanomagnets revolutionized the study of magnetic tunneling in quantum systems [94].

4.5. *Magnets with spin-singlet ground states*

Section 3 introduced several ways in which spin-singlet ground states can arise. Antiferromagnetic dimers (Section 3.3.2) have non-magnetic ground states separated from moment-bearing states by energy gaps Δ proportional to the size of the exchange interactions. In addition, crystal field splittings and single-ion anisotropy of the correct sign can create a

[†]See Section 3.1.5 in Ref. [23c].

singlet-ground state for integer-spin ions such as Fe(II) and Ni(II), also with an energy gap Δ.

An interaction J' between each dimer (or singlet-ground state ion) and its z neighbors *may* lead to a state of LRO, depending on the relative strength of zJ' and Δ. Broadly speaking, if $zJ' > \Delta$, the gap is closed by the interaction and an ordered state will occur at sufficiently low temperatures. However, if $zJ' < \Delta$, Δ the gap will remain finite but at a reduced value. At temperatures low compared to the reduced gap, the system will fall into the ground state and become diamagnetic. This is known as the condition of *subcritical exchange*. A number of examples are known [95, 96].

Antiferromagnetic dimers, alternating chains, and spin ladders all have singlet ground states. As seen in figures 21 and 23, their gaps can be closed by external magnetic fields. Likewise, the gap of a subcritical exchange system can be closed at which point the ground state becomes magnetic. At a sufficiently low temperature, LRO will appear, with the critical temperature being a function of the applied field. This is an example of *field-induced ordering*. The compounds Ni(pyridine-N-oxide)$_6$(NO$_3$)$_2$ [97] and $NiCl_2{\cdot}4SC(NH_2)_2$ [96] were the first two examples of subcritical exchange systems to be identified in 1979 and 1981. Recently, the nickel chloride compound has been extensively studied [98, 99] as an example of a quantum phase transition, in which the transition is driven by a change in a term in the Hamiltonian, rather than a change of temperature.

Two spin ladders have been found to undergo field-induced ordering: *bis*piperidinium copper tetrabromide (BPCB, *strong rung*) and *bis*(2,3-dimethylpyridinium) copper tetrabromide (DIMPY, *strong rail*) (Section 3.3). Both have shown evidence of Luttinger Liquid (LL) behavior, which is restricted to 1-D systems. The gaps can be closed by fields of 6.8 and 3.0 T, respectively; beyond these fields, the ladders have magnetic moments and excitations that can travel along them. Careful studies at low temperature show each undergoes a transition to LRO with the transition temperature varying with the applied field. The highest transition temperature for BPBC occurs at 0.105 K in a field of 8.5 T, although the LL behavior persists up to 1.5 K [100, 101]. For DIMPY, the largest ordering temperature is found near 0.300 K in a field of 8.5 T [102, 103].

4.6. *Highly frustrated magnets*

There is another class of magnets which fails to order until very low temperatures, if at all. Many of the compounds in this class are 3-D transition metal/rare earth oxides with large moments and large exchange interactions; nevertheless, their ordering temperatures are much less than the Curie–Weiss parameter, θ. The explanations for their behavior are the particular magnetic lattices involved and the concept of frustration [36].

Frustration in magnetic systems is defined as the inability of any moment to simultaneously satisfy all of its magnetic interactions, resulting in ground state degeneracy [35a, 104–109]. This concept is illustrated with magnetic triangles in figure 29. Figure (29a) represents an Ising antiferromagnetic triangle in which all three interactions are identical and the easy axis points towards the top and bottom of the page. The two moments at the bottom of the triangle are antiferromagnetically aligned with each other but the remaining moment is frustrated. Either choice of orientation opposes one of the interactions, creating a twofold degenerate ground state.

There is an important distinction between frustration and competing interactions. Figure (29b) shows an Ising antiferromagnetic triangle with two strong (J_1) and one weaker

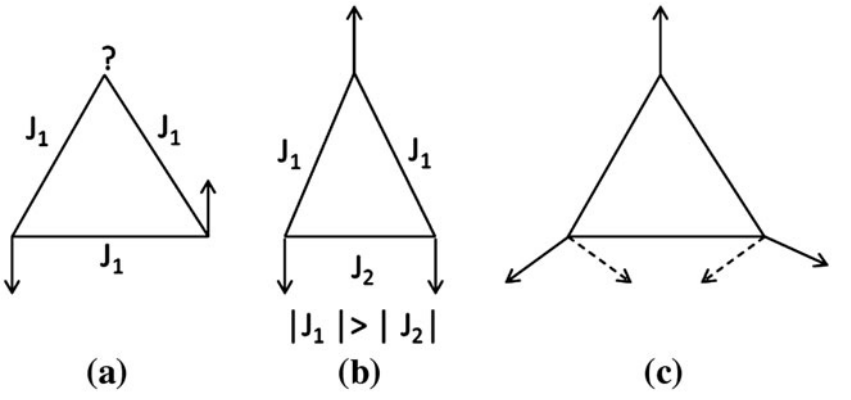

Figure 29. (a) Equilateral Ising antiferromagnetic triangle with frustration. (b) Isosceles Ising antiferromagnetic triangle with competing interactions (not frustrated). (c) Equilateral Heisenberg antiferromagnetic triangle with frustration.

(J_2) interaction. The two moments at the bottom do experience competing interactions but their unambiguous alignment, as shown, represents a unique ground state. This triangle is not frustrated.

Figure (29c) represents an equilateral antiferromagnetic triangle with either *XY* or Heisenberg exchange so the moments can orient to minimize their exchange energy. For every antiferromagnetic system, the ground state is one in which the total spin equals zero. For the triangle, an energy minimum is reached when the moments are inclined at 120° to each other ($S_{tot} = 0$), even though no interaction is completely satisfied since no two spins are antiparallel. The two lower spins can exchange their orientations (dotted lines), creating a twofold degenerate ground state and frustrating the triangle.

Extended lattices can be constructed from antiferromagnetically coupled triangles and tetrahedra, but frustration for triangles only occurs when they share corners, not edges. The triangular lattice consists of edge-sharing triangles, two of which are shown in

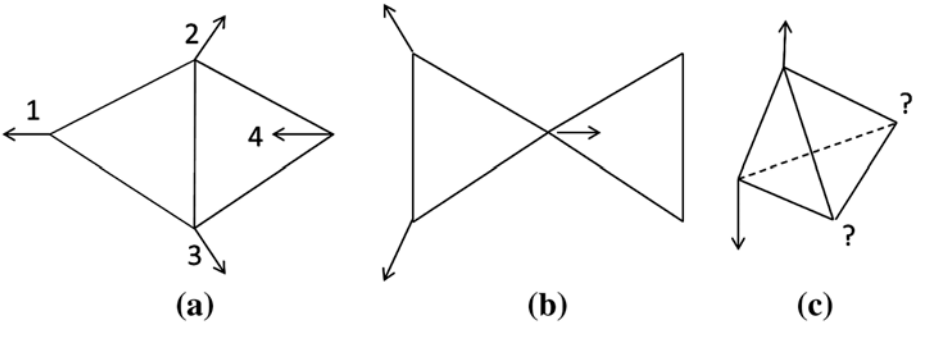

Figure 30. (a) Edge-sharing triangles which exhibit no additional frustration. (b) Corner-sharing triangles which exhibit a doubling of degeneracy. (c) A frustrated isotropic antiferromagnetic tetrahedron.

figure (30a). The triangle with spins 1, 2, and 3 is twofold degenerate, but when the fourth spin is added to the edge-sharing triangle (4), its alignment is predetermined. No additional degeneracy is added as the lattice is extended so the triangular lattice [figure (31a)] has a twofold degeneracy no matter how many spins are added. It undergoes a normal ordering process [110].

Antiferromagnetic tetrahedra with uniform interactions are also frustrated, much more so than triangles. As seen in figure (30c), any pair of moments can align antiferromagnetically. The $S_{tot} = 0$ ground state can be achieved by the remaining pair being antiferromagnetic to each other, no matter their orientation to the first pair so the ground state of the tetrahedron is much more degenerate.

In contrast to the edge-shared case, when triangles share corners, each triangle has a unique twofold degeneracy. This point is illustrated in figure (30b) which shows that only one moment is shared between the triangles, leaving the two remaining moments to have two degenerate orientations. The kagomé lattice [figure (31b)] consists of corner-sharing triangles, so its degeneracy scales as the number of triangles, causing the kagomé lattice to be considered the holy grail of frustrated antiferromagnets. The best-known representation of a kagomé lattice is Herbertsmithite, $ZnCu_3(OH)_6Cl_2$ [111], which consists of Cu(II)-based kagomé planes separated by diamagnetic Zn(II) ions. In spite of a strong ($J/k_B \approx 190$ K) nearest-neighbor interaction, no long range order has been determined above 50 mK [112].

What is the experimental evidence for the presence of frustration in a magnet? The most common signature of frustration is a temperature dependence of the magnetic susceptibility similar to that found in low-dimensional antiferromagnets, although *for very different reasons*. At high temperatures compared to the dominant exchange interaction, the material is paramagnetic and the susceptibility follows Curie–Weiss behavior (Section 3.1) with a Weiss constant proportional to the product of J and the number of nearest neighbors [equation (52)]. As the temperature is lowered, the susceptibility shows a broad maximum and continues to decrease. If the ground state is a singlet, the susceptibility decreases to zero at the lowest temperatures, as in figure 22, while it will remain finite if there is a ground state moment [figure (18)]. The presence of ordering will appear as an abrupt change in the slope of the susceptibility, usually at a temperature at T_N that is much lower than the value of θ. An index of the degree of frustration is the ratio of the (negative) Curie–Weiss constant to that of the ordering temperature [35a]:

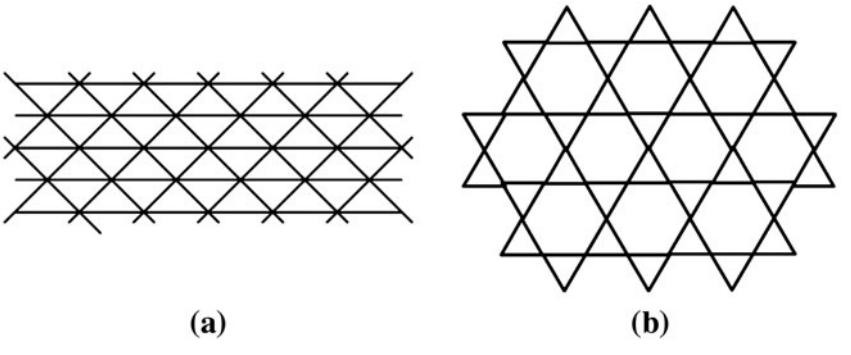

Figure 31. (a) An extended triangular lattice. (b) The kagomé lattice.

$$f = -\frac{\theta}{T_N} \tag{80}$$

Magnetic materials with f-values greater than ten are considered frustrated. The value for Herbertsmithite holds the current record, $f > 1800$!

Why do frustrated magnets fail to order? The answer to this question can be given in terms of the correlation length ξ. The correlation length needs to grow upon cooling; so at some temperature, the total exchange energy will overcome the randomizing effects of thermal energy, equation (73). This growth does not occur in frustrated magnets, for reasons apparent in figure (29c). The spin at the top of the triangle is not strongly correlated to either of its neighbors, for they are fluctuating between their two degenerate orientations. If this triangle is part of a kagomé lattice, neither of the bottom spins are strongly correlated to the moments in the adjacent triangle, due to that triangle's twofold degeneracy. The correlation lengths in frustrated magnets are short, and do not increase upon cooling when well below the Curie–Weiss temperature. These features have been observed by neutron scattering on Herbertsmithite [113] as well as predicted by calculations for the kagomé lattice [114]. Note that this explanation is very different from the reason low-dimensional magnets do not order until low temperatures. For low-D materials, the correlation lengths do grow upon cooling, but only along one axis (1-D) or along a plane (2-D); the correlations do not span the entire sample until temperatures comparable to the interchain or interlayer interaction strength J', equations (76) and (77).

Nevertheless, most frustrated magnets do ultimately order; Herbertsmithite is the exception, not the rule. The magnets discussed in this section are examples of *Geometrically Frustrated Magnets* for which the frustration is inherent in the lattice. Any perturbation that breaks the symmetry of the lattice will break the ground-state degeneracy and lead to order. Examples of such perturbations are grain boundaries in crystals, impurities in the magnetic sites, voids, an external magnetic field, and even applied pressure [115]. Other sources of symmetry-breaking are spin-canting contributions to the Hamiltonian as well as interactions between moments that are not nearest neighbors.

The 3-D analog of the kagomé lattice is the cubic pyrochlore structure of formula $A_2B_2O_7$ [105] which consists of corner sharing antiferromagnetically coupled tetrahedral units, figure (29c). The A-site is occupied by a trivalent rare earth element and the B-site by a tetravalent transition metal ion; a well-studied example is $Ho_2Ti_2O_7$. While the nearest neighbor exchange leads to a degenerate lattice, the Ho(III) ion has a magnetic moment of nearly $10\mu_B$, so the dipolar fields are large and contribute to the breaking of the degeneracies at low temperature [104].

Frustration has other origins besides the lattice-symmetry imposed type characteristic of the geometrically frustrated magnets. Uniform linear chains with nearest-neighbor exchange J_1 and antiferromagnetic next-nearest neighbor exchange J_2 become frustrated for certain ratios of J_2/J_1. The earliest experimental evidence of frustration was found in metallic copper that had been doped with small amounts ($\approx 0.5\%$) of a 3-D transition metal such as Mn or Fe. The magnetic interactions between the dopant atoms decrease with distance while oscillating in sign (RKKY interaction); consequently, different moments experience different combinations of competing ferro- and antiferromagnetic interactions and frustration results. Due to the randomness in these metals, known as spin glasses [116], they are more difficult to study and understand than the geometrically frustrated magnets.

Acknowledgments

The authors are grateful for all the contributions of their students over the past three decades which has made the work fun, and especially to Dr Fan Xiao for assistance with the figures.

References

[1] O.Kahn, *Molecular Magnetism*, VCH Publishers, New York (1993).
[2] J.H. Van Vleck. *The Theory of Electric and Magnetic Susceptibilities*, Oxford University Press, London (1932).
[3] A.H. Morrish. *The Physical Principles of Magnetism*, IEEE Press, New York (2001).
[4] D.H. Martin. *Magnetism in Solids*, MIT Press, Cambridge Massachusetts (1967).
[5] P.W. Selwood. *Magnetochemistry*, 2nd Edn, Interscience Publishers, New York (1956).
[6] J. Crangle. *Solid State Magnetism*, Van Nostrand Reinhold, New York (1991).
[7] S. Chikazumi. *Physics of Ferromagnetism*, 2nd Edn, Oxford University Press, Oxford (1997).
[8] S. Blundell. *Magnetism in Condensed Matter*, Oxford University Press, Oxford (2001).
[9] A.F. Orchard. *Magnetochemistry*, Oxford University Press, Oxford (2003).
[10] L.J. De Jongh, A.R. Miedema. *Adv. Phys.*, **23**, 1 (1974); Republished *Adv. Phys.*, **50**, 947 (2001)
[11] L.J. de Jongh (Ed.). *Magnetic Properties of Layered Transition Metal Compounds*, Kluwer Academic Publishers, Dordrecht (1990).
[12] A. Earnshaw. *Introduction to Magnetochemistry*, Academic Press, London (1968).
[13] A. Thompson, B.N. Taylor, *Guide for the Use of the International System of Units (SI)*, NIST Special Publication 811, 2008 Edn. Available online at: www.nist.gov
[14] (a) T.I. Quickenden, R. Marshall. *J. Chem. Ed.*, **49**, 114 (1979); (b) S. Hatscher, H. Schilder, H. Lueken, W. Urland. *Pure. Appl. Chem.*, **77**, 497 (2005).
[15] R. Kuhlman, G.L. Schimek, J.W. Kolis. *Polyhedron*, **18**, 1379 (1999).
[16] F. Xiao, M.M. Turnbull, C.P. Landee (in press).
[17] A.M. Ako, I.J. Hewitt, V. Mereacre, R. Clérac, W. Wernsdorfer, C.E. Anson, A.K. Powell. *Angew. Chem. Inter. Ed.*, **45**, 4926 (2006).
[18] P. Weiss. *J. Physique*, **6**, 667 (1907).
[19] J.S. Smart. *Effective Field Theories of Magnetism*, Saunders, Philadelphia, PA (1966).
[20] J.A. Schlueter, H. Park, G.J. Halder, W.R. Armand, C. Dunmars, K.W. Chapman, J.L. Manson, J. Singleton, R. McDonald, A. Plonczak, J. Kang, C. Lee, M.-H. Whangbo, T. Lancaster, A.J. Steele, I. Franke, J.D. Wright, S.J. Blundell, F.L. Pratt, J. de George, M.M. Turnbull, C.P. Landee. *Inorg. Chem.*, **51**, 2121 (2012).
[21] J.H. Van Vleck. *Physica*, **69**, 177 (1973).
[22] T. Lis. *Acta Crystal. B*, **36**, 2042 (1980).
[23] R. Sessoli, H.L. Tsai, A.R. Schake, S. Wang, J.B. Vincent, K. Folting, D. Gatteschi, G. Christou, D.N. Hendrickson. *J. Am. Chem. Soc.*, **115**, 1804 (1993).
[24] Recent review articles: (a) S. Hill, S. Datta, J. Liu, R. Inglis, C.J. Milios, P.L. Feng, J.J. Henderson, E. del Barco, E.K. Brechin, D.N. Hendrickson. *Dalton Trans.*, **39**, 4693 (2010); (b) T.C. Stamatatos, C.G. Efthymiou, C.C. Stoumpos, S.P. Perlepes. *Eur. J. Inorg. Chem.*, **2009**, 3361 (2009); (c) T.C. Stamatatos, G. Christou. *Inorg. Chem.*, **48**, 3308 (2009); (d) O. Roubeau, R. Clerac. *Eur. J. Inorg. Chem.*, **28**, 4325 (2008); (e) K.E. Vostrikova. *Coord. Chem. Rev.*, **252**, 1409 (2008); (f) H. Oshio, M. Nihei. *Bull. Chem. Soc. Jpn.*, **80**, 608 (2007); (g) P. Przychodzen, T. Korzeniak, R. Podgajny, B. Sieklucka. *Coord. Chem. Rev.*, **250**, 2234 (2006); (h) E.K. Brechin. *Chem. Commun.*, **41**, 5141 (2005).
[25] Recent books on molecular magnets: (a) M.M. Turnbull, T. Sugimoto, L.K. Thompson (Eds.). *Molecular-based Magnetic Materials: Theory, Techniques, and Applications*, American Chemical Society, Washington, DC (1996); (b) K. Itoh, M. Kinoshita (Eds.). *Molecular Magnetism: New Magnetic Materials*, copublished by Kodansha LTD (Tokyo) and Gordon and Breach, Amsterdam (2000); (c) D. Gatteschi, R. Sessoli, J. Villain. *Molecular Nanomagnets*, Oxford University Press, Oxford (2006); (d) R. Winpenny (Ed.). *Molecular Cluster Magnets*, World Scientific Publishing, Singapore (2012).
[26] Recent book chapters on molecular magnets: (a) J.R. Long. In *Chemistry of Nanostructured Materials*, P. Yang (Ed.), pp. 291–315, World Scientific Publishing, Hong Kong (2003); (b) M. Baumgarten. In *EPR of free radicals in solids, Trends in methods and application*, A. Lund, M. Shiotani (Eds), pp. 491–528, Kluwer, Dordrecht (2003/2004); (c) T. Takui, H. Matsuoka, K. Furukawa, S. Nakazawa, K. Sato, D. Shiomi. In *EPR of free radicals in solids, Trends in methods and application*, A. Lund, M. Shiotani (Eds), pp. 407–490, Kluwer, Dordrecht (2003/2004); (d) N. Robertson, G.T. Yee. In *Molecular Materials*, D.W. Bruce, D. O'Hare, R.I. Walton (Eds), pp. 143–210, Wiley, Chichester (2010).
[27] A.F. Albuquerque, F. Alet, P. Corboz, P. Dayal, A. Feiguin, S. Fuchs, L. Gamper, E. Gull, S. Guertler, A. Honecker, R. Igarashi, M. Koerner, A. Kozhevnikov, A. Laeuchli, S.R. Manmana, M. Matsumoto, I.P. McCulloch, F. Michel, R.M. Noack, G. Pawlowski, L. Pollet, T. Pruschke, U. Schollwock, S. Todo,

S. Trebst, M. Troyer, P. Werner, S. Wessel. *The ALPS project release 1.3: open source software for strongly correlated systems*. arXiv:0801.1765
[28] C. Yasuda, S. Todo, K. Hukushima, F. Alet, M. Keller, M. Troyer, H. Takayama. *Phys. Rev. Lett.*, **94**, 217201 (2005).
[29] (a) A. Santoro, A.D. Mighell, C.W. Reimann. *Acta Cryst. B*, **26**, 9979 (1970); (b) P.R. Hammar, M.B. Stone, D.H. Reich, C. Broholm, P.J. Gibson, M.M. Turnbull, C.P. Landee, M. Oshikawa. *Phys. Rev. B*, **59**, 1008 (1999).
[30] (a) B. Morosin. *Acta Cryst. B*, **31**, 632 (1975); (b) W. Duffy Jr, J.E. Venneman, D.L. Strandburg, P.M. Richards. *Phys. Rev. B*, **9**, 2220 (1974).
[31] D.C. Johnston, R.K. Kremer, M. Troyer, X. Wang, A. Klümper, S.L. Bud'ko, A.F. Panchula, P.C. Canfield. *Phys. Rev. B*, **61**, 9558 (2000).
[32] J.C. Bonner, M.E. Fisher. *Phys. Rev.*, **135**, A 640 (1964).
[33] (a) C.P. Landee, R.D. Willett. *Phys. Rev. Lett.*, **43**, 463–466 (1979); (b) D.D. Swank, C.P. Landee, R.D. Willett. *Phys. Rev. B*, **20**, 2154 (1979).
[34] (a) M. Takahashi. *Phys. Rev. Lett.*, **58**, 168 (1987); (b) J. Oitmaa, E. Bornilla. *Phys. Rev. B*, **53**, 14228 (1996).
[35] (a) A.P. Ramirez. *Ann. Rev. Mater. Sci.*, **24**, 453–480 (1994); (b) H.T. Diep (Ed.). *Frustrated Spin Systems*, World Scientific, Singapore (2004); (c) C. LaCroix, P. Mendels, F. Mila (Eds). *Introduction to Frustrated Magnetism: Materials, Experiments, Theory*, Springer, Berlin (2011).
[36] R.J. Birgeneau. *Am. J. Phys.*, **58**, 17 (1990) and references therein.
[37] (a) E. Manousakis. *Rev. Mod. Phys.*, **63**, 1 (1991); (b) J.-K. Kim, M. Troyer. *Phys. Rev. Lett.*, **80**, 2705 (1998).
[38] F.M. Woodward, A.S. Albrecht, C.M. Wynn, C.P. Landee, M.M. Turnbull. *Phys. Rev. B*, **65**, 144412 (2002). The expression in this paper was in error by failing to include the factor of one that is added to the ratio of the sums.
[39] J. Darriet, M.S. Haddad, E.N. Duesler, D.N. Hendrickson. *Inorg. Chem.*, **18**, 2679 (1979).
[40] F.M. Woodward, P.J. Gibson, G. Jameson, C.P. Landee, M.M. Turnbull, R.D. Willett. *Inorg. Chem.*, **46**, 4256 (2007).
[41] F. Xiao, F.M. Woodward, C.P. Landee, M.M. Turnbull, C. Mielke, N. Harrison, T. Lancaster, S.J. Blundell, P.J. Baker, P. Babkevich, F.L. Pratt. *Phys. Rev. B*, **79**, 134412 (2009).
[42] F.M. Woodward, C.P. Landee, J. Giantsidis, M.M. Turnbull, C. Richardson. *Inorg. Chim. Acta*, **324**, 324 (2001).
[43] F.M. Woodward, A.S. Albrecht, C.M. Wynn, C.P. Landee, M.M. Turnbull. *Phys. Rev. B*, **65**, 144412 (2002).
[44] R.T. Butcher, M.M. Turnbull, C.P. Landee, A. Shapiro, F. Xiao, D. Garrett, W.T. Robinson, B. Twamley. *Inorg. Chem.*, **49**, 427 (2010).
[45] M.M. Turnbull, C.P. Landee, B.M. Wells. *Coord. Chem. Rev.*, **249**, 2567–2576 (2005).
[46] J. Oitmass, E. Bornilla. *Phys. Rev. B*, **53**, 14228 (1996).
[47] M. Takahashi. *Phys. Rev. Lett.*, **58**, 168 (1987).
[48] T. Fetzer, A. Lentz, T. Debaerdemaeker. *Z. Naturforsch., B: Chem. Sci.*, **44**, 553 (1989).
[49] B.C. Keith, C.P. Landee, T. Valleau, M.M. Turnbull, N. Harrison. *Phys. Rev. B*, **84**, 104442 (2011). Erratum: *Phys. Rev. B*, **84**, 229901 (2011).
[50] J.J. Borrás-Almenar, E. Coronado, J. Curely, R. Georges. *Inorg. Chem.*, **34**, 2699 (1995).
[51] M. Hase, I. Terasaki, K. Uchinokura. *Phys. Rev. Lett.*, **70**, 3651 (1993).
[52] J.L. Musfeldt, In *Magnetism: Molecules to Materials I: Models and Experiments*, J.S. Miller, M. Drillon (Eds), Wiley-VCH Verlag GmbH & Co. KGaA, pp. 90–135, Weinheim (2002).
[53] (a) S.A. Roberts, D.R. Bloomquist, R.D. Willett, H.W. Dodgen. *J. Am. Chem. Soc.*, **103**, 2603 (1981); (b) H. Manaka, I. Yamada, K. Yamaguchi. *J. Phys. Soc. Jpn.*, **66**, 564 (1997).
[54] (a) J.J. Borrás-Almenar, E. Coronado, J. Curely, R. Georges, J.C. Gianduzzo. *Inorg. Chem.*, **33**, 5171 (1994); (b) R. Georges, J.J. Borrás-Almenar, E. Coronado, J. Curély, M. Drillon. In *Magnetism: Molecules to Materials I: Models and Experiments*, J.S. Miller, M. Drillon (Eds), Wiley-VCH Verlag GmbH & Co. KGaA, pp. 1–47, Weinheim (2002).
[55] (a) M. Julve, F. Lloret, J. Faus, G. De Munno, M. Verdaguer, A. Caneschi. *Angew. Chem. Int. Ed. Eng.*, **32**, 1046 (1993); (b) G. De Munno, M. Julve, F. Lloret, J. Faus, M. Verdaguer. A. Caneschi, *Inorg. Chem.*, **34**, 157 (1995).
[56] E. Dagotto, T.M. Rice. *Science*, **271**, 618 (1996).
[57] T. Barnes, E. Dagotto, J. Riera, E.S. Swanson. *Phys. Rev. B*, **47**, 3196 (1993).
[58] D.C. Johnston, M. Troyer, S. Miyahara, D. Lidsky, K. Ueda, M. Azuma, Z. Hiroi, M. Takano, M. Isobe, Y. Ueda, M.A. Korotin, V.I. Anisimov, A.V. Mahajan, L.L. Miller. arXiv:cond-mat/0001147. Note that this article is a preprint and contains numerous typographical errors. The tables of coefficients for the basic spin ladder are correct.
[59] M. Azuma, Z. Hiroi, M. Takano, K. Ishida, Y. Kitaoka. *Phys. Rev. Lett.*, **73**, 3463 (1994).
[60] R. Eccleston, M. Azuma, M. Takano. *Phys. Rev. B*, **53**, 14721 (2006).
[61] T. Imai, K.R. Thurber, K.M. Shen, A.W. Hunt, F.C. Chou. *Phys. Rev. Lett.*, **81**, 220 (1998).
[62] (a) M. Uehara, T. Nagata, J. Akimitsu, H. Takahashi, N. Mori, K. Kinoshita. *J. Phys. Soc. Jpn.*, **65**, 2764 (1996); (b) H. Mayaffre, P. Auban-Senzier, M. Nardone, D. Jérome, D. Poilblanc, C. Bourbonnais, U. Ammerahl, G. Dhalenne, A. Revcolevschi. *Science*, **279**, 345 (1998); (c) T. Nagata, M. Uehara, J. Goto, N. Motoyama, H. Eisakai, S. Uchida, H. Takahashi, T. Makashishi, N. Mori. *Phys. Rev. Lett.*, **98**, 1090 (1998).

[63] C.P. Landee, M.M. Turnbull, C. Galeriu, J. Giantsidis, F.M. Woodward. *Phys. Rev. B, Rapid Comm.*, **63**, 100402 (2001).
[64] (a) B.R. Patyal, B.L. Scott, R.D. Willett. *Phys. Rev. B*, **41**, 1657 (1990); (b) B.C. Watson, V.N. Kotov, M.W. Meisel, D.W. Hall, G.E. Granoth, W.T. Montfrooij, S.E. Nagle, D.A. Jensen, R. Backov, M.A. Petruska, G.E. Fanucci, D.R. Talham. *Phys. Rev. Lett.*, **86**, 5168 (2001).
[65] J. Jornet-Somoza, N. Codina-Castillo, M. Deumal, F. Mota, J.J. Novoa, R.T. Butcher, M.M. Turnbull, B. Keith, C.P. Landee, J.L. Wikaira. *Inorg. Chem.*, **51**, 6315–6325 (2012).
[66] M.M. Turnbull, C. Galeriu, J. Giantsidis, C.P. Landee. *Mol. Cryst. Liq. Cryst.*, **376**, 469–476 (2002).
[67] (a) C.P. Landee, A. Delcheva, C. Galeriu, G. Pena, M.M. Turnbull, R.D. Willett. *Polyhedron*, **22**, 2325 (2006); (b) T. Hong, M. Kenzelmann, M.M. Turnbull, C.P. Landee, B.D. Lewis, K.P. Schmidt, G.S. Uhrig, Y. Qiu, C. Broholm, D.H. Reich. *Phys. Rev. B*, **74**, 094434 (2006).
[68] (a) R.D. Willett, C. Galeriu, C.P. Landee, M.M. Turnbull, B. Twamley, *Inorg. Chem.*, **43**, 3804−3811 (2004); (b) J.D. Woodward, J. Choi, J.L. Musfeldt, J.T. Haraldsen, X. Wei, H.-J. Koo, D. Dai, M.-H. Wangbo, C.P. Landeee, M.M. Turnbull. *Phys. Rev. B*, **71**, 174416 (2005).
[69] A. Shapiro, C.P. Landee, M.M. Turnbull, J. Jornet, M. Deumal, J.J. Novoa, M.A. Robb, W. Lewis. *J. Am. Chem. Soc.*, **129**, 952 (2007).
[70] F. Awwadi, R.D. Willett, B. Twamley, R. Schneider, C.P. Landee. *Inorg. Chem.*, **47**, 9327 (2008).
[71] T. Hong, M. Kenzelmann, M.M. Turnbull, C.P. Landee, B.D. Lewis, K.P. Schmidt, G.S. Uhrig, Y. Qiu, C. Broholm, D.H. Reich. *Phys. Rev. B*, **74**, 094434-1/9 (2006).
[72] M. Klanjšek, H. Mayaffre, C. Berthier, M. Horvatić, B. Chiari, O. Piovesana, P. Bouillot, C. Kollath, E. Orignac, R. Citro, T. Giamarchi. *Phys. Rev. Lett.*, **101**, 137207 (2008).
[73] T. Hong, Y.H. Kim, C. Hotta, Y. Takano, G. Tremelling, M.M. Turnbull, C.P. Landee, H.-J. Kang, N.B. Christensen, K. Lefman, K.P. Schmidt, G.S. Uhrig, C. Broholm. *Phys. Rev. Lett.*, **105**, 137201 (2010).
[74] P.R. Hammar, M.B. Stone, D.H. Reich, C. Broholm, P.J. Gibson, M.M. Turnbull, C.P. Landee, M. Oshikawa. *Phys. Rev. B*, **59**, 1008–1015 (1999).
[75] J.S. Griffith. *The Theory of Transition Metal Ions*, Cambridge University Press, Cambridge (1961).
[76] F. Lloret, M. Julve, J. Cano, R. Ruiz-García, E. Pardo. *Inorg. Chim. Acta*, **361**, 3432 (2008).
[77] J. Villain. *J. Physique*, **35**, 27 (1974).
[78] D.J. Scalapino, Y. Imry, P. Pincus. *Phys. Rev. B*, **11**, 2042 (1975).
[79] H. Schulz. *Phys. Rev. Lett.*, **77**, 2790 (1996).
[80] S. Todo. *Phys. Rev. B*, **74**, 104415 (2006).
[81] S. Todo, A. Shibasaki. *Phys. Rev. B*, **78**, 224411 (2008).
[82] A. Furrer, J. Mesot, Th. Strässle (Eds.). *Neutron Scattering in Condensed Matter Physics*, World Scientific Publishing C. Pte. Ltd., Singapore (2009).
[83] S. Chakravarty, B.I. Halperin, D.R. Nelson. *Phys. Rev. Lett.*, **60**, 1057 (1988).
[84] L. Onsager. *Phys. Rev.*, **65**, 117 (1944).
[85] K. Harada, N. Kawashima. *Phys Rev. B*, **55**, R11949 (1997).
[86] (a) V.L. Berezinskii. *Soviet Physics JETP*, **32**, 493 (1971); (b) J.M. Kosterlitz, D.J. Thouless. *J. Phys. C*, **6**, 1181 (1973); (c) J.M. Kosterlitz. *J. Phys. C*, **7**, 1046 (1974).
[87] L.P. Regnault, J. Rossat-Mignod, p. 271 in Ref. [11].
[88] A. Cuccoli, T. Roscilde, V. Tognetti, R. Vaia, P. Verrucchi. *Phys. Rev. B*, **67**, 104414 (2003).
[89] A. Cuccoli, T. Roscilde, R. Vaia, P. Verrucchi. *Phys. Rev. B*, **68**, 060402 (2003).
[90] L. Néel. *J. Phys. Radium*, **11**, 49 (1950).
[91] J. Tejada, X.X. Zhang. *J. Phys.: Cond. Matt.*, **6**, 263 (1993).
[92] (a) J.R. Friedman, M.P. Sarachik, J. Tejada, R. Ziolo. *Phys. Rev. Lett.*, **76**, 3830 (1996); (b) L. Thomas, F. Lionti, R. Ballou, D. Gatteschi, R. Sessoli, B. Barbara, *Nature*, **383**, 145 (1996).
[93] L. Gunther, B. Barbara (Eds.). *Quantum Tunneling of Magnetization*, Kluwer, Dordrecht (1995).
[94] E. Chudnovsky, J. Tejada. *Macroscopic Quantum Tunneling of the Magnetic Moment* (Cambridge Studies in Magnetism), Cambridge University Press, Cambridge (1998).
[95] A. Paduan-Filho, R.D. Chirico, K.O. Joung, R.L. Carlin. *J. Chem. Phys.*, **74**, 4103 (1981).
[96] M. Orendáč, S. Zvyagin, A. Orendáčová, M. Sieling, B. Lüthi, A. Feher, M.W. Meisel. *Phys. Rev. B*, **60**, 4170 (1999).
[97] R.L. Carlin, K.O. Joung, A. Paduan-Filho, C.J. O'Connor, E. Sinn. *J. Phys. C*, **12**, 293 (1979).
[98] V.S. Zapf, D. Zocco, B.R. Hansen, M. Jaime, N. Harrison, C.D. Batista, M. Kenzelmann, C. Niedermayer, A. Lacerda, A. Paduan-Filho. *Phys. Rev. Lett.*, **96**, 077204 (2006).
[99] S.A. Zvyagin, J. Wosnitza, A.K. Kolezhuk, V.S. Zapf, M. Jaime, A. Paduan-Filho, V.N. Glazkov, S.S. Sosin, A.I. Smirnov. *Phys. Rev. B*, **77**, 092413 (2008).
[100] M. Klanjšek, H. Mayaffre, C. Berthier, M. Horvatić, B. Chiari, O. Piovesana, P. Bouillot, C. Kollath, E. Orignac, R. Citro, T. Giamarchi. *Phys. Rev. Lett.*, **101**, 137207 (2008).
[101] Ch. Rüegg, K. Kiefer, B. Thielemann, D.F. McMorrow, V. Zapf, B. Normand, M.B. Zvonarev, P. Bouillot, C. Kollath, T. Giamarchi, S. Capponi, D. Poilblanc, D. Biner, K.W. Krämer. *Phys. Rev. Lett.*, **101**, 247202 (2008).

[102] D. Schmidiger, P. Bouillot, S. Mühlbauer, S. Gvasaliya, C. Kollath, T. Giamarchi, A. Zheludev. *Phys. Rev. Lett.*, **108**, 167201 (2012).
[103] K. Ninios, T. Hong, T. Manabe, C. Hotta, S.N. Herringer, M.M. Turnbull, C.P. Landee, Y. Takano, H.B. Chan. *Phys. Rev. Lett.*, **108**, 097201 (2012).
[104] S.T. Bramwell, M.J.P. Gingras. *Science*, **294**, 1495 (2001).
[105] J.E. Greedan. *J. Mater. Chem.*, **11**, 37 (2001).
[106] R. Moessner, A.P. Ramirez. *Physics Today*, 24 (2006).
[107] M. Murrie, D.J. Price. *Ann. Rep. Prog. Chem., Sect. A*, **103**, 20 (2007).
[108] J.F. Sadoc, R. Mosseri. *Geometrical Frustration*, Cambridge University Press, Cambridge (2006).
[109] J. Schnack. *Dalton Trans.*, 4677 (2010).
[110] B. Bernu, C. Lhuillier, L. Pierre. *Phys. Rev. Lett.*, **69**, 2590 (1992).
[111] M.P. Shores, E.A. Nytko, B.M. Bartlett, D.G. Nocera. *J. Am. Chem. Soc.*, **127**, 13462 (2005).
[112] P. Mendels, F. Bert, M.A. de Vries, A. Olariu, A. Harrison, F. Duc, J.C. Trombe, J.S. Lord, A. Amato, C. Baines. *Phys. Rev. Lett.*, **98**, 077204 (2007).
[113] M.A. de Vries, J.R. Stewart, P.P. Deen, J. Piatek, G. Nilsen, H. Rønnow. *Phys. Rev. Lett.*, **103**, 237201 (2009).
[114] S. Depenbrock, I.P. McCulloch, U. Schollwöck. *Phys. Rev. Lett.*, **109**, 067201 (2012).
[115] D.P. Kozlenko, A.F. Kusmartseva, E.V. Lukin, D.A. Keen, W.G. Marshall, M.A. de Vries, K.V. Kamenev. *Phys. Rev. Lett.*, **108**, 187207 (2012).
[116] D. Chowdhury. *Spin Glasses and Other Frustrated Systems*, Princeton University Press, Princeton, NJ (1986).

Appendix A. Relationship between Gaussian and rationalized MKSA units

Quantity	Symbol	Gaussian unit	Conversion*	MKSA unit
Force	F	dyne	10^{-5}	newton (N)
Energy	U	erg	10^{-7}	joule (J)
Energy density	U/V	erg cm^{-3}	10^{-1}	J m^{-3}
Current	I	abampere	10	Ampere (A)
Magnetic field	**H**	oersted (Oe)	$\frac{1}{4\pi} \times 10^3$	amp-turns m^{-1}
Magnetic induction	**B**	Gauss (G)	10^{-4}	tesla (T)
Magnetic moment	$\boldsymbol{\mu}$	erg G^{-1} (emu)	10^{-3}	J T^{-1} = A m^2
Volume magnetization	**M**	erg G^{-1} cm^{-3} (emu cm^{-3})	10^3	A m^{-1} = J T^{-1} m^{-3}
Mass magnetization	M_{mass}	erg G^{-1} g^{-1} (emu g^{-1})	1	A m^2 kg^{-1} = J T^{-1} kg^{-1}
Molar magnetization	M_{mol}	erg G^{-1} mol^{-1} (emu mol^{-1}, cm^3 mol^{-1})	10^{-3}	A m^2 mol^{-1} = J T^{-1} mol^{-1}
Susceptibility	χ_{vol}	dimensionless	4π	dimensionless
Mass susceptibility	χ_g, χ_{kg}	cm^3 g^{-1}	$4\pi \times 10^{-3}$	m^3 kg^{-1}
Molar susceptibility	χ_{mol}	cm^3 mol^{-1}	$4\pi \times 10^{-6}$	m^3 mol^{-1}
Demagnetization	D, N	dimensionless	$1/(4\pi)$	dimensionless factor

*One dyne = 10^{-5} newton; one erg = 10^{-7} joule, etc.
A more comprehensive version of this table, plus a second table on converting Gaussian/cgs units to the SI equivalents, are available at http://www.nist.gov/pml/electromagnetics/magnetics/magnetics-publications.cfm.

Appendix B. Fundamental physics constants

Quantity	SI value and unit	CGS value and unit
Avogadro constant (N_A)	$6.022\ 141 \times 10^{23}$ mol^{-1}	$6.022\ 141 \times 10^{23}$ mol^{-1}
Bohr magneton (m_B)	$927.400\ \times 10^{-26}$ J T^{-1}	$927.400\ \times 10^{-23}$ erg G^{-1}
Boltzmann constant (k_B)	$1.380\ 64 \times 10^{-23}$ J K^{-1}	$1.380\ 64 \times 10^{-16}$ erg K^{-1}
electron charge ($-e$)	$1.602\ 176 \times 10^{-19}$ C	$1.602\ 176 \times 10^{-20}$ abC
electron mass (m_e)	$9.109\ 382 \times 10^{-31}$ kg	$9.109\ 382\ \times 10^{-28}$ g
permeability of vacuum (m_0)	$4\pi \times 10^{-7}$ N A^{-2} (exact)	1 (exact, dimensionless)
Planck constant (h)	$6.626\ 069 \times 10^{-34}$ J s	$6.626\ 069 \times 10^{-27}$ erg s
Speed of light in vacuum (c)	299 792 458 m s^{-1} (exact)	$2.997\ 924\ 58 \times 10^{10}$ cm s^{-1} (exact)

Source: 2010 CODATA.
http://physics.nist.gov/cuu/Constants/

Appendix C. Energy units and conversion factors

The fundamental (SI) unit of energy, the joule, is too large for the atomic scale. In practice, alternative units are used which are on the order of the energy scale being studied. Each of these units is directly related to energy through fundamental constants. For example, the thermal energy of one kelvin can be found by the equation $E(J) = k_B T(\mathrm{K})$, where $k_B T$ is Boltzmann's constant of $1.380\ 6488(13) \times 10^{-23}$ J K^{-1}. Similarly, the energy of an electromagnetic wavelength of one centimeter is found from the Planck's equation:

$$E = hf = h\frac{c}{\lambda} = \frac{1.986 \times 10^{-25}\, J\, m}{0.01m} = 1.986 \times 10^{-23} J$$

Similarly, it can be shown that a millielectron volt (meV) = 1.602×10^{-19} J and a 1 GHz electromagnetic wave has an energy of 6.626×10^{-25} J. The energy of a moment (spin S) in an applied field is given by the Zeeman equation [equation (21)]: $E = g\mu_B m_s B$. Assuming $g = 2.00$ and $S = 1/2$, the magnetic energy in a field of B tesla can be compared to the other practical units. One kelvin of thermal energy equals the Zeeman energy in a field of 1.489 T.

This table can be read horizontally or vertically. Moving horizontally from the left-hand side, 1 K is an equivalent energy to those of 0.695 cm^{-1}, 0.08617 meV, 20.84 GHz, and 1.489 tesla. Moving vertically, the table displays how many K are required to match the energies of the other energy units. 1.439 K equal 1 cm^{-1}, 11.605 K equal 1 meV, etc.

Unit	K	cm^{-1}	meV	GHz	Tesla
K	1	0.695	8.617×10^{-2}	20.84	1.489

(*Continued*)

Appendix D

Equations for susceptibilities of various model systems. Each expression is based on the single-J form of the Hamiltonian (53a).

1-D HEISENBERG SUSCEPTIBILITIES

Uniform 1-D QHAF [equation (60)]
Single J format, positive J is antiferromagnetic.
Parameter 1: CC, the Curie Constant.
Parameter 2: Jk, the exchange strength *expressed as a temperature*
Parameter 3: PARA, the percentage of paramagnetic contribution

Chi = (1-0.01* PARA)*(CC/T)*(1.+(-0.053837836)*(Jk/T) +0.097401365*(Jk/T)^2 +0.0144 67437*(Jk/T)^3 +0.0013925193*(Jk/T)^4 +0.00011393434*(Jk/T)^5)/ (1. +0.44616216*(Jk/T) +0.32048245*(Jk/T)^2 +0.13304199*(Jk/T)^3 +0.037184126*(Jk/T)^4 +0.0028136088*(Jk/T) ^5+0.00026467628*(Jk/T)^6) +0.01* PARA *CC/T

Alternating 1-D QHAF
Single J format, positive J is antiferromagnetic.
Parameter 1: CC, the Curie Constant.
Parameter 2: Jk, the exchange strength *expressed as a temperature*
Parameter 3: alpha, the alternation parameter
Parameter 4: PARA, the percentage of paramagnetic contribution

chi = (PARA*0.01*CC/T) + (1-0.01*PARA)*(CC/T)*exp(-(Jk/T)*(1-0.5*alpha -2* alpha^2 +1.5*alpha^3))*(1.+(Jk/T)*(0.63427990 -2.06777217*alpha -0.70972219*alpha^2 + 4.89720885 *alpha^3 -2.80783223*alpha^4)+ (Jk/T)^2*(0.18776962 -2.84847225*alpha + 5.96899688* alpha^2 - 3.85145137*alpha^3 +0.64055849* alpha^4) + (Jk/T)^3*(0.033603617 -0.757981757* alpha +4.137970390*alpha^2 -6.100241386*alpha^3 +2.701116573*alpha^4) +(Jk/T)^4* (0.0038611069 + 0.5750352896*alpha -2.3359243110*alpha^2 +2.934083364* alpha^3 -1.1756629304*alpha^4) + (Jk/T)^5*(0.00027331430 -0.10724895512*alpha + 0.403 45647304* alpha^2 -0.48608843641*alpha^3 + 0.18972153852*alpha^4) + (Jk/T)^6*(0 + 0.005 78123759*alpha -0.02313572892*alpha^2 +0.02892774508*alpha^3 -0.01157325374*alpha^4) + (Jk/T)^7*(2.59870347E-7*alpha -2.39236193E-7*alpha^2) * ((Jk/T)*(1.-alpha)^0.75*(1. + alpha)^0.25 + 0.38658545*alpha*(1-alpha)-0.20727806 *alpha^2*(1- alpha)^2)^4.69918784)/ (1.+ (Jk/T)*(-0.11572010 -1.31777217*alpha +1.29027781*alpha^2 + 3.39720885*alpha^3- 2.80783223 *alpha^4) + (Jk/T)^2*(0.08705969 -1.44693321*alpha +5.09401919*alpha^2

-10.51861382*alpha^3 +8.97655318*alpha^4 + 5.75312680*alpha^5 -11.83647774*alpha^6 + 4.21174835*alpha^7) + (Jk/T)^3*(0.00563137 + 0.65986015*alpha -1.38069533*alpha^2 -0.09849603*alpha^3 + 7.54214913*alpha^4 - 22.31810507*alpha^5 +27.60773633*alpha^6 -6.39966673*alpha^7 -15.69691721*alpha^8 +13.37035665*alpha^9 -3.15881126*alpha^10) + (Jk/T)^4*(0.0010408866 + 0.1008789796*alpha -0.9188446197*alpha^2 +1.6052570070* alpha^3 -0.7511481272*alpha^4) + (Jk/T)^5*(0.0000683286 -0.1410232710*alpha + 0.6939435 034*alpha^2 -0.9608700949*alpha^3 +0.4106951428*alpha^4) + (Jk/T)^6*(0+ 0.0367159872* alpha -0.1540749976*alpha^2 + 0.19826671*alpha^3 -0.0806430233*alpha^4) + (Jk/T)^7*(0 -0.00314381636*alpha + 0.01140642324*alpha^2 -0.01338139741*alpha^3 + 0.00511879 053*alpha^4) + (Jk/T)^8*(1.25124679E-7*alpha -1.03824523E-7*alpha^2) *((Jk/T)*((1-alpha) ^0.75*(1+alpha)^0.25 + 0.38658545*alpha*(1-alpha) -0.20727806*alpha^2*(1-alpha)^2))^3.556 92695)

Strong *Rung* Spin Ladder ($J_{rung} > J_{rail}$)

Single J format, positive J is antiferromagnetic.
Parameter 1: CC, the Curie Constant.
Parameter 2: j_rail the exchange strength *expressed as a temperature*
Parameter 3: j_rung, the exchange strength *expressed as a temperature*
Parameter 4: PARA, the percentage of paramagnetic contribution

chi =(1-0.01* PARA)*(CC/T)*exp(-(1-1.462084*j_rail/j_rung+1.382207*(j_rail/j_rung)^2-0.4182226*(j_rail/j_rung)^3)/(T/j_rung))*(1+(j_rung/T)*(0.6342799-0.4689967*(j_rail/j_rung)-0.1224498*(j_rail/j_rung)^2-0.6316720*(j_rail/j_rung)^3-0.08782728*(j_rail/j_rung)^4) + (j_rung/T)^2 * (0.1877696-0.1498959*(j_rail/j_rung)-0.4760102*(j_rail/j_rung)^2 +0.2714945*(j_rail/j_rung)^3 +0.3686003*(j_rail/j_rung)^4) + (j_rung/T)^3*(0.03360362-0.0131970*(j_rail/j_rung)-0.3269535*(j_rail/j_rung)^2 +0.7854194*(j_rail/j_rung)^3-0.5140804*(j_rail/j_rung)^4) + (j_rung/T)^4*(0.003861107-0.01530859*(j_rail/j_rung)+0.1567169*(j_rail/j_rung)^2-0.2790342*(j_rail/j_rung)^3+0.1304374*(j_rail/j_rung)^4) + (j_rung/T)^5*(0.0002733143+0.008596509*(j_rail/j_rung)-0.03444813*(j_rail/j_rung)^2 + 0.05010183*(j_rail/j_rung)^3-0.02274661*(j_rail/j_rung)^4) + (j_rung/T)^6*(-0.0002501523*(j_rail/j_rung)+0.001069419*(j_rail/j_rung)^2-0.001893068*(j_rail/j_rung)^3+0.001088651*(j_rail/j_rung)^4))/(1+(j_rung/T)*(-0.1157201+1.493088*(j_rail/j_rung)-1.5046567*(j_rail/j_rung)^2-0.2134494*(j_rail/j_rung)^3-0.08782728*(j_rail/j_rung)^4) + (j_rung/T)^2*(0.08705969-0.1502010*(j_rail/j_rung)+0.9054526*(j_rail/j_rung)^2-1.607161*(j_rail/j_rung)^3+0.9440189*(j_rail/j_rung)^4+0.07149545*(j_rail/j_rung)^5-0.05532895*(j_rail/j_rung)^6-0.03673135*(j_rail/j_rung)^7)
+(j_rung/T)^ 3* (0.005631367+0.07738460*(j_rail/j_rung)-0.1639982*(j_rail/j_rung)^2+0.3932678*(j_rail/j_rung)^3-0.7370737*(j_rail/j_rung)^4 +0.6755368*(j_rail/j_rung)^5 -0.2865834*(j_rail/j_rung)^6 -0.1009833*(j_rail/j_rung)^7+0.07759403*(j_rail/j_rung)^8 +0.007719311*(j_rail/j_rung)^9-0.007680941*(j_rail/j_rung)^10)
+(j_rung/T)^4*(0.001040887+0.01252745*(j_rail/j_rung) + 0.1183833*(j_rail/j_rung)^2
-0.2857871*(j_rail/j_rung)^3+0.1510432*(j_rail/j_rung)^4)
+(j_rung/T)^5*(0.00006832857+0.004243732*(j_rail/j_rung)-0.03901711*(j_rail/j_rung)^2
+0.1055626*(j_rail/j_rung)^3-0.06948651*(j_rail/j_rung)^4)
+(j_rung/T)^6*(-0.0001868979*(j_rail/j_rung)+0.009010690*(j_rail/j_rung)^2
-0.019630625*(j_rail/j_rung)^3+0.01131886*(j_rail/j_rung)^4)) + 0.01* PARA *CC/T

Strong *Rail* Spin Ladder ($J_{rail} > J_{rung}$)

Single J format, positive J is antiferromagnetic.
Parameter 1: CC, the Curie Constant.
Parameter 2: j_rail, the exchange strength *expressed as a temperature*
Parameter 3: j_rung, the exchange strength *expressed as a temperature*
Parameter 4: PARA, the percentage of paramagnetic contribution

chi = (1-0.01*PARA)*(CC/T)*exp(-(0.4030*(j_rung/j_rail)+0.0989*(j_rung/j_rail)^3)/(T/j_rail))*
(1+(j_rail/T)*(-0.05383784-0.67282213*(j_rung/j_rail)+0.03896299*(j_rung/j_rail)^2 + 0.01103114*(j_rung/j_rail)^3)
+(j_rail/T)^2*(0.09740136+0.12334838*(j_rung/j_rail)-0.0253489*(j_rung/j_rail)^2 +0.00655748*(j_rung/j_rail)^3)

+(j_rail/T)^3*(0.01446744-0.03965984*(j_rung/j_rail)-0.03120146*(j_rung/j_rail)^2 +0.02118588*(j_rung/j_rail)^3)
+(j_rail/T)^4*(0.001392519+0.006657608*(j_rung/j_rail)-0.020207553*(j_rung/j_rail)^2+0.008830122*(j_rung/j_rail)^3)
+ (j_rail/T)^5*(0.0001139343 + 0.0001341951*(j_rung/j_rail) + 0.0016684229*(j_rung/j_rail)^2 -0.0001396407*(j_rung/j_rail)^3)
+(j_rail/T)^6*(0.0000422531*(j_rung/j_rail)-0.000160983*(j_rung/j_rail)^2 +0.0001335788*(j_rung/j_rail)^3))/
(1+(j_rail/T)*(0.44616216-0.82582213*(j_rung/j_rail) + 0.03896299*(j_rung/j_rail)^2 -0.08786886*(j_rung/j_rail)^3)
+(j_rail/T)^2*(0.32048245-0.40632550*(j_rung/j_rail) +0.20252880*(j_rung/j_rail)^2 -0.03801372*(j_rung/j_rail)^3+0.07998604*(j_rung/j_rail)^4-0.00385344*(j_rung/j_rail)^5
+0.00379963*(j_rung/j_rail)^6)
+(j_rail/T)^3*(0.13304199-0.25099527*(j_rung/j_rail) + 0.11749096*(j_rung/j_rail)^2-0.07871375*(j_rung/j_rail)^3 +0.4106834*(j_rung/j_rail)^4 -0.01886681*(j_rung/j_rail)^5
+0.00157755*(j_rung/j_rail)^6 -0.00387185*(j_rung/j_rail)^7 +0.00019055*(j_rung/j_rail)^8-0.00010728*(j_rung/j_rail)^9)
+(j_rail/T)^4*(0.03718413-0.10249898*(j_rung/j_rail)+0.04316152*(j_rung/j_rail)^2 +0.01936105*(j_rung/j_rail)^3)
+(j_rail/T)^5*(0.002813608+0.000402749*(j_rung/j_rail)+0.001958564*(j_rung/j_rail)^2 -0.003803837*(j_rung/j_rail)^3)
+(j_rail/T)^6*(0.0002646763-0.0010424633*(j_rung/j_rail)+0.0015813041*(j_rung/j_rail)^2 -0.000291445*(j_rung/j_rail)^3)) + (0.01*PARA*CC/T)

Alternating FM/AFM Heisenberg Chain
Single J format, positive J is antiferromagnetic.
Parameter 1: CC, the Curie Constant.
Parameter 2: Jk, the *magnitude* of the antiferromagnetic exchange strength *expressed as a temperature*
Parameter 3: alpha, the alternation parameter defined as $J_{FM}/|J_{AF}|$
Parameter 4: PARA, the percentage of paramagnetic contribution
This expression is valid over the range $0 \leq \text{alpha} \leq 2$.

chi = (1-.01*PARA)*(CC/T)*((T/Jk)^3 + 5*(T/Jk)^2 - T/Jk + .05)/((T/Jk)^4 +(5.2623 - .33021*alpha)*(T/Jk)^3 + (.44976686 - .99234827*alpha - .00881524*alpha^2 + .15481517*alpha^3)*(T/Jk)^2 + (.18948031 + .36766434*alpha + .51001414*alpha^2 - .2795751*alpha^3)*(T/Jk) + (.28437797 -.16749925*alpha - .18725364*alpha^2 + .09374817*alpha^3)) + (.01*PARA*CC/T)

Uniform 1-D QH FM [equation (60)]
Single J format, positive J is *ferromagnetic*
Parameter 1: CC, the Curie Constant.
Parameter 2: Jk, the exchange strength *expressed as a temperature*

chi = (CC/T)*(1.+1.736278*(Jk/T)+1.07588*(Jk/T)^2+0.12081*(Jk/T)^3) / (1.+1.24008*(Jk/T)+0.42784*(Jk/T)^2+0.00272*(Jk/T)^3-0.00002*(Jk/T)^4)

2-D HEISENBERG SUSCEPTIBILITIES
Uniform 2-D QHAF: [equation (61)]
Single J format, positive J is antiferromagnetic.
Parameter 1: CC, the Curie Constant.
Parameter 2: Jk, the exchange strength *expressed as a temperature*
Parameter 3: xx, the percentage of paramagnetic contribution

Chi = (1-0.01*xx)*(CC/T)*(1.+ (-0.998586*(Jk/T) -1.28534*(Jk/T)^2 -0.656313*(Jk/T)^3 + 0.235862*(Jk/T)^4 -0.277527*(Jk/T)^5) /(1. +1.84279*(Jk/T)+1.14141*(Jk/T)^2+0.704192*(Jk/T)^3 -0.189044*(Jk/T)^4 +0.277545)*(Jk/T)^5)) + (0.01*xx*CC/T)

Rectangular 2-D QHAF: [equation (64)]
Single J format, positive J is antiferromagnetic.
Parameter 1: CC, the Curie Constant.
Parameter 2: Jk, the exchange strength *expressed as a temperature*
Parameter 3: alpha, the exchange anisotropy parameter
Parameter 4: PARA, the percentage of paramagnetic contribution

chi = (1.-0.01*PARA)*(0.25*CC/T)*(1.+ (Jk/T)*(1519.2 +533.43*alpha-77.687*alpha^2 -153.13*alpha^3 -169.91* alpha^4) +(Jk/T)^2*(-215.7+100.15*alpha+124.18*alpha^2-127.28 *alpha^3+169.16*alpha^4) + (Jk/T)^3*(218.14-57.494*alpha+10.684*alpha^2 +169.44*alpha^3 + 82.555*alpha^4) + (Jk/T)^4*(-10.769 + 12.189*alpha -227.21*alpha^2 + 45.305*alpha^3 -79.075 *alpha^4) + (Jk/T)^5*(0.094304 + 0.26961*alpha + 27.093*alpha^2 + 128.89*alpha ^3 - 21.344 *alpha^4) + (Jk/T)^6*(-0.00089531 + 0.0093003*alpha – 0.17427*alpha^2 +0.46488*alpha^3 – 0.38915*alpha^4)) / (1.+ (Jk/T)*(369.44 + 126.42*alpha + 13.757*alpha^2 -126.75*alpha^3 +10.215*alpha^4) + (Jk/T)^2*(179.27 +254.16*alpha +234.59*alpha^2 +69.668*alpha^3 -154.58 *alpha^4) +(Jk/T)^3*(50.271 + 106.25*alpha -500.56*alpha^2 +114.28*alpha^3 + 67.521* alpha^4) +(Jk/T)^4*(95.893 -39.055*alpha +548*alpha^2 +190.2*alpha^3 +41.573*alpha^4) + (Jk/ T)^5*(-4.1906 + 13.921*alpha -234.91*alpha^2 -252.49*alpha^3 -24.395*alpha^4) + (Jk/T)^6* (-0.00059343 – 0.43284*alpha + 27.795*alpha^2 + 117.38*alpha^3 + 43.919*alpha^4)) + (0.25*CC*PARA*0.01)/T

Uniform 2-D QH FM [equation (62)]
Single J format, positive J is *ferromagnetic*.
Parameter 1: CC, the Curie Constant.
Parameter 2: Jk, the exchange strength expressed as a temperature

chi = (CC/T)*(1. + 3*(Jk/(2.*T)) + 6*(Jk/(2.*T))^2 + 11.*(Jk/(2.*T))^3 + 20.625*(Jk/(2.*T))^4 + 39.025*(Jk/(2.*T))^5 + 68.777*(Jk/(2.*T))^6 + 119.43*(Jk/(2.*T))^7 + 216.162*(Jk/(2.*T))^8 + 387.194*(Jk/(2.*T))^9 + 658.342*(Jk/(2.*T))^10 + 1136.229*(Jk/(2.*T))^11 + 2036.605*(Jk/ (2.*T))^12 + 3538.639*(Jk/(2.*T))^13)